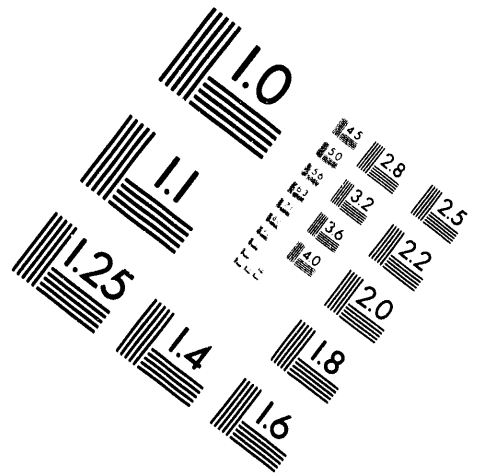




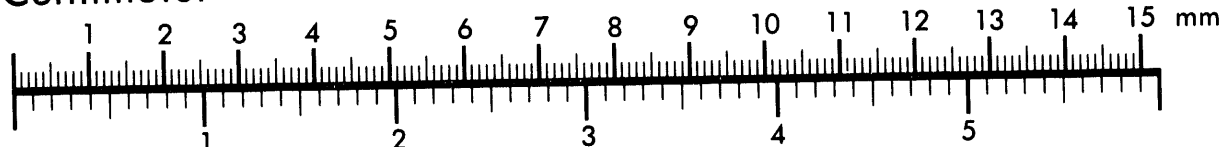
AIIM

Association for Information and Image Management

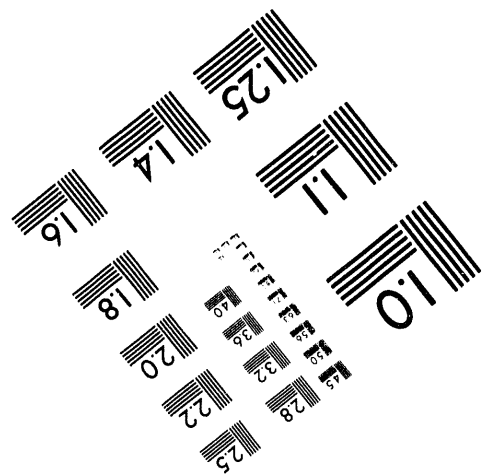
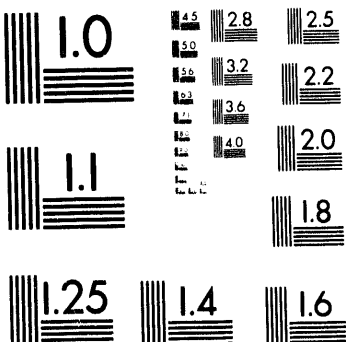
1100 Wayne Avenue, Suite 1100
Silver Spring, Maryland 20910
301/587-8202



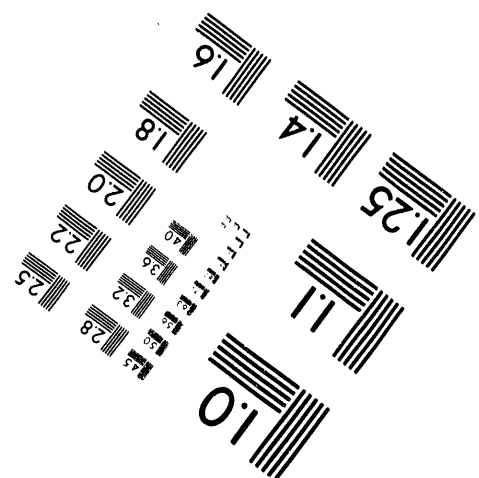
Centimeter



Inches



MANUFACTURED TO AIIM STANDARDS
BY APPLIED IMAGE, INC.



1 of 2

Physics Division

**Electron-Impact Ionization of Multicharged Ions
at ORNL: 1985 - 1992**

D. C. Gregory
*Office of Radiation Protection
Oak Ridge National Laboratory*

and

M. E. Bannister
*Physics Division
Oak Ridge National Laboratory*

Date Published: July 1994

Prepared for the
Office of Fusion Energy
Budget Activity No. AT 05 30 04 0

Prepared by the
OAK RIDGE NATIONAL LABORATORY
Oak Ridge, Tennessee 37831-6285
managed by
MARTIN MARIETTA ENERGY SYSTEMS, INC.
for the
U.S. DEPARTMENT OF ENERGY
under contract DE-AC05-84OR21400

MASTER

ols
DISTRIBUTION OF THIS DOCUMENT IS UNLIMITED

TABLE OF CONTENTS

REACTION CHART	v
INDEX OF TABLES, FIGURES, AND REFERENCES	vii
ABSTRACT	1
I. INTRODUCTION	1
II. EXPERIMENTAL METHOD	2
Ion Source	2
Ion Optics	4
Electron Gun	5
Cross Section Determination	6
Uncertainties	7
III. UNPUBLISHED DATA	8
O^{2+}	8
Kr^{4+}	9
Kr^{7+}	9
Kr^{9+}	10
Xe^{6+}	11
Ta^{8+}	12
CD_4^+	13
IV. EXPLANATION OF TABLES AND FIGURES	14
V. ACKNOWLEDGMENTS	15
REFERENCES	16
DATA TABLES	19
FIGURES	71
DISTRIBUTION	135

Element		Initial Charge State														
		1	2	3	4	5	6	7	8	9	10	11	12	13	14	15
27	Co															
28	Ni			2		■	■	■	■			■		■		
29	Cu		2	2												
30	Zn															
31	Ga															
32	Ge															
33	As															
34	Se															
35	Br															
36	Kr		2	2	■			■	■	■						
	Kr [†]				2											
40	Zr			2												
51	Sb			2												
54	Xe		2	2	2	2	2■		■							
	Xe [†]				2		2■		■							
	Xe [‡]						2■									
72	Hf			2												
73	Ta			2					■							
92	U										■		■			■
	U [†]									■		■				

¹ Reference 1, ORNL/TM-7020.

² Reference 2, ORNL/TM-9501.

■ This report.

Index of Tables, Figures, and References. List of electron-impact ionization and dissociation processes for which cross sections have been measured at ORNL. Page numbers for the tables and figures are listed in the appropriate columns, except where the reader is referred to previous reports ORNL/TM-7020 (Ref. 1) and ORNL/TM-9501 (Ref. 2). The fourth column lists the reference number for a given cross section. (See the reference list beginning on page 16.)

Reaction	Table	Figure	Reference	Previous Report
$B^{2+} \rightarrow B^{3+}$			3	TM-9501
$B^{3+} \rightarrow B^{4+}$			1	TM-7020
$C^{2+} \rightarrow C^{3+}$			4	TM-9501
$C^{3+} \rightarrow C^{4+}$			5	TM-7020, 9501
$C^{4+} \rightarrow C^{5+}$			1	TM-7020
$N^{2+} \rightarrow N^{3+}$			2	TM-9501
$N^{3+} \rightarrow N^{4+}$			4	TM-7020, 9501
$N^{4+} \rightarrow N^{5+}$			5	TM-7020
$N^{5+} \rightarrow N^{6+}$			1	TM-7020
$O^{2+} \rightarrow O^{3+}$	text p. 8		2,6	TM-9501
$O^{3+} \rightarrow O^{4+}$			1	TM-7020
$O^{4+} \rightarrow O^{5+}$			4	TM-7020, 9501
$O^{5+} \rightarrow O^{6+}$	21,22	73-76	3,5,7	TM-7020
$F^{2+} \rightarrow F^{3+}$			8	TM-9501
$Ne^{3+} \rightarrow Ne^{4+}$			9	TM-9501
$Al^{2+} \rightarrow Al^{3+}$			10	TM-9501
$Si^+ \rightarrow Si^{2+}$	23	77	11	
$Si^{2+} \rightarrow Si^{3+}$	24	78	11	
$Si^{3+} \rightarrow Si^{4+}$			10	TM-9501
$Si^{4+} \rightarrow Si^{5+}$	25	79	12	
$Si^{5+} \rightarrow Si^{6+}$	26	80	12	
$Si^{6+} \rightarrow Si^{7+}$	27	81	13	
$Si^{7+} \rightarrow Si^{8+}$	27	82	13	
$S^{4+} \rightarrow S^{5+}$	28	83,84	14	

Reaction	Table	Figure	Reference	Previous Report
$\text{Cl}^{2+} \rightarrow \text{Cl}^{3+}$		8		TM-9501
$\text{Cl}^{5+} \rightarrow \text{Cl}^{6+}$	29	85	14	
$\text{Ar}^{2+} \rightarrow \text{Ar}^{3+}$		8		TM-9501
$\text{Ar}^{3+} \rightarrow \text{Ar}^{4+}$		9		TM-9501
$\text{Ar}^{4+} \rightarrow \text{Ar}^{5+}$		1		TM-7020
$\text{Ar}^{4+} \rightarrow \text{Ar}^{6+}$		15		TM-9501
$\text{Ar}^{5+} \rightarrow \text{Ar}^{6+}$		2		TM-9501
$\text{Ar}^{6+} \rightarrow \text{Ar}^{7+}$	30	86	14	
$\text{Ar}^{7+} \rightarrow \text{Ar}^{8+}$	31	87	16	
$\text{Ar}^{8+} \rightarrow \text{Ar}^{9+}$	32,33	88,89	17	
$\text{Ti}^{2+} \rightarrow \text{Ti}^{3+}$			8	TM-9501
$\text{Ti}^{3+} \rightarrow \text{Ti}^{4+}$			18	TM-9501
$\text{Ti}^{5+} \rightarrow \text{Ti}^{6+}$	34	90	19	
$\text{Ti}^{11+} \rightarrow \text{Ti}^{12+}$	35	91	20	
$\text{Cr}^{6+} \rightarrow \text{Cr}^{7+}$	36	92	21	
$\text{Cr}^{7+} \rightarrow \text{Cr}^{8+}$	37	93	21	
$\text{Cr}^{8+} \rightarrow \text{Cr}^{9+}$	38	94	21	
$\text{Cr}^{10+} \rightarrow \text{Cr}^{11+}$	39	95	21	
$\text{Cr}^{13+} \rightarrow \text{Cr}^{14+}$	39	96	20	
$\text{Fe}^{2+} \rightarrow \text{Fe}^{3+}$			8	TM-9501
$\text{Fe}^{5+} \rightarrow \text{Fe}^{6+}$	40	97	22	
$\text{Fe}^{6+} \rightarrow \text{Fe}^{7+}$	41	98	22	
$\text{Fe}^{9+} \rightarrow \text{Fe}^{10+}$	42	99	22	
$\text{Fe}^{11+} \rightarrow \text{Fe}^{12+}$	43	100,101	23	
$\text{Fe}^{13+} \rightarrow \text{Fe}^{14+}$	43	102	23	
$\text{Fe}^{15+} \rightarrow \text{Fe}^{16+}$	44	103	23	
$\text{Ni}^{3+} \rightarrow \text{Ni}^{4+}$			24	TM-9501
$\text{Ni}^{5+} \rightarrow \text{Ni}^{6+}$	45	104	25	
$\text{Ni}^{6+} \rightarrow \text{Ni}^{7+}$	46	105	25	
$\text{Ni}^{7+} \rightarrow \text{Ni}^{8+}$	47	106	25	
$\text{Ni}^{8+} \rightarrow \text{Ni}^{9+}$	48	107	25	

Reaction	Table	Figure	Reference	Previous Report
$\text{Ni}^{12+} \rightarrow \text{Ni}^{13+}$	49	108	25	
$\text{Ni}^{14+} \rightarrow \text{Ni}^{15+}$	49	109	25	
$\text{Cu}^{2+} \rightarrow \text{Cu}^{3+}$			24	TM-9501
$\text{Cu}^{3+} \rightarrow \text{Cu}^{4+}$			24	TM-9501
$\text{Kr}^{2+} \rightarrow \text{Kr}^{3+}$			26	TM-9501
$\text{Kr}^{3+} \rightarrow \text{Kr}^{4+}$			9	TM-9501
$\text{Kr}^{4+} \rightarrow \text{Kr}^{5+}$	50	110	27	
$\text{Kr}^{4+} \rightarrow \text{Kr}^{6+}$			15	TM-9501
$\text{Kr}^{7+} \rightarrow \text{Kr}^{8+}$	51,52	111	28	
$\text{Kr}^{8+} \rightarrow \text{Kr}^{9+}$	53	112	29	
$\text{Kr}^{9+} \rightarrow \text{Kr}^{10+}$	54	113	30	
$\text{Zr}^{3+} \rightarrow \text{Zr}^{4+}$			18	TM-9501
$\text{Sb}^{3+} \rightarrow \text{Sb}^{4+}$			24	TM-9501
$\text{Xe}^{2+} \rightarrow \text{Xe}^{3+}$			31	TM-9501
$\text{Xe}^{3+} \rightarrow \text{Xe}^{4+}$			9	TM-9501
$\text{Xe}^{4+} \rightarrow \text{Xe}^{5+}$			31	TM-9501
$\text{Xe}^{4+} \rightarrow \text{Xe}^{6+}$			15	TM-9501
$\text{Xe}^{5+} \rightarrow \text{Xe}^{6+}$			31	TM-9501
$\text{Xe}^{6+} \rightarrow \text{Xe}^{7+}$	55	114	32,33	TM-9501
$\text{Xe}^{6+} \rightarrow \text{Xe}^{8+}$	56	115	34	TM-9501
$\text{Xe}^{6+} \rightarrow \text{Xe}^{9+}$	56	116	34	TM-9501
$\text{Xe}^{8+} \rightarrow \text{Xe}^{9+}$	57	117	29	
$\text{Xe}^{8+} \rightarrow \text{Xe}^{10+}$	58	118	35	
$\text{Hf}^{3+} \rightarrow \text{Hf}^{4+}$			18	TM-9501
$\text{Ta}^{3+} \rightarrow \text{Ta}^{4+}$			18	TM-9501
$\text{Ta}^{8+} \rightarrow \text{Ta}^{9+}$	59	119	36	
$\text{U}^{10+} \rightarrow \text{U}^{11+}$	60	120	37	
$\text{U}^{10+} \rightarrow \text{U}^{12+}$	61	121	37	
$\text{U}^{13+} \rightarrow \text{U}^{14+}$	62	122,123	37	
$\text{U}^{13+} \rightarrow \text{U}^{15+}$	63	124	37	
$\text{U}^{16+} \rightarrow \text{U}^{17+}$	64	125,126	37	

Reaction	Table	Figure	Reference	Previous Report
D ₃ O ⁺ → D ₂ O ⁺	65	127	38	
H ₃ O ⁺ → OH ⁺	65	128	38	
H ₃ O ⁺ → O ⁺	65	129	38	
CD ₄ ⁺ → CD ₄ ²⁺	66	130	39	
CD ₄ ⁺ → CD ₃ ⁺	66	131	39	
CD ₄ ⁺ → CD ₂ ⁺	67	132	39	
CD ₄ ⁺ → CD ⁺	68	133	39	
CD ₄ ⁺ → C ⁺	69	134	39	

Electron-Impact Ionization of Multicharged Ions at ORNL: 1985 - 1992

D. C. Gregory and M. E. Bannister

ABSTRACT

Absolute cross sections are presented in graphs and tables for single ionization of forty-one ions, multiple ionization of four ions, and for dissociation and ionization of two molecular ions by electron impact. This memo is the third in a series of manuscripts summarizing previously published as well as unpublished ionization cross section measurements at ORNL; contents of the two previous memos are also referenced in this work. All work tabulated in this memo involved ion beams generated in the ORNL-ECR ion source and utilized the ORNL electron-ion crossed beams apparatus. Target ions range from atomic number $Z=8$ (oxygen) to $Z=92$ (uranium) in initial charge states from +1 to +16. Electron impact energies typically range from threshold to 1500 eV.

I. INTRODUCTION

Our understanding of the atomic processes which are important in the ionization of atomic ions has progressed greatly in the last decade, primarily due to numerous collaborations between theoreticians and experimentalists involving ions of widely varying atomic number and charge. Advances on the experimental side in ion sources, energy resolution, and data collection and analysis techniques have inspired more sophisticated theoretical models and calculations. Similarly, theoretical insights and advanced computational techniques have led to predictions which guided experimentalists toward more meaningful work.

As a result of the understanding gained from this symbiotic relationship, the cross section for ionization of any given ion by electron impact could probably be calculated within 20% today, given relatively modest resources and attention. This was certainly not true 15 years ago, when direct ionization was considered by most modelers and other cross section users to be the only important process for almost all ions. It is now

understood that various indirect processes contribute to, and indeed often dominate, total ionization.

One of the purposes behind the collection of measurements summarized here is a search for "interesting" cross sections, those that reveal unexpected or seemingly unexplainable features. It is these surprises that lead to advances in our understanding of the ionization process. Another theme behind the measurements involves the interests of the fusion energy community. This research project receives primary support from DOE's Office of Fusion Energy, and it has emphasized specific data needs of the fusion program as an important part of the quest for general understanding discussed above. The targets presented here are dominated by metallic ions in relatively high charge states, typical of impurities commonly found in fusion research plasmas. The final theme found in this data collection is the study of trends along isoelectronic (same number of electrons) and isonuclear (same element) sequences. These sequences seem to provide the simplest trends to guide our understanding of the processes being studied. In addition, some of the measurements were made because they were interesting to the experimenters, convenient, or being used to test and confirm our experimental capabilities.

II. EXPERIMENTAL METHOD

The experimental technique and ion source have been described previously,²² and the references provide considerable detail which will not be repeated here. In general, the experiment consists of well-characterized ion and electron beams which intersect at 90°. Ions which are further ionized by the electron beam are selected by charge state and counted. Accurate measurement of critical quantities allows the cross sections to be put on an absolute scale.

Ion Source

Figure 1 shows a schematic of the ORNL-ECR (Oak Ridge National Laboratory Electron Cyclotron Resonance) ion source.⁴⁰ The source includes unique features in its design, although it is similar to several other ECR sources currently in use. For most of

ORNL-DWG 94-6018

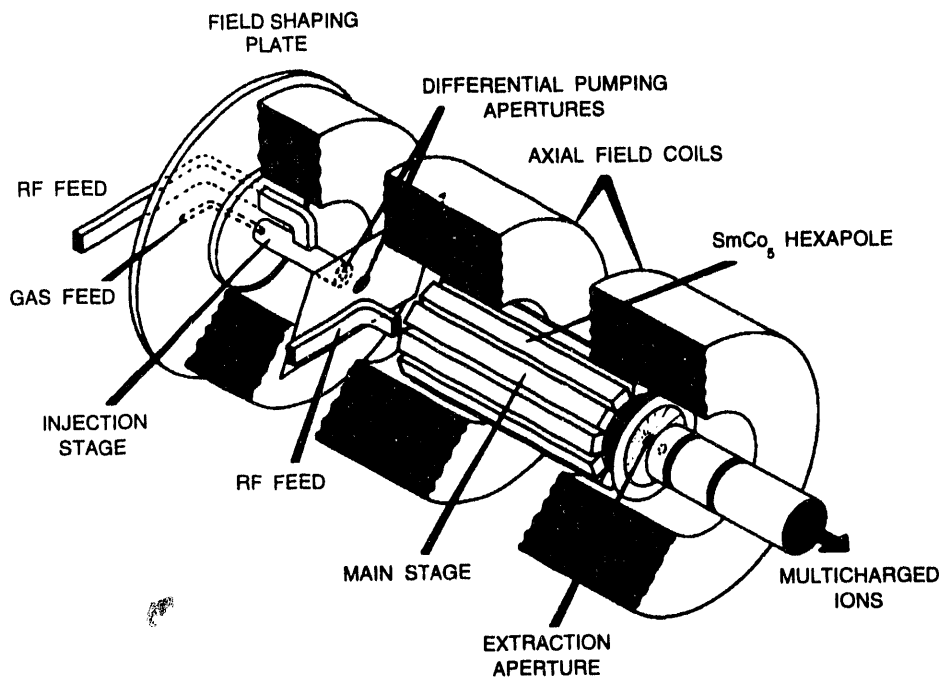


Fig. 1. ORNL ECR Multicharged Ion Source.

its eight-year tenure as the primary source for this research group, it was the only ECR source in the world dedicated solely to atomic physics research. The source is currently inactive, having just been replaced by a more powerful unit, but will be repositioned for further use in the same laboratory in the near future.

In general use, a gas is introduced into the first stage, where a small ECR surface produces low charge-state ions. These ions drift into the low-pressure second stage, where they are further ionized by electrons accelerated by a larger ECR surface. The entire source floats at the acceleration potential (generally 10 kV), and ions are extracted by acceleration to the ground potential at the exit of the source. A mixture of gases is sometimes used to influence the distribution of charges in the extracted beam, enhancing the production of either higher or lower charges. Most metals are not readily available in acceptable gases, and another method had to be found to introduce metal vapor into the source. Usually, a thin foil is attached to an insulated arm in the second stage of the ECR

source; the foil can then be raised using an external manipulator until it approaches the ECR region. The foil then melts or, if thin enough, slowly vaporizes. There is some evidence that a major source of metal vapor is recycled material deposited on the chamber walls.

The metastable content of ion beams extracted from ECR ion sources is still under study. In general, ECR sources are "hot," producing extracted ion beams with a wide range of charge states. As a rule of thumb, if a source has the energy to produce a significant number of ions in charge states higher than the one of interest, it has plenty of energy to produce metastable ions in the species of interest. If such metastables live long enough to reach the experimental region, the threshold for electron-impact ionization will be observed at an energy lower than that expected for ground-state ions. For most of the measurements summarized here, the metastable fraction of the target beam was determined, or estimated as accurately as possible.

Ion Optics

Two different techniques were used to separate signal ions from the main ion beam for this data. Prior to 1985, a parallel-plate analyzer was utilized to separate the signal ("ionized ions") from the main ion beam.¹⁸ Using that apparatus, physical space limitations in the collision chamber limited the range of charge states that could be studied. The parallel plate separator could not be made large enough to effectively separate beams with initial/final charge ratios greater than 6/7. In addition, apertures had to be used to separate the beam paths in order to block scattered particles and even photons from the ionized ion detector. Tens of counts/sec of false signal (out of 10^{12} ions/sec in the main beam) would dominate the real signal. A final drawback to the parallel-plate analyzer was that the chamber had to be opened and modifications made for almost every change in initial-to-final-ion charge ratio. In order to overcome these limitations, a new ion analysis apparatus was developed.

Figure 2 shows the apparatus used for the great majority of the measurements presented here. The main chamber houses the initial ion optics, a parallel-plate analyzer to reject ions which change charge along the flight path from the ion source, the electron gun and interaction volume, and some post-collision steering optics. The ion beams then enter a double-focusing 90° analyzing magnet. The signal ions are directed into a channel

electron multiplier, while the main beam is captured in a deep Faraday cup. The ions effectively see no apertures after the collision volume so that the possibility of "slit-scattering" is virtually eliminated. The double-focusing magnet focuses the collision volume onto the signal ion detector so that a "spot" signal is obtained. The ion analyzer is known as "PACMAG" because of the physical resemblance of the analyzing magnet to the video game creature. The original design was intended to be used for initial-to-final charge ratios between 4/5 and 15/16. An additional main beam cup extended that range down to approximately 1/2, and measurements have been made up to 16/17. Further details and an explanation of the available diagnostics are published elsewhere.²²

URNL-DWG 94-6016

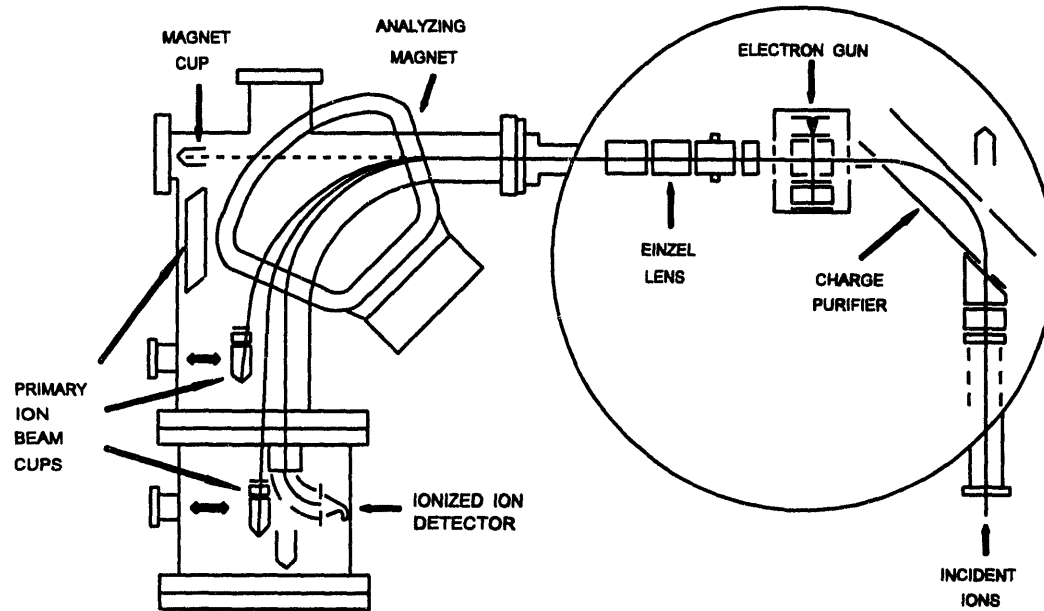


Fig. 2. Electron-ion crossed beams apparatus.

Electron Gun

The electron gun used in this series of experiments is essentially the same as that described by Taylor *et al.*⁴¹ Electrons emitted from an indirectly heated cathode are confined and compressed by an axial magnetic field. It was designed to produce an

intense, homogeneous, low-divergence electron beam at energies from a few eV to at least 3000 eV. In practice, power supplies, feed-thrus, and power dissipation in the beam collector limit the electron gun operation to 1500 eV or less. The energy resolution of the gun at low energies was measured during early excitation experiments, while the resolution at higher energies must be estimated based on excitation-autoionization features observed during ionization measurements. The energy resolution of the gun is known to be 2 eV or less at 350 eV or less beam energy. This resolution may be a conservative estimate since sharp ionization features tend to be "softened" or "smeared" by recombination resonances associated with the feature being observed. Typical operating electron beam currents range from 300 μ A at 100 eV to 5 mA at 1000 eV.

Cross Section Determination

The one-dimensional spatial distributions of the ion and electron beams, and the overlap of these two beams in the collision region is determined using a movable slit assembly. The current transmitted through a narrow horizontal slit is measured as the probe is moved through the beam vertically. The probe can be rotated so that both the ion and electron beam profiles are measured through the same slit. The probe position and current measurements are computer-controlled so that the overlap of the beams at any absolute vertical position can be determined. The beam profiles and overlap determine the "form factor," given by the relation

$$F = \frac{\int I_i(z) dz \int I_e(z) dz}{\int I_i(z) I_e(z) dz}$$

where $I_i(z)$ and $I_e(z)$ are the beam intensity profiles in the direction (z) perpendicular to both beams.

The quantities which must be measured in order to determine an absolute cross section are the ion and electron currents (I_i and I_e , in amperes), ion and electron velocities (v_i and v_e , in cm/sec), the form factor (F , in cm), the signal event rate (R , in events/sec), and the signal detection efficiency (D , unitless). The charge state of the incident ions (q_i) must also be known. Given these quantities, the absolute cross section (σ , in cm^2) as a function of the interaction energy (E) is given by

$$\sigma(E) = \frac{R}{I_e I_i} \frac{q_i e^2 v_e v_i}{\sqrt{v_e^2 + v_i^2}} \frac{F}{D}$$

where e is the electronic charge (1.6×10^{-19} C) and the ion velocity is assumed to be much less than the electron velocity. The interaction energy (E) is largely determined by the electron beam accelerating voltage, but must be corrected for contact potentials in the electron gun, space charge potentials, and the finite velocity of the target ions. In practice, there is always a background count rate in the signal detector, so the true signal event rate is taken to be the difference between signal-plus-background and background-only count rates.

Uncertainties

Each cross section measurement at each energy is independently absolute, but some quantities in the above formula are assumed constant for a given target ion. For example, the signal event detection efficiency will affect the measured signal rate at each energy by the same multiplicative factor, and the contact potential (a constant) offsets each interaction energy by almost the same amount. In contrast, the statistical uncertainty is independent for each measurement. Thus, to accurately convey the measurement uncertainty, we must specify both "absolute" and "relative" uncertainties for each set of cross section data.

In the data presented here, relative uncertainties are listed and plotted at the equivalent of one standard deviation for a purely statistical uncertainty, unless specified otherwise. The relative uncertainty includes (and is usually dominated by) statistical uncertainties, but also includes (combined in quadrature) relative form factor uncertainties and any other factors which are found to vary during a set of measurements. For a given data set, the shape of the cross section curve and any features observed in the curve may be judged in light of the relative uncertainties. For most of the cross section curves, one-standard-deviation relative uncertainty error bars are plotted when they are larger than the plotted points.

The absolute uncertainty is a combination of the relative uncertainty discussed above with any other factors which would affect all data points the same. The detection

efficiency, ion velocity and current, and some aspects of the beams overlap measurement are examples of additional sources of uncertainty in the absolute measurement. The shape and features of the cross section curve will not be affected by the absolute uncertainty, but the vertical scale of the entire curve could vary within the limits of the absolute uncertainty. The absolute uncertainty is generally specified in this report as a percentage of the cross section measurement for a typical point near the peak of the curve. It is given here at the equivalent of two standard deviations for purely statistical uncertainty, corresponding to approximately a 90% certainty for a limited number of measurement sets. For most of these measurements, the absolute uncertainty amounts to approximately 7% before combining it (in quadrature) with the relative uncertainty, which must also be taken at the two-standard-deviation level.

III. UNPUBLISHED DATA

A number of the data sets included in this report have never been published. Some were not considered to be sufficiently detailed to constitute a "complete" measurement. Others were not understood in sufficient detail to allow interpretation of the observed features. A few simply never fit into the pattern of data sets being published and were not of sufficient interest to be published alone. In order to make this report complete, and for the benefit of users who might find the data interesting (even given the limitations), tables and plots of the unpublished data are included. A brief description of each unpublished data set is given below, with warnings and such interpretation as can be made at this time.

O²⁺

There is no data table or plot presented here for O²⁺. The measurement was made in 1980 as an incidental part of another experiment and was not analyzed for several years. The data were collected by Dunn *et al.*,⁶ analyzed by D. C. Gregory, and first printed in the second of this series of memos (ORNL/TM-9501). A re-evaluation of the original data by Phaneuf⁶ for an IAEA-sponsored project revealed that a factor had been left out of the original data analysis. The Redbook analysis is now considered to be correct, and the O²⁺ cross sections in ORNL/TM-9501 need to be multiplied by 0.87 to correct them.

Kr⁴⁺

The data²⁷ for ionization of Kr⁴⁺, with a nominal 4s²4p² electron configuration and a 64 eV ground configuration ionization threshold, indicate a high percentage of metastable ions in the incident beam as well as some excitation-autoionization at energies above the ground ionization threshold. The observed threshold is near 41 eV. There are some interesting features with sharp energy dependence in the 80 to 100 eV range which could indicate the presence of resonances. The resolution of the present data, however, does not allow any firm conclusions about the presence of resonances based on the data alone. This was one of the last measurements made before the PACMAG energy analyzer was installed.

The absolute magnitude of the overall cross section curve is in some doubt. The measurements, which are all independently absolute, shifted by about 5% in magnitude from one day to the next during the experiment. We were unable to reproduce the first data, but are also unable to find any fault with those initial measurements. A subtle change in source conditions could produce a different metastable fraction, or some factor involved in the absolute normalization may have changed slightly. The uncertainty in the absolute magnitude of the curve made the data suspect, even though only by a small percentage, and it has never been published in the open literature. An average of the two sets of data is shown and tabulated here. A recent remeasurement of the data at ORNL is in good agreement with the data presented here.

The experimental results are compared in the figure to distorted-wave calculations by T. W. Gorczyca, M. S. Pindzola, N. R. Badnell, and D. C. Griffin⁴² for ground-configuration ions. Calculations are shown for both direct and total ionization. The total ionization calculation (which includes indirect effects) shows good agreement with the present data in magnitude, and fairly good agreement in shape. Permission by the authors to use these results prior to publication is acknowledged and greatly appreciated.

Kr⁷⁺

This measurement²⁸ was a quick first trial of the PACMAG energy analyzer. The electron gun was not fully baked before the data collection, and the expected instability in electron beam profiles was observed at high energies. The ground electron

configuration is $3d^{10}4s$. Two high points very close to the 3d direct-ionization onset could indicate the presence of resonances, but the possibility was not explored. Despite the beam profile instability mentioned above, the energy dependence of the curve at high energies is consistent with expectations.

We should clearly expect the ion source to produce metastable ions for a configuration as "unsettled" as this one, although the lifetimes and energy differential from the ground configuration are not at all obvious. In fact, as the measurements were extended to lower energies the cross section appeared to increase, a phenomenon which is normally taken as an indication of the spurious effect known as space-charge modulation. Another process which has been invoked to explain several other similar curves since this data was collected is the presence of autoionizing metastables in the incident beam. Any perturbation, such as a collision with a low energy electron, would stimulate the autoionization process. Lower energy electrons have "longer" collisions, and the probability of "stimulated autoionization" might well increase with decreasing electron energy. When this data analysis was carried out in 1985, the energy-dependence at low energies was assumed to be due to space-charge modulation, and a fit to the below-threshold points was subtracted from the raw data. This "corrected" data is presented here. There is a negligible change in the magnitude of the points above threshold due to this "correction." The overall absolute uncertainty in the curve for a point near the peak cross section is estimated to be 10%.

The experimental results are compared in the figure to distorted-wave calculations by T. W. Gorczyca, M. S. Pindzola, N. R. Badnell, and D. C. Griffin⁴² for ground-configuration ions. Calculations are shown for both direct and total ionization. The total ionization calculation (which includes indirect effects) shows fairly good agreement with the present data over the energy range covered by the calculation. Permission by the authors to use these results prior to publication is acknowledged and greatly appreciated.

Kr⁹⁺

This measurement³⁰ was a quick study carried out in preparation for the much more difficult Fe¹⁵⁺ experiment. The relatively large signal found for ionization of Kr⁹⁺ was used to obtain approximate settings of various lenses and steering elements which were then used as a starting point for Fe¹⁵⁺ diagnostics. The Kr⁹⁺ data were collected in

a short time to show that the apparatus was ready for the arduous experiment to come. The Lotz calculation shown is for the expected $3p^63d^9$ ground configuration. The data follow the general shape of the Lotz prediction, and the experimental curve is only about 12% higher than direct ionization theory. The measurement was considered incomplete due to the relatively large energy steps between data points, and uninteresting since there is good agreement with the Lotz prediction.

Xe⁶⁺

This is probably the second most interesting and detailed measurement in the entire series (after ionization of O⁵⁺). The initial data,³² published in 1983, was a very fruitful collaborative effort between theory and experiment. The near-threshold region is dominated by excitation-autoionization, and several major excitation features are clearly distinguishable. Overall agreement between theory and experiment is quite good, in shape and magnitude. However, there are also several interesting points on which theory and experiment disagree, indicating additional processes which could be explored. These include early onsets for several major excitation features (indicative of resonant recombination features) and a dip in the measured cross section at 120 eV (perhaps some sort of interference process). It was decided to remeasure the threshold region in early 1987 in greater detail, with the advantages of the more intense (and stable) beams from the ECR ion source, as well as improved post-collision optics available with PACMAG. The 1983 data utilized the old Penning Ion Gauge (PIG) ion source and parallel plate analyzer.

The ECR ion source, as expected, is a "hotter" source than the PIG source which provided beams for the initial 1983 data. An unexpected result is that approximately 50% of the Xe⁶⁺ beam for the present data³³ were in a metastable configuration 12 eV above ground. The ionization threshold thus moved 12 eV lower, including a major excitation feature which was below the ionization threshold for the 1983 data but which was noted (at the insistence of Chris Bottcher) in the original publication. By combining the theory for that feature with the published 1983 above-threshold theory, and assuming 50% metastables in the incident beam, excellent agreement with theory is again observed. The relative uncertainty of the new data is smaller than the plotted points, and it can be seen that the density of points has been greatly increased over the 1983 data. The two features

mentioned above are still present (early excitation onsets and the dip at 120 eV), but theoretical analysis would be complicated by the presence of the metastables, and has never been attempted.

The only sure method of measuring the resolution of an electron gun is to measure a sharp feature and fit the smoothed edge with a Gaussian shape. An additional hope for this data was that a sharp excitation onset could be obtained which would provide a measurement of the electron gun resolution. We have since concluded that if Nature abhors a vacuum, She also dislikes sharp edges. As has been mentioned here, physical processes such as recombination resonances tend to "smear" many sharp features. A relatively sharp onset at 98 eV can be fit with Gaussian distributions of 1.5 eV or 2.0 eV, depending on how many data points are included in the fit. This is, then, an upper limit on the resolution for this electron gun at 100 eV.

The 1987 cross section data were never published. While the analysis was under way, a subsequent collaborative study of this system was carried out in Giessen utilizing their ECR ion source and excellent high-resolution electron gun and scanning technique. Although a bit more detail was revealed by the Giessen data (some resonances emerged that were lost in the ORNL data), the overall shapes agree amazingly well. In fact, the 1987 ORNL and the Giessen data overlay almost exactly, with less than 10% difference in absolute magnitude. The ORNL data was no longer the most detailed available, and so unfortunately was never published. The Giessen data did not reveal any real surprises after seeing the ORNL data, and so was not considered worth a priority publication effort. As a result, this most interesting curve has not been updated in the literature since the initial 1983 data.

Ta⁸⁺

An effort was made to extend ionization measurements into the heavier metals when it appeared that this data would be useful to the fusion effort. Subsequent efforts in the fusion program seem to de-emphasize this area of research. It was also found that stable beams of refractory metals are quite difficult to produce in ECR ion sources. Uncertain identification of beams produced and almost universal charge-to-mass ratio overlaps with other more common species make the optimization of high charge states of refractory metal beams an adventure in frustration. After several false starts, a very weak

beam of Ta⁸⁺ was produced. The ground configuration is calculated to be 4f¹³5s²5p⁴, and the theory shown is the Lotz direct ionization calculation for that configuration. Unfortunately, a short in the electron gun somewhat limited the available electron beam. Combining a weak electron beam with a very weak ion beam, only limited data³⁶ could be collected. In general, the experimental curve appears to be about twice the Lotz prediction. The two points which do not seem to follow the experimental curve are not far enough off to indicate a significant real deviation in light of the experimental difficulties.

CD₄⁺

Dissociation of CD₄⁺ is of great interest to plasma modelers because of its expected presence near the edges of fusion plasma devices. It is, however, a difficult system for both experimentalists and theoreticians. The theory is difficult because of the complex energy levels available and the large number of particles involved in a collision. Experimentally, the threshold for dissociation extends to relatively low energies (compared to ionization), and the multiple dissociation channels scatter "stray" beams throughout the apparatus. It is also difficult to produce a beam of molecular ions with low internal energy.

The measurements reported here³⁹ extend from 4 to 300 eV interaction energies, and investigated the cross sections for dissociation of the parent ion into all possible ion fragments. Briefly, it was found that the cross section for ionization of CD₄⁺ to stable CD₄²⁺ was smaller than could be measured by this apparatus, as predicted by theory. The peak cross sections for dissociation to C⁺, CD⁺, and CD₂⁺ were all roughly equal (within a factor of three), a result which was surprising. All of the cross sections were measured against a "background" cross section which increased with decreasing electron energy. This indicates either that the signal detector background (dominated by "stray" dissociation products) was modulated by the electron beam, producing an "apparent signal" on top of the real signal, or that some of the incident ions were in highly excited states. This last view is supported by the fact that this "apparent signal" could be changed by a factor of 10 by simple adjustments to the ion source. It also indicates that this set of measurements was made with incident ions in unknown energy states, probably not in the lowest available ones.

For ionization of CD_4^+ , the best we can do is to estimate the magnitude of cross section which could be "hidden" in the observed background signal. Any peak cross section greater than approximately $1 \times 10^{-17} \text{ cm}^2$ should be visible, so this value is our estimated maximum, with zero being a likely value.

The cross section for dissociation to CD_3^+ was dominated by the false "apparent signal," which registers a cross section of 10^{-15} cm^2 at 9 eV interaction energy. The predicted cross section for this dissociation channel, with a peak value of $2 \times 10^{-16} \text{ cm}^2$, is not visible against this overwhelming background. The number of data points and the statistics were limited by considerations of time efficiency considering the high background count rate.

The cross sections for dissociation to C^+ , CD^+ , and CD_2^+ are all similar. Thresholds are in the 8 to 10 eV range and peak cross sections are approximately 27, 80, and $80 \times 10^{-18} \text{ cm}^2$, respectively. The apparent signal background was less important for the more complete dissociation products. One can imagine seeing two dissociation channels with different energy dependences in the cross sections for CD^+ and, less definitely, for C^+ . These energy dependences are reminiscent of those for dipole-allowed and non-dipole-allowed transitions in electron-impact excitation. Given this distinction, dissociation to CD_2^+ appears to be dominated by the process which falls off faster with increasing energy.

The data were reported at a meeting,³⁹ but have never been published in a refereed journal. The primary obstacles were lack of theoretical understanding and the complicating presence of the apparent signal background under the cross section being studied. A long-term commitment would have been required to become literate in the molecular dissociation research field, and other efforts had priority. Follow-up studies are under way at ORNL and in Japan which may lead to some use of this data.

IV. EXPLANATION OF TABLES AND FIGURES

The tables in the front of the publication provide keys to the available data. The first table shows all charge states up to 16+ of all elements up to Kr, along with heavier elements of interest here, indicating all ions for which electron-impact ionization cross sections have been measured by this research group through 1992 (although some of the data was published as late as 1994). A "1" or "2" indicates that data tables and plots are

found in references 1 or 2, the previous memos in this series. A "■" indicates that information is provided in this memo. Single, double, and triple ionization measurements are indicated on separate lines.

The second table again lists all reactions for which cross sections have been measured, listed by increasing target charge and increasing atomic number. Subsequent columns list the page numbers where data tables and figures can be found, and the publication reference number. For species found in the previous memos, "TM-7020" and/or "TM-9501" are noted in the final column.

Following this text, the reference list includes all data from all three reports. The target ions are listed at the end of each reference. Data tables follow the references, with headings adapted from the original publications. Figures follow the data tables, with captions again adapted from the publications on the page with the figure. References for the experimental data are included in each data table heading and figure caption. References for other experiments and theoretical calculations shown in the figures are given in the original publications.

V. ACKNOWLEDGMENTS

In addition to the numerous experimentalists who developed the apparatus and measured the cross sections, close collaborations with theoreticians were essential in the selection of targets and interpretation of results. Drs. Don Griffin, Mitch Pindzola, and Chris Bottcher were the most frequent and helpful theoretical collaborators. Jerry Hale and Fay Ownby provided technical and administrative support for all of these measurements. This research was supported by DOE's Office of Fusion Energy. One of us (MEB) acknowledges an appointment to the ORNL Postdoctoral Research Associates Program administered jointly by ORNL and Oak Ridge Associated Universities.

REFERENCES

[NOTE: Double ionization (\dagger), triple ionization (\ddagger), and molecular dissociation (*) are noted; all others are for single ionization.]

1. D. H. Crandall, R. A. Phaneuf, and D. C. Gregory, *Electron Impact Ionization of Multicharged Ions*, ORNL/TM-7020, Oak Ridge Natl. Lab., 1979. [B^{3+} , C^{4+} , N^{5+} , O^{3+} , Ar^{4+} , and published results]
2. D. C. Gregory, D. H. Crandall, R. A. Phaneuf, A. M. Howald, G. H. Dunn, R. A. Falk, D. W. Mueller, and T. J. Morgan, *Electron Impact Ionization of Multicharged Ions at ORNL: 1980 - 1984*, ORNL/TM-9501, Oak Ridge Natl. Lab., 1985. [C^{3+} , N^{2+} , N^{3+} , O^{2+} , Ar^{5+} , and published results]
3. D. H. Crandall, R. A. Phaneuf, D. C. Gregory, A. M. Howald, D. W. Mueller, T. J. Morgan, G. H. Dunn, D. C. Griffin, and R. J. W. Henry, Phys. Rev. A **34**, 1757 (1986). [B^{2+} , O^{5+}]
4. R. A. Falk, G. Stefani, R. Camilloni, G. H. Dunn, R. A. Phaneuf, D. C. Gregory, and D. H. Crandall, Phys. Rev. A **28**, 91 (1983). [C^{2+} , N^{3+} , O^{4+}]
5. D. H. Crandall, R. A. Phaneuf, B. E. Hasselquist, and D. C. Gregory, J. Phys. B **12**, L249 (1979). [C^{3+} , N^{4+} , O^{5+}]
6. R. A. Phaneuf, R. K. Janev, and M. S. Pindzola, *Atomic Data for Fusion, Volume 5: Collisions of Carbon and Oxygen Ions with Electrons, H, H₂, and He*, ORNL-6090, Oak Ridge Natl. Lab., Feb. 1987; original data collected by G. H. Dunn, R. A. Falk, and R. A. Phaneuf, unpublished (1980). [O^{2+}]
7. K. Rinn, D. C. Gregory, L. J. Wang, R. A. Phaneuf, and A. Müller, Phys. Rev. A **36**, 595 (1987). [O^{5+}]
8. D. W. Mueller, T. J. Morgan, G. H. Dunn, D. C. Gregory, and D. H. Crandall, Phys. Rev. A **31**, 2905 (1985). [F^{2+} , Cl^{2+} , Ar^{2+} , Ti^{2+} , Fe^{2+}]
9. D. C. Gregory, P. F. Dittner, and D. H. Crandall, Phys. Rev. A **27**, 724 (1983). [Ne^{3+} , Ar^{3+} , Kr^{3+} , Xe^{3+}]
10. D. H. Crandall, R. A. Phaneuf, R. A. Falk, D. S. Belić, and G. H. Dunn, Phys. Rev. A **25**, 143 (1982). [Al^{2+} , Si^{3+}]
11. N. Djurić, E. W. Bell, X. Q. Guo, G. H. Dunn, R. A. Phaneuf, M. E. Bannister, M. S. Pindzola, and D. C. Griffin, Phys. Rev. A **47**, 4786 (1993). [Si^+ , Si^{2+}]

12. J. S. Thompson and D. C. Gregory, Phys. Rev. A, to be published (August 1994). [Si⁴⁺, Si⁵⁺]
13. P. A. Zeijlmans van Emmichoven, M. E. Bannister, D. C. Gregory, C. C. Havener, R. A. Phaneuf, E. W. Bell, X. Q. Guo, J. S. Thompson, and M. Sataka, Phys. Rev. A **47**, 2888 (1993). [Si⁶⁺, Si⁷⁺]
14. A. M. Howald, D. C. Gregory, F. W. Meyer, R. A. Phaneuf, A. Müller, N. Djurić, and G. H. Dunn, Phys. Rev. A **33**, 3779 (1986). [S⁴⁺, Cl⁵⁺, Ar⁶⁺]
15. M. S. Pindzola, D. C. Griffin, C. Bottcher, D. H. Crandall, R. A. Phaneuf, and D. C. Gregory, Phys. Rev. A **29**, 1749 (1984). [Ar^{4+†}, Kr^{4+†}, Xe^{4+†}]
16. Y. Zhang, C. B. Reddy, R. S. Smith, D. E. Golden, D. W. Mueller, and D. C. Gregory, Phys. Rev. A **45**, 2929 (1992). [Ar⁷⁺]
17. Y. Zhang, C. B. Reddy, R. S. Smith, D. E. Golden, D. W. Mueller, and D. C. Gregory, Phys. Rev. A **44**, 4368 (1991). [Ar⁸⁺]
18. R. A. Falk, G. H. Dunn, D. C. Gregory, and D. H. Crandall, Phys. Rev. A **27**, 762 (1983). [Ti³⁺, Zr³⁺, Hf³⁺, Ta³⁺]
19. S. J. Chantrenne, D. C. Gregory, M. J. Buie, and M. S. Pindzola, Phys. Rev. A **41**, 140 (1990). [Ti⁵⁺]
20. D. C. Gregory, L. J. Wang, D. R. Swenson, M. Sataka, and S. J. Chantrenne, Phys. Rev. A **41**, 6512 (1990). [Ti¹¹⁺, Cr¹³⁺]
21. M. Sataka, S. Ohtani, D. Swenson, and D. C. Gregory, Phys. Rev. A **39**, 2397 (1989). [Cr⁶⁺, Cr⁷⁺, Cr⁸⁺, Cr¹⁰⁺]
22. D. C. Gregory, F. W. Meyer, A. Müller, and P. Defrance, Phys. Rev. A **34**, 3657 (1986). [Fe⁵⁺, Fe⁶⁺, Fe⁹⁺]
23. D. C. Gregory, L. J. Wang, F. W. Meyer, and K. Rinn, Phys. Rev. A **35**, 3256 (1987). [Fe¹¹⁺, Fe¹³⁺, Fe¹⁵⁺]
24. D. C. Gregory and A. M. Howald, Phys. Rev. A **34**, 97 (1986). [Ni³⁺, Cu²⁺, Cu³⁺, Sb³⁺]
25. L. J. Wang, K. Rinn, and D. C. Gregory, J. Phys. B **21**, 2117 (1988). [Ni⁵⁺, Ni⁶⁺, Ni⁷⁺, Ni⁸⁺, Ni¹²⁺, Ni¹⁴⁺]
26. D. C. Gregory, Nucl. Instrum. Methods Phys. Res. B **10/11**, 87 (1985). [Kr²⁺]

27. A. M. Howald, D. C. Gregory, N. Djurić, G. H. Dunn, and A. Müller, unpublished ORNL data (1985). [Kr⁴⁺]
28. D. C. Gregory and A. M. Howald, unpublished ORNL data (1985). [Kr⁷⁺]
29. M. E. Bannister, D. W. Mueller, L. J. Wang, M. S. Pindzola, D. C. Griffin, and D. C. Gregory, Phys. Rev. A **38**, 38 (1988). [Kr⁸⁺, Xe⁸⁺]
30. D. C. Gregory, K. Rinn, and L. J. Wang, unpublished ORNL data (1986). [Kr⁹⁺]
31. D. C. Griffin, C. Bottcher, M. S. Pindzola, S. M. Younger, D. C. Gregory, and D. H. Crandall, Phys. Rev. A **29**, 1729 (1984). [Xe²⁺, Xe⁴⁺, Xe⁵⁺]
32. D. C. Gregory and D. H. Crandall, Phys. Rev. A **27**, 2338 (1983). [Xe⁶⁺]
33. D. C. Gregory, K. Rinn, and L. J. Wang, unpublished ORNL data (1986). [Xe⁶⁺]
34. A. M. Howald, D. C. Gregory, R. A. Phaneuf, D. H. Crandall, and M. S. Pindzola, Phys. Rev. Lett. **56**, 1675 (1986). [Xe^{6+†}, Xe^{6+‡}]
35. D. W. Mueller, L. J. Wang, and D. C. Gregory, Phys. Rev. A **39**, 2381 (1989). [Xe^{8+†}]
36. D. C. Gregory and F. W. Meyer, unpublished ORNL data (1988). [Ta⁸⁺]
37. D. C. Gregory, M. S. Huq, F. W. Meyer, D. R. Swenson, M. Sataka, and S. Chantrenne, Phys. Rev. A **41**, 106 (1990). [U¹⁰⁺, U^{10+†}, U¹³⁺, U^{13+†}, U¹⁶⁺]
38. P. A. Schulz, D. C. Gregory, F. W. Meyer, and R. A. Phaneuf, J. Chem. Phys. **85**, 3386 (1986). [H₃O^{+*}, D₃O^{+*}]
39. D. C. Gregory, D. W. Mueller, and H. Tawara, unpublished ORNL data (1989); D. C. Gregory and H. Tawara, Abstracts of Contributed Papers, XVI ICPEAC, New York City (1989), p. 10. [CD₄^{+*}]
40. F. W. Meyer, Nucl. Instrum. Methods Phys. Res. B **9**, 532 (1985).
41. P. O. Taylor, K. T. Dolder, W. E. Kauppila, and G. H. Dunn, Rev. Sci. Instrum. **45**, 538 (1974).
42. T. W. Gorczyca, M. S. Pindzola, N. R. Badnell, and D. C. Griffin, Phys. Rev. A **49**, 4682 (1994).

DATA TABLES

Corrected experimental cross sections for electron-impact ionization of O⁵⁺. The relative uncertainties are one-standard-deviation counting statistics only. Corrections applied to these data to compensate for apparent spurious signal are explained in the reference. Total absolute uncertainty is $\pm 11\%$ at good confidence corresponding to 90% confidence level. Reference: D. H. Crandall *et al.*, Phys. Rev. A **34**, 1757 (1986).

Energy (eV)	σ (10^{-18} cm 2)	Energy (eV)	σ (10^{-18} cm 2)
97	0.005 ± 0.018	394	0.713 ± 0.014
137	-0.005 ± 0.018	443	0.752 ± 0.012
147	0.072 ± 0.018	493	0.741 ± 0.008
157	0.203 ± 0.049	519	0.723 ± 0.009
167	0.255 ± 0.027	543	0.719 ± 0.009
177	0.352 ± 0.028	568	0.756 ± 0.008
196	0.426 ± 0.018	593	0.759 ± 0.008
216	0.559 ± 0.026	618	0.764 ± 0.009
236	0.614 ± 0.026	693	0.717 ± 0.016
256	0.639 ± 0.026	793	0.707 ± 0.016
276	0.676 ± 0.029	892	0.642 ± 0.017
295	0.695 ± 0.012	995	0.634 ± 0.011
344	0.685 ± 0.013		

Electron-impact ionization cross sections for O⁵⁺. Uncertainties listed here are one-standard-deviation relative only; absolute uncertainty for a typical point near the peak cross section is $\pm 8\%$ at 90% confidence level. Reference: K. Rinn *et al.*, Phys. Rev. A 36, 595 (1987).

Energy (eV)	σ (10^{-18} cm 2)	Energy (eV)	σ (10^{-18} cm 2)
122.9	0.0008 \pm 0.0158	543.5	0.6963 \pm 0.0031
132.7	0.0440 \pm 0.0176	544.7	0.6999 \pm 0.0031
137.5	0.0073 \pm 0.0100	545.8	0.6996 \pm 0.0031
157.1	0.2224 \pm 0.0124	547.0	0.6958 \pm 0.0030
176.7	0.3650 \pm 0.0105	548.2	0.7020 \pm 0.0030
196.3	0.4529 \pm 0.0064	548.4	0.6985 \pm 0.0035
215.8	0.5194 \pm 0.0064	549.4	0.6967 \pm 0.0030
235.4	0.5861 \pm 0.0080	550.6	0.6998 \pm 0.0030
254.9	0.6405 \pm 0.0072	551.8	0.7025 \pm 0.0030
274.5	0.6468 \pm 0.0070	553.0	0.7057 \pm 0.0030
293.9	0.6806 \pm 0.0051	554.2	0.7158 \pm 0.0030
313.5	0.6856 \pm 0.0052	555.3	0.7200 \pm 0.0030
332.8	0.7004 \pm 0.0071	556.5	0.7258 \pm 0.0030
352.4	0.7004 \pm 0.0075	557.7	0.7359 \pm 0.0030
372.0	0.6946 \pm 0.0066	558.4	0.7314 \pm 0.0035
391.5	0.7035 \pm 0.0039	558.9	0.7411 \pm 0.0030
411.2	0.7106 \pm 0.0037	560.1	0.7398 \pm 0.0030
431.1	0.7036 \pm 0.0033	561.3	0.7460 \pm 0.0030
439.8	0.7039 \pm 0.0044	562.5	0.7412 \pm 0.0030
450.0	0.7086 \pm 0.0031	563.7	0.7404 \pm 0.0030
459.5	0.7029 \pm 0.0042	564.9	0.7401 \pm 0.0030
469.8	0.7107 \pm 0.0032	566.0	0.7458 \pm 0.0030
479.3	0.7025 \pm 0.0040	567.2	0.7510 \pm 0.0030
489.4	0.7168 \pm 0.0029	568.4	0.7522 \pm 0.0030
499.1	0.6992 \pm 0.0038	569.6	0.7554 \pm 0.0030
508.9	0.7037 \pm 0.0033	570.8	0.7571 \pm 0.0030
518.8	0.6981 \pm 0.0037	572.0	0.7588 \pm 0.0030
528.7	0.7032 \pm 0.0031	573.1	0.7625 \pm 0.0030
538.6	0.6942 \pm 0.0036	574.4	0.7592 \pm 0.0030
541.1	0.7009 \pm 0.0031	575.5	0.7603 \pm 0.0030
542.3	0.6994 \pm 0.0031		

Experimental electron-impact single-ionization cross sections for Si⁺. The total relative uncertainties listed are at 90% confidence level. Total systematic uncertainties are estimated to be $\pm 9\%$. Also included are data using Si⁺ formed by charge exchange of Si²⁺; this eliminated N₂⁺ impurity ions in the beam. Reference: N. Djurić *et al.* Phys. Rev. A **47**, 4786 (1993).

Energy (eV)	σ (10^{-18} cm 2)	Energy (eV)	σ (10^{-18} cm 2)
16.3	1.22 \pm 0.39	27.1	15.7 \pm 0.4
16.4	1.00 \pm 0.32	27.4	15.4 \pm 0.4
16.6	1.55 \pm 0.19	27.6	15.6 \pm 0.4
16.9	2.05 \pm 0.19	27.9	15.4 \pm 0.4
17.1	3.09 \pm 0.21	28.3	15.5 \pm 0.4
17.4	3.98 \pm 0.19	28.7	15.2 \pm 0.4
17.6	4.23 \pm 0.19	29.1	15.0 \pm 0.4
17.9	4.96 \pm 0.20	29.4	15.0 \pm 0.4
18.1	5.30 \pm 0.20	29.8	15.3 \pm 0.4
18.4	5.62 \pm 0.20	33.2	16.1 \pm 0.5
18.6	5.87 \pm 0.28	38.2	16.3 \pm 0.4
18.9	6.26 \pm 0.27	43.1	15.3 \pm 0.4
19.1	7.39 \pm 0.31	57.7	14.2 \pm 0.3
19.3	8.21 \pm 0.30	67.4	13.5 \pm 0.3
19.6	8.33 \pm 0.30	77.1	12.8 \pm 0.3
19.8	9.90 \pm 0.31	87.2	11.9 \pm 0.3
20.1	10.2 \pm 0.3	96.9	11.2 \pm 0.2
20.3	11.3 \pm 0.3	117.1	10.7 \pm 0.2
20.7	11.8 \pm 0.4	137.0	9.77 \pm 0.22
21.0	12.1 \pm 0.4	156.8	8.78 \pm 0.21
21.4	12.9 \pm 0.4	176.9	8.22 \pm 0.20
21.7	13.1 \pm 0.4	196.0	7.75 \pm 0.17
22.1	13.2 \pm 0.4	246.2	6.77 \pm 0.15
22.4	13.4 \pm 0.4	295.6	5.98 \pm 0.14
22.8	13.4 \pm 0.4	344.2	5.51 \pm 0.12
23.1	13.5 \pm 0.4	393.2	5.01 \pm 0.11
23.4	13.7 \pm 0.3	492.1	4.13 \pm 0.09
23.7	14.4 \pm 0.4	492.4	4.30 \pm 0.09
23.9	14.5 \pm 0.4	591.3	3.75 \pm 0.08
24.2	14.1 \pm 0.3	689.5	3.25 \pm 0.07
24.5	15.1 \pm 0.4	788.8	2.89 \pm 0.06
24.8	14.5 \pm 0.4	887.7	2.72 \pm 0.06
25.2	14.5 \pm 0.4	987.5	2.67 \pm 0.06
25.4	15.0 \pm 0.4		
25.7	14.7 \pm 0.4	38.1	17.6 \pm 1.1
25.9	14.7 \pm 0.4	98.3	12.3 \pm 0.6
26.2	15.3 \pm 0.4	245.5	7.23 \pm 0.30
26.6	15.2 \pm 0.4	491.8	4.27 \pm 0.12
26.9	15.3 \pm 0.4		

Si⁺ from charge transfer:

Experimental electron-impact single-ionization cross sections for Si²⁺. The total relative uncertainties listed are at 90% confidence level. Total systematic uncertainties are estimated to be $\pm 9\%$. Reference: N. Djurić *et al.* Phys. Rev. A **47**, 4786 (1993).

Energy (eV)	σ (10^{-18} cm 2)	Energy (eV)	σ (10^{-18} cm 2)
25.6	0.002 ± 0.17	137.8	2.07 ± 0.07
28.2	0.22 ± 0.12	146.0	1.89 ± 0.06
30.4	0.28 ± 0.12	157.4	1.92 ± 0.06
32.1	0.29 ± 0.15	170.2	1.87 ± 0.05
33.1	0.42 ± 0.14	177.2	1.88 ± 0.05
34.0	0.45 ± 0.15	195.8	1.75 ± 0.04
38.0	1.08 ± 0.13	245.6	1.67 ± 0.04
47.7	1.75 ± 0.09	296.1	1.51 ± 0.03
57.8	1.81 ± 0.11	346.7	1.36 ± 0.03
67.7	1.89 ± 0.08	395.2	1.26 ± 0.03
77.5	1.94 ± 0.07	446.8	1.20 ± 0.03
87.2	1.97 ± 0.06	494.5	1.18 ± 0.03
97.1	1.85 ± 0.05	594.8	1.07 ± 0.02
106.9	1.82 ± 0.05	693.5	0.96 ± 0.02
116.6	1.94 ± 0.06	723.0	0.92 ± 0.02
118.0	2.16 ± 0.07	893.6	0.91 ± 0.02
126.4	1.98 ± 0.05	992.6	0.89 ± 0.02

Experimental electron-impact single-ionization cross sections for Si⁴⁺. Relative uncertainties listed are at the two-standard-deviation level. The absolute uncertainties at a 90% confidence level are listed in parentheses. Reference: J. S. Thompson and D. C. Gregory, Phys. Rev. A, to be published (August 1994).

Energy (eV)	σ (10^{-18} cm 2)	Energy (eV)	σ (10^{-18} cm 2)
33.4	-0.002 ± 0.044 (0.044)	337	4.491 ± 0.026 (0.319)
46.5	0.043 ± 0.028 (0.028)	385	4.62 ± 0.16 (0.36)
48.4	0.034 ± 0.040 (0.040)	434	4.929 ± 0.042 (0.351)
60.8	0.043 ± 0.036 (0.036)	483	5.081 ± 0.034 (0.361)
72.4	0.151 ± 0.030 (0.032)	532	5.270 ± 0.050 (0.376)
84.6	0.240 ± 0.026 (0.031)	581	5.349 ± 0.102 (0.392)
96.0	0.276 ± 0.026 (0.032)	639	5.316 ± 0.016 (0.376)
97.4	0.282 ± 0.028 (0.034)	688	5.07 ± 0.30 (0.47)
121	0.474 ± 0.028 (0.044)	738	5.01 ± 0.04 (0.36)
146	0.681 ± 0.032 (0.057)	788	4.82 ± 0.06 (0.35)
169	0.847 ± 0.030 (0.067)	836	4.78 ± 0.04 (0.34)
181	1.344 ± 0.022 (0.098)	886	4.77 ± 0.02 (0.34)
194	1.892 ± 0.022 (0.136)	936	4.68 ± 0.04 (0.33)
206	2.289 ± 0.024 (0.163)	986	4.85 ± 0.16 (0.38)
218	2.634 ± 0.034 (0.190)	1085	4.62 ± 0.04 (0.33)
242	3.242 ± 0.028 (0.231)	1181	4.52 ± 0.10 (0.33)
266	3.718 ± 0.028 (0.264)	1330	4.62 ± 0.20 (0.38)
290	4.043 ± 0.024 (0.287)	1487	4.14 ± 0.14 (0.32)

Experimental electron-impact single-ionization cross sections for Si⁵⁺. Relative uncertainties listed are at the two-standard-deviation level. The absolute uncertainties (listed in parentheses) are reported at a 90% confidence level. J. S. Thompson and D. C. Gregory, Phys. Rev. A, to be published (August 1994).

Energy (eV)	σ (10^{-18} cm 2)	Energy (eV)	σ (10^{-18} cm 2)
196	0.010 ± 0.060 (0.060)	573	3.136 ± 0.040 (0.225)
208	0.093 ± 0.044 (0.044)	588	3.03 ± 0.22 (0.31)
220	0.510 ± 0.052 (0.063)	635	3.136 ± 0.030 (0.224)
231	0.841 ± 0.036 (0.070)	683	3.121 ± 0.034 (0.223)
243	1.108 ± 0.040 (0.088)	733	3.069 ± 0.020 (0.218)
268	1.483 ± 0.038 (0.112)	783	3.036 ± 0.016 (0.215)
293	1.816 ± 0.028 (0.131)	831	3.068 ± 0.026 (0.218)
317	2.042 ± 0.034 (0.148)	887	2.879 ± 0.036 (0.207)
341	2.288 ± 0.032 (0.165)	936	2.870 ± 0.028 (0.205)
365	2.421 ± 0.038 (0.175)	987	2.804 ± 0.036 (0.202)
390	2.566 ± 0.030 (0.184)	1085	2.726 ± 0.036 (0.196)
415	2.687 ± 0.036 (0.193)	1185	2.69 ± 0.22 (0.291)
440	2.804 ± 0.042 (0.202)	1284	2.515 ± 0.030 (0.180)
463	2.861 ± 0.024 (0.204)	1382	2.56 ± 0.13 (0.22)
487	2.95 ± 0.16 (0.26)	1481	2.52 ± 0.10 (0.20)

Electron-impact single ionization cross sections for Si⁶⁺. Uncertainties are one-standard-deviation relative only; absolute uncertainties are $\pm 9\%$ at the two standard deviation level. Reference: P. A. Zeijlmans van Emmichoven *et al.*, Phys. Rev. A 47, 2888 (1993).

Energy (eV)	σ (10^{-18} cm^2)	Energy (eV)	σ (10^{-18} cm^2)
196	0.056 ± 0.064	440	1.546 ± 0.037
220	0.061 ± 0.058	463	1.662 ± 0.073
245	0.106 ± 0.060	491	1.601 ± 0.067
254	0.202 ± 0.067	516	1.580 ± 0.064
269	0.382 ± 0.047	536	1.656 ± 0.048
279	0.564 ± 0.068	566	1.680 ± 0.066
294	0.685 ± 0.034	588	1.811 ± 0.043
317	0.909 ± 0.073	638	1.802 ± 0.046
342	1.047 ± 0.029	687	1.779 ± 0.064
365	1.206 ± 0.054	735	1.809 ± 0.051
373	1.123 ± 0.094	784	1.750 ± 0.054
382	1.080 ± 0.093	987	1.745 ± 0.084
391	1.271 ± 0.041	1085	1.652 ± 0.078
402	1.410 ± 0.091	1183	1.670 ± 0.078
411	1.359 ± 0.090	1403	1.626 ± 0.076
421	1.354 ± 0.089		

Electron-impact single ionization cross sections for Si⁷⁺. Uncertainties are one-standard-deviation relative only; absolute uncertainties range from 9% to 12% for the peak cross section at the two-standard-deviation level. Reference: P. A. Zeijlmans van Emmichoven *et al.*, Phys. Rev. A 47, 2888 (1993).

Energy (eV)	σ (10^{-18} cm^2)	Energy (eV)	σ (10^{-18} cm^2)
200	0.019 ± 0.072	494	0.756 ± 0.059
249	-0.009 ± 0.115	519	0.781 ± 0.067
298	0.004 ± 0.047	544	0.826 ± 0.041
323	0.127 ± 0.046	593	0.860 ± 0.067
347	0.298 ± 0.033	642	0.877 ± 0.040
372	0.355 ± 0.044	740	0.917 ± 0.055
386	0.397 ± 0.065	789	0.878 ± 0.069
396	0.500 ± 0.036	888	0.952 ± 0.056
421	0.552 ± 0.045	986	0.890 ± 0.064
445	0.662 ± 0.040	1182	0.821 ± 0.057
470	0.642 ± 0.037	1363	0.812 ± 0.056

Electron-impact ionization cross sections for S⁴⁺. Uncertainties are one standard deviation on counting statistics. Total uncertainties are $\pm 9\%$ at 90% confidence level for a typical point near the peak cross section. Reference: A. M. Howald *et al.*, Phys. Rev. A **33**, 3779 (1986).

Energy (eV)	σ (10^{-18} cm 2)	Energy (eV)	σ (10^{-18} cm 2)
37.3	0.12 \pm 0.17	186	6.17 \pm 0.14
47.2	0.25 \pm 0.14	191	6.27 \pm 0.08
57.1	0.20 \pm 0.11	194	6.24 \pm 0.07
61.2	0.18 \pm 0.14	198	6.74 \pm 0.07
64.2	0.28 \pm 0.15	200	6.57 \pm 0.14
67.0	0.56 \pm 0.16	203	6.62 \pm 0.14
69.9	0.80 \pm 0.15	206	6.75 \pm 0.14
72.0	1.14 \pm 0.18	209	6.73 \pm 0.14
74.0	1.23 \pm 0.12	216	6.98 \pm 0.09
76.8	1.37 \pm 0.11	236	7.21 \pm 0.09
79.0	1.84 \pm 0.16	256	7.30 \pm 0.09
81.9	2.19 \pm 0.17	265	7.10 \pm 0.09
83.1	2.03 \pm 0.15	275	6.89 \pm 0.07
86.9	2.46 \pm 0.11	285	6.93 \pm 0.09
91.7	2.92 \pm 0.15	292	6.94 \pm 0.07
102.4	3.59 \pm 0.13	317	6.74 \pm 0.09
112.3	3.75 \pm 0.13	341	6.57 \pm 0.09
122.9	4.48 \pm 0.13	367	6.44 \pm 0.09
127	4.48 \pm 0.13	391	6.31 \pm 0.09
127	4.33 \pm 0.13	440	6.26 \pm 0.09
137	4.47 \pm 0.13	490	6.29 \pm 0.07
142	4.35 \pm 0.10	539	6.16 \pm 0.18
147	4.93 \pm 0.12	589	5.76 \pm 0.09
152	4.75 \pm 0.10	638	5.72 \pm 0.09
157	4.66 \pm 0.13	689	5.56 \pm 0.06
162	4.83 \pm 0.13	839	4.97 \pm 0.07
167	4.95 \pm 0.13	992	4.40 \pm 0.07
171	5.31 \pm 0.13	1195	3.97 \pm 0.07
177	5.44 \pm 0.13	1392	3.68 \pm 0.07
181	5.92 \pm 0.13		

Electron-impact single ionization cross sections for Cl³⁺. The listed uncertainties are relative only, while the absolute uncertainty for a typical point near the peak cross section is $\pm 10\%$ at 90% confidence level. Reference: A. M. Howald *et al.*, Phys. Rev. A **33**, 3779 (1986).

Energy (eV)	σ (10^{-18} cm 2)	Energy (eV)	σ (10^{-18} cm 2)
66.5	0.10 ± 0.19	235	3.96 ± 0.08
76.4	0.02 ± 0.27	250	4.43 ± 0.07
86.9	0.04 ± 0.15	255	4.55 ± 0.08
96.5	0.34 ± 0.14	275	4.70 ± 0.09
107.4	0.65 ± 0.13	294	4.95 ± 0.05
116.7	0.85 ± 0.17	306	4.83 ± 0.05
126.9	1.26 ± 0.13	319	4.62 ± 0.05
136.4	1.67 ± 0.14	344	4.72 ± 0.05
147.2	1.83 ± 0.13	368	4.47 ± 0.15
156.1	1.92 ± 0.13	393	4.60 ± 0.05
176	2.34 ± 0.11	441	4.59 ± 0.09
186	2.37 ± 0.11	491	4.50 ± 0.05
195	2.48 ± 0.08	540	4.46 ± 0.09
202	2.93 ± 0.10	591	4.25 ± 0.05
210	2.99 ± 0.09	690	4.03 ± 0.05
211	3.30 ± 0.09	840	3.71 ± 0.05
214	3.82 ± 0.09	992	3.54 ± 0.05
215	3.72 ± 0.07	1193	3.25 ± 0.05
220	3.51 ± 0.09	1393	3.05 ± 0.05
225	3.82 ± 0.07		

Electron-impact ionization cross sections for Ar⁶⁺. Uncertainties are typical relative uncertainties, which combine one standard deviation on counting statistics with uncertainties in the form factor. Total uncertainty for a typical point near the peak cross section is $\pm 8\%$ at 90% confidence level. Reference: A. M. Howald *et al.*, Phys. Rev. A **33**, 3779 (1986).

Energy (eV)	σ (10^{-18} cm 2)	Energy (eV)	σ (10^{-18} cm 2)
36.5	0.00	270	2.81
56.5	-0.02 \pm 0.05	275	2.98
76.5	0.01	295	3.24
96.5	0.04	320	3.47 \pm 0.07
107	0.08	345	3.58
117	0.08 \pm 0.05	370	3.70
126	0.32	395	3.68
137	0.66	445	3.62
147	0.92	495	3.57 \pm 0.05
156	1.05	543	3.47
166	1.19 \pm 0.07	593	3.38
176	1.34	642	3.27
186	1.48	693	3.20
196	1.51	793	2.96 \pm 0.05
216	1.67	893	2.80
236	1.86 \pm 0.07	996	2.69
241	1.94	1100	2.58
246	2.09	1202	2.52
251	2.14	1298	2.45 \pm 0.05
255	2.30	1398	2.41
260	2.53	1503	2.34
265	2.77		

Cross sections for electron impact ionization of Ar⁷⁺, with relative uncertainties. The absolute uncertainty is $\pm 12\%$ for the measured data and $\pm 20\%$ for the corrected data* at the two-standard-deviation level for a typical point near the peak cross section. Reference: Y. Zhang *et al.*, Phys. Rev. A 45, 2929 (1992).

Electron energy (eV)	Ionization cross sections σ (10^{-18} cm 2)	
	Measured data	Corrected data*
18.1	26.63 ± 4.34	-2.29 ± 8.21
28.8	18.15 ± 2.41	1.30 ± 4.73
48.0	11.24 ± 1.41	2.25 ± 2.87
73.8	4.23 ± 0.67	-0.83 ± 1.88
97.2	0.81 ± 0.44	-0.58 ± 1.49
122.3	2.91 ± 0.40	0.56 ± 1.27
170.2	3.11 ± 0.69	1.82 ± 1.18
195.0	1.83 ± 0.14	0.87 ± 0.89
243.0	1.56 ± 0.21	1.02 ± 0.80
267.1	1.76 ± 0.26	1.37 ± 0.77
291.8	1.83 ± 0.29	1.56 ± 0.75
364.3	3.19 ± 0.23	3.16 ± 0.64
390.0	3.28 ± 0.29	3.31 ± 0.65
413.0	3.45 ± 0.20	3.53 ± 0.59
440.0	2.99 ± 0.26	3.12 ± 0.60
489.0	3.21 ± 0.24	3.40 ± 0.56
538.0	3.09 ± 0.36	3.33 ± 0.60
561.0	3.51 ± 0.22	3.78 ± 0.52
586.9	3.04 ± 0.08	3.32 ± 0.46
593.6	2.91 ± 0.13	3.20 ± 0.47
643.5	2.77 ± 0.23	3.10 ± 0.49
692.7	2.88 ± 0.18	3.22 ± 0.45
742.3	2.76 ± 0.17	3.13 ± 0.43
792.1	2.94 ± 0.16	3.32 ± 0.42
840.0	3.07 ± 0.27	3.46 ± 0.46
890.0	2.85 ± 0.23	3.25 ± 0.43
988.0	2.56 ± 0.23	2.99 ± 0.41
1087.0	2.31 ± 0.22	2.75 ± 0.39
1186.0	2.20 ± 0.22	2.64 ± 0.38

*The data have been corrected for below-threshold apparent signal which is assumed to be due to a combination of spurious space charge effects and excitation autoionization from highly metastable ions.

Ionization cross section data for Ar⁸⁺: The second column lists the measured data with their absolute uncertainties. The third column gives data reduced by $0.30/\sqrt{E}$ (where E is in eV). Absolute uncertainties in the third column include the contribution from the uncertainties due to correction for space-charge modulation. The absolute uncertainties listed are at the one-standard-deviation level. Reference: Y. Zhang *et al.*, Phys. Rev. A **44**, 4368 (1991).

Energy (eV)	Ionization cross sections (10^{-18} cm^2)	
	Measured data	Data after the correction for space-charge modulation
50.0	0.053 ± 0.018	0.006 ± 0.019
70.3	0.052 ± 0.028	0.012 ± 0.028
74.5	0.039 ± 0.019	0.001 ± 0.019
98.4	0.034 ± 0.002	0.001 ± 0.003
121.1	0.011 ± 0.015	-0.019 ± 0.015
145.1	0.014 ± 0.013	-0.014 ± 0.013
148.1	0.024 ± 0.012	-0.003 ± 0.012
169.1	0.036 ± 0.011	0.010 ± 0.011
193.0	0.035 ± 0.016	0.011 ± 0.017
196.8	0.034 ± 0.011	0.010 ± 0.011
200.0	0.006 ± 0.012	-0.017 ± 0.012
210.8	0.033 ± 0.010	0.010 ± 0.010
221.0	0.050 ± 0.014	0.028 ± 0.014
235.0	0.028 ± 0.012	0.006 ± 0.012
241.0	0.026 ± 0.008	0.004 ± 0.008
245.6	0.046 ± 0.003	0.024 ± 0.003
258.1	0.022 ± 0.001	0.001 ± 0.011
264.9	0.018 ± 0.008	-0.003 ± 0.008
268.3	0.018 ± 0.007	-0.002 ± 0.008
281.8	0.040 ± 0.009	0.020 ± 0.009
289.0	0.041 ± 0.008	0.022 ± 0.008
294.0	0.065 ± 0.004	0.045 ± 0.004
304.5	0.050 ± 0.008	0.031 ± 0.008
313.1	0.052 ± 0.007	0.033 ± 0.007
328.0	0.064 ± 0.008	0.045 ± 0.008
342.3	0.088 ± 0.010	0.070 ± 0.010
351.9	0.068 ± 0.007	0.051 ± 0.007
374.9	0.082 ± 0.006	0.065 ± 0.006
385.6	0.073 ± 0.005	0.056 ± 0.005
391.8	0.089 ± 0.005	0.072 ± 0.005
407.3	0.092 ± 0.010	0.075 ± 0.010
421.6	0.110 ± 0.011	0.094 ± 0.011
441.0	0.174 ± 0.010	0.159 ± 0.011

(Continued)

Ionization cross sections (10^{-18} cm^2)

Energy (eV)	Measured data	Data after the correction for space-charge modulation
445.2	0.218 ± 0.016	0.203 ± 0.016
489.0	0.374 ± 0.024	0.359 ± 0.024
492.0	0.354 ± 0.024	0.339 ± 0.024
538.0	0.514 ± 0.032	0.500 ± 0.032
542.0	0.481 ± 0.033	0.466 ± 0.034
588.0	0.597 ± 0.037	0.584 ± 0.037
591.3	0.615 ± 0.038	0.602 ± 0.038

Experimental cross sections for ionization of Ti⁵⁺. Relative uncertainties are quoted at the statistical one-standard-deviation level or equivalent. The absolute uncertainty for a typical point near the peak cross section is $\pm 7\%$ at good confidence level (two standard deviations). Reference: S. Chanrenne *et al.*, Phys. Rev. A **41**, 140 (1990).

Energy (eV)	σ (10^{-18} cm 2)	Energy (eV)	σ (10^{-18} cm 2)
75.9	-0.68 ± 0.071	405.0	7.41 ± 0.08
80.7	0.10 ± 0.08	420.0	7.20 ± 0.08
86.0	0.288 ± 0.063	441.2	7.24 ± 0.03
95.6	0.80 ± 0.08	460.1	7.60 ± 0.09
105.7	1.04 ± 0.07	479.5	7.37 ± 0.09
115.3	1.38 ± 0.07	489.9	7.39 ± 0.02
125.0	2.26 ± 0.07	499.5	7.58 ± 0.09
135.1	3.61 ± 0.07	519.0	7.60 ± 0.08
144.7	4.51 ± 0.07	539.0	7.28 ± 0.04
154.9	5.05 ± 0.08	588.0	7.04 ± 0.05
164.3	5.51 ± 0.06	637.2	6.96 ± 0.04
174.4	5.79 ± 0.06	687.0	6.63 ± 0.02
184.0	6.05 ± 0.06	736.3	6.48 ± 0.03
194.3	6.39 ± 0.06	785.3	6.32 ± 0.03
214.1	6.84 ± 0.09	834.0	6.19 ± 0.03
233.9	7.20 ± 0.08	884.0	6.06 ± 0.03
253.0	7.34 ± 0.08	984.0	5.99 ± 0.02
272.9	7.51 ± 0.06	1082.0	5.58 ± 0.07
292.9	7.36 ± 0.03	1179.0	5.29 ± 0.07
317.5	7.28 ± 0.05	1273.0	4.94 ± 0.05
342.7	7.29 ± 0.04	1372.0	4.89 ± 0.09
367.3	7.20 ± 0.04	1467	4.57 ± 0.07
391.8	7.09 ± 0.04		

Cross-section measurements for electron-impact ionization of Ti¹¹⁺. The uncertainties listed are relative at the equivalent of one standard deviation for statistics; absolute uncertainties are dominated by the statistics. Reference: D. C. Gregory *et al.*, Phys. Rev. A **41**, 6512 (1990).

Energy (eV)	σ (10^{-18} cm 2)	Energy (eV)	σ (10^{-18} cm 2)
292	-0.022 ± 0.067	569	0.684 ± 0.025
341	-0.009 ± 0.072	578	0.817 ± 0.058
391	0.154 ± 0.056	589	0.824 ± 0.038
440	0.067 ± 0.043	599	0.897 ± 0.046
490	0.365 ± 0.082	608	0.813 ± 0.032
539	0.811 ± 0.034	624	0.812 ± 0.049
549	0.696 ± 0.027	639	0.780 ± 0.028
554	0.802 ± 0.038	688	0.711 ± 0.038
559	0.834 ± 0.028	738	0.740 ± 0.037
564	0.851 ± 0.035	788	0.785 ± 0.021

Electron-impact single ionization cross sections for Cr⁶⁺. Uncertainties are typical relative uncertainties, which combine one standard deviation on counting statistics with uncertainties in the form factor. Total uncertainty for a typical point near the peak cross section is $\pm 8\%$ to 10% at 90% confidence level. Reference: M. Sataka *et al.*, Phys. Rev. A **39**, 2397 (1989).

Energy (eV)	σ (10^{-18} cm 2)	Energy (eV)	σ (10^{-18} cm 2)
55.0	0.07 ± 0.10	217	5.59 ± 0.05
65.0	0.11 ± 0.16	242	5.97 ± 0.06
75.1	0.20 ± 0.12	267	6.14 ± 0.05
85.0	0.05 ± 0.08	291	6.49 ± 0.03
94.2	0.11 ± 0.08	316	6.63 ± 0.04
104.3	0.10 ± 0.06	341	6.42 ± 0.07
114.2	0.18 ± 0.08	366	6.60 ± 0.03
116.5	0.31 ± 0.08	391	6.68 ± 0.03
118.2	0.50 ± 0.08	415	6.61 ± 0.04
118.8	0.84 ± 0.09	440	6.34 ± 0.05
120.4	0.88 ± 0.08	465	6.44 ± 0.04
122.0	1.17 ± 0.08	489	6.43 ± 0.07
124.5	1.55 ± 0.05	514	6.37 ± 0.04
125.9	1.71 ± 0.08	539	6.40 ± 0.05
128.3	1.84 ± 0.08	564	6.45 ± 0.04
129.0	1.81 ± 0.08	589	6.54 ± 0.04
129.9	1.93 ± 0.08	637	6.37 ± 0.04
132.1	2.05 ± 0.08	687	6.45 ± 0.03
134.2	2.54 ± 0.08	736	6.29 ± 0.03
139.0	2.81 ± 0.08	785	6.05 ± 0.02
143.6	2.80 ± 0.05	883	6.11 ± 0.04
148.9	3.20 ± 0.08	931	5.75 ± 0.04
153.7	3.22 ± 0.04	982	5.55 ± 0.04
163.4	3.60 ± 0.04	1080	5.26 ± 0.04
168.1	3.73 ± 0.04	1173	4.80 ± 0.04
173.6	4.18 ± 0.04	1267	4.60 ± 0.03
178.2	4.77 ± 0.04	1363	4.39 ± 0.04
192.8	4.96 ± 0.03	1460	4.17 ± 0.02

Electron-impact single ionization cross sections for Cr⁷⁺. Uncertainties are typical relative uncertainties, which combine one standard deviation on counting statistics with uncertainties in the form factor. Total uncertainty for a typical point near the peak cross section is $\pm 8\%$ to 10% at 90% confidence level. Reference: M. Sataka *et al.*, Phys. Rev. A **39**, 2397 (1989).

Energy (eV)	σ (10^{-18} cm 2)	Energy (eV)	σ (10^{-18} cm 2)
118.9	0.01 ± 0.05	292	3.05 ± 0.05
124.5	0.00 ± 0.07	312	3.27 ± 0.04
134.5	0.03 ± 0.08	331	3.32 ± 0.04
143.7	0.11 ± 0.08	341	3.33 ± 0.04
153.8	0.28 ± 0.06	351	3.31 ± 0.04
163.7	0.53 ± 0.05	371	3.45 ± 0.04
173.9	0.51 ± 0.05	391	3.45 ± 0.01
183.0	0.58 ± 0.04	440	3.53 ± 0.03
185.5	0.70 ± 0.05	489	3.57 ± 0.03
187.8	0.79 ± 0.04	539	3.55 ± 0.03
189.3	0.78 ± 0.06	589	3.65 ± 0.04
191.7	1.05 ± 0.05	639	3.74 ± 0.03
193.1	0.98 ± 0.08	686	3.74 ± 0.01
195.3	1.24 ± 0.04	737	3.75 ± 0.02
197.1	1.28 ± 0.05	786	3.69 ± 0.02
199.2	1.37 ± 0.05	833	3.72 ± 0.03
200.8	1.34 ± 0.05	883	3.59 ± 0.03
202.9	1.53 ± 0.04	932	3.64 ± 0.03
213	1.80 ± 0.04	983	3.51 ± 0.02
223	2.19 ± 0.05	1081	3.27 ± 0.02
232	2.40 ± 0.04	1171	3.08 ± 0.03
242	2.46 ± 0.06	1275	2.81 ± 0.02
252	2.61 ± 0.05	1370	2.71 ± 0.02
272	2.89 ± 0.04	1465	2.67 ± 0.02

Electron-impact single ionization cross sections for Cr⁸⁺. Uncertainties are typical relative uncertainties, which combine one standard deviation on counting statistics with uncertainties in the form factor. Total uncertainties for a typical point near the peak cross section is $\pm 8\%$ to 10% at 90% confidence level. Reference: M. Sataka *et al.*, Phys. Rev. A **39**, 2397 (1989).

Energy (eV)	σ (10^{-18} cm 2)	Energy (eV)	σ (10^{-18} cm 2)
154.0	0.06 \pm 0.11	391	2.10 \pm 0.06
164.0	0.17 \pm 0.10	415	2.03 \pm 0.08
174.1	0.05 \pm 0.10	440	2.08 \pm 0.07
183.2	0.20 \pm 0.09	465	2.23 \pm 0.07
193.3	0.26 \pm 0.09	489	2.15 \pm 0.06
203.1	0.22 \pm 0.12	539	2.28 \pm 0.07
213	0.31 \pm 0.08	589	2.49 \pm 0.01
215	0.45 \pm 0.07	638	2.45 \pm 0.05
218	0.43 \pm 0.08	688	2.40 \pm 0.05
220	0.68 \pm 0.07	738	2.53 \pm 0.05
223	0.84 \pm 0.06	786	2.53 \pm 0.04
233	0.86 \pm 0.06	834	2.51 \pm 0.04
243	1.05 \pm 0.07	883	2.48 \pm 0.04
253	1.28 \pm 0.07	932	2.40 \pm 0.03
263	1.36 \pm 0.07	983	2.42 \pm 0.04
273	1.48 \pm 0.06	1032	2.39 \pm 0.04
282	1.60 \pm 0.07	1081	2.31 \pm 0.04
292	1.68 \pm 0.07	1175	2.14 \pm 0.04
312	1.78 \pm 0.08	1271	2.01 \pm 0.04
331	1.85 \pm 0.07	1369	1.95 \pm 0.04
351	1.84 \pm 0.08	1489	1.92 \pm 0.04
371	2.01 \pm 0.08		

Electron-impact single ionization cross sections for Cr¹⁰⁺. Uncertainties are typical relative uncertainties, which combine one standard deviation on counting statistics with uncertainties in the form factor. Total uncertainty for a typical point near the peak cross section is $\pm 8\%$ to 10% at 90% confidence level. Reference: M. Sataka *et al.*, Phys. Rev. A **39**, 2397 (1989).

Energy (eV)	σ (10^{-18} cm 2)	Energy (eV)	σ (10^{-18} cm 2)
242	-0.06 ± 0.08	588	1.03 ± 0.05
252	-0.01 ± 0.07	613	1.11 ± 0.05
262	-0.04 ± 0.07	638	1.18 ± 0.04
272	0.13 ± 0.09	663	1.19 ± 0.04
282	0.41 ± 0.13	686	1.22 ± 0.05
292	0.29 ± 0.11	736	1.24 ± 0.04
312	0.36 ± 0.09	786	1.29 ± 0.03
331	0.52 ± 0.09	833	1.23 ± 0.04
351	0.50 ± 0.08	882	1.32 ± 0.04
371	0.70 ± 0.08	932	1.22 ± 0.04
390	0.71 ± 0.06	982	1.25 ± 0.03
415	0.62 ± 0.07	1032	1.14 ± 0.05
440	0.72 ± 0.09	1078	1.17 ± 0.03
465	0.71 ± 0.07	1174	1.10 ± 0.07
489	0.84 ± 0.05	1269	1.09 ± 0.06
514	0.80 ± 0.06	1364	0.97 ± 0.05
539	0.83 ± 0.05	1461	0.90 ± 0.05
564	0.96 ± 0.05		

Cross-section measurements for electron-impact ionization of Cr¹³⁺. The uncertainties listed are relative at the equivalent of one standard deviation for statistics; absolute uncertainties are dominated by the statistics. Reference: D.C. Gregory *et al.*, Phys. Rev. A **41**, 6512 (1990).

Energy (eV)	σ (10^{-18} cm 2)	Energy (eV)	σ (10^{-18} cm 2)
490	0.024 ± 0.034	885	0.449 ± 0.043
539	0.129 ± 0.036	931	0.379 ± 0.033
686	0.371 ± 0.050	1028	0.387 ± 0.032
720	0.373 ± 0.032	1225	0.481 ± 0.048
835	0.369 ± 0.035	1480	0.422 ± 0.038

Experimental electron-impact ionization cross sections for Fe⁵⁺. Uncertainties here are one-standard-deviation relative only. Absolute uncertainty for a typical point near the peak cross section is $\pm 8\%$ at 90% confidence level. Reference: D.C. Gregory *et al.*, Phys. Rev. A **34**, 3657 (1986).

Energy (eV)	σ (10^{-18} cm 2)	Energy (eV)	σ (10^{-18} cm 2)
81.5	0.04 ± 0.12	216	14.17 ± 0.13
91.3	-0.03 ± 0.11	235	15.02 ± 0.14
97.0	0.60 ± 0.10	255	15.21 ± 0.13
99.8	1.58 ± 0.13	275	15.56 ± 0.12
101.9	2.75 ± 0.19	292	15.40 ± 0.23
106.8	4.57 ± 0.17	317	15.48 ± 0.06
111.8	5.84 ± 0.16	342	15.26 ± 0.10
114.7	6.61 ± 0.16	366	14.90 ± 0.08
116.9	7.07 ± 0.15	391	14.62 ± 0.05
118.7	7.30 ± 0.15	415	14.51 ± 0.04
120.6	7.48 ± 0.15	465	14.26 ± 0.06
122	7.79 ± 0.28	490	14.18 ± 0.05
126	8.74 ± 0.29	539	13.91 ± 0.04
132	9.74 ± 0.15	588	13.69 ± 0.03
136	10.41 ± 0.26	638	13.23 ± 0.06
141	11.13 ± 0.13	688	13.05 ± 0.05
146	11.45 ± 0.11	787	12.19 ± 0.02
151	12.01 ± 0.16	885	11.29 ± 0.06
156	12.43 ± 0.12	988	10.72 ± 0.03
166	12.92 ± 0.10	1236	9.11 ± 0.07
176	13.32 ± 0.11	1484	8.37 ± 0.07
196	14.07 ± 0.06		

Experimental electron-impact ionization cross sections for Fe⁶⁺. Uncertainties here are one-standard-deviation relative only. Absolute uncertainty for a typical point near the peak cross section is $\pm 8\%$ at 90% confidence level. Reference: D.C. Gregory *et al.*, Phys. Rev. A **34**, 3657 (1986).

Energy (eV)	σ (10^{-18} cm 2)	Energy (eV)	σ (10^{-18} cm 2)
96.6	0.06 ± 0.23	255	9.03 ± 0.09
106.2	-0.14 ± 0.23	275	9.29 ± 0.09
111.3	-0.17 ± 0.24	295	9.50 ± 0.05
116.5	0.13 ± 0.17	317	9.57 ± 0.21
121.2	-0.05 ± 0.21	342	9.69 ± 0.15
126	0.52 ± 0.19	367	9.39 ± 0.15
131	1.96 ± 0.30	391	9.45 ± 0.10
136	2.61 ± 0.15	441	9.30 ± 0.13
141	4.10 ± 0.19	490	9.10 ± 0.10
146	4.46 ± 0.15	540	9.01 ± 0.07
151	5.62 ± 0.18	589	9.03 ± 0.06
155	5.65 ± 0.27	638	9.02 ± 0.06
166	6.20 ± 0.36	689	8.85 ± 0.06
176	7.08 ± 0.26	788	8.16 ± 0.07
186	7.53 ± 0.28	888	7.79 ± 0.05
195	7.70 ± 0.08	990	7.28 ± 0.04
215	8.34 ± 0.09	1236	6.69 ± 0.08
235	8.76 ± 0.09	1485	5.85 ± 0.05
245	9.10 ± 0.16		

Experimental electron-impact ionization cross sections for Fe⁹⁺. Uncertainties here are one-standard-deviation relative only. Absolute uncertainty for a typical point near the peak cross section is $\pm 8\%$ at 90% confidence level. Reference: D.C. Gregory *et al.*, Phys. Rev. A **34**, 3657 (1986).

Energy (eV)	σ (10^{-18} cm 2)	Energy (eV)	σ (10^{-18} cm 2)
145	0.09 ± 0.07	565	2.03 ± 0.07
170	-0.02 ± 0.09	589	1.99 ± 0.04
182	0.19 ± 0.11	639	2.04 ± 0.04
194	0.04 ± 0.06	690	2.03 ± 0.03
211	-0.05 ± 0.08	740	2.04 ± 0.04
219	0.23 ± 0.07	789	2.16 ± 0.03
243	0.42 ± 0.05	839	1.97 ± 0.06
268	0.52 ± 0.05	888	2.07 ± 0.03
293	0.96 ± 0.04	992	1.95 ± 0.16
318	1.13 ± 0.05	1094	1.87 ± 0.07
343	1.38 ± 0.04	1191	1.68 ± 0.05
367	1.50 ± 0.05	1247	1.78 ± 0.05
392	1.64 ± 0.05	1299	1.65 ± 0.05
443	1.73 ± 0.05	1400	1.67 ± 0.05
492	1.80 ± 0.03	1504	1.50 ± 0.05
540	1.91 ± 0.06		

Experimental electron-impact ionization cross sections for Fe¹¹⁺. Uncertainties listed here are one-standard-deviation relative only, while the absolute uncertainty for a typical point near the peak cross section is $\pm 14\%$ at 90% confidence level. Reference: D.C. Gregory *et al.*, Phys. Rev. A 35, 3256 (1987).

Energy (eV)	σ (10^{-18} cm 2)	Energy (eV)	σ (10^{-18} cm 2)
293	0.02 ± 0.05	788	1.17 ± 0.03
317	-0.02 ± 0.07	812	1.09 ± 0.04
342	0.19 ± 0.06	838	1.16 ± 0.04
391	0.36 ± 0.05	862	1.09 ± 0.05
440	0.52 ± 0.06	887	1.11 ± 0.04
490	0.60 ± 0.06	935	1.08 ± 0.05
540	0.73 ± 0.04	988	1.12 ± 0.04
590	0.79 ± 0.04	1039	1.15 ± 0.03
639	0.80 ± 0.04	1090	1.04 ± 0.04
664	0.83 ± 0.05	1138	1.07 ± 0.05
688	0.84 ± 0.06	1189	1.05 ± 0.04
713	0.90 ± 0.05	1288	1.04 ± 0.04
738	0.95 ± 0.04	1385	0.93 ± 0.04
763	1.06 ± 0.05	1481	0.80 ± 0.03

Experimental electron-impact ionization cross sections for Fe¹³⁺. Uncertainties listed here are one-standard-deviation relative only, while the absolute uncertainty for a typical point near the peak cross section is $\pm 23\%$ at 90% confidence level. Reference: D.C. Gregory *et al.*, Phys. Rev. A 35, 3256 (1987).

Energy (eV)	σ (10^{-18} cm 2)	Energy (eV)	σ (10^{-18} cm 2)
342	-0.04 ± 0.09	763	0.50 ± 0.09
392	-0.006 ± 0.077	788	0.68 ± 0.08
416	0.02 ± 0.14	838	0.71 ± 0.06
442	0.28 ± 0.08	885	0.78 ± 0.07
490	0.21 ± 0.10	935	0.85 ± 0.10
540	0.27 ± 0.09	986	0.68 ± 0.07
590	0.13 ± 0.08	1086	0.54 ± 0.10
639	0.20 ± 0.11	1183	0.64 ± 0.09
688	0.38 ± 0.10	1282	0.63 ± 0.10
739	0.44 ± 0.08	1381	0.58 ± 0.09

Experimental electron-impact ionization cross sections for Fe¹⁵⁺. Uncertainties listed here are one-standard-deviation relative only, while the absolute uncertainty for a typical point near the peak cross section is $\pm 21\%$ at the two-standard-deviation level. Reference: D.C. Gregory *et al.*, Phys. Rev. A 35, 3256 (1987).

Energy (eV)	σ (10^{-18} cm 2)	Energy (eV)	σ (10^{-18} cm 2)
634.2	0.071 \pm 0.048	806.2	0.150 \pm 0.050
686.1	0.076 \pm 0.042	806.7	0.210 \pm 0.025
727.3	0.058 \pm 0.043	807.3	0.355 \pm 0.042
741.5	0.155 \pm 0.046	816.0	0.253 \pm 0.028
751.1	0.105 \pm 0.026	820.8	0.298 \pm 0.065
757.0	0.151 \pm 0.026	835.2	0.257 \pm 0.027
760.4	0.172 \pm 0.032	850.2	0.353 \pm 0.033
769.1	0.190 \pm 0.056	855.6	0.278 \pm 0.047
778.1	0.175 \pm 0.043	870.4	0.287 \pm 0.029
785.7	0.242 \pm 0.046	872.0	0.349 \pm 0.045
796.6	0.198 \pm 0.051	904.5	0.271 \pm 0.027
800.9	0.317 \pm 0.042	924.6	0.302 \pm 0.034
804.8	0.305 \pm 0.042	956.9	0.339 \pm 0.034
805.7	0.250 \pm 0.027	988.0	0.321 \pm 0.047

Electron-impact single ionization cross sections for Ni⁵⁺. Uncertainties are one-standard-deviation relative only, while the absolute uncertainty is about $\pm 10\%$ at 90% confidence level for a typical point near the peak cross section. Reference: L.J. Wang *et al.*, J. Phys. B **21**, 2117 (1988).

Energy (eV)	σ (10^{-18} cm 2)	Energy (eV)	σ (10^{-18} cm 2)
91.6	0.064 ± 0.144	292.6	15.29 ± 0.10
96.1	0.255 ± 0.123	316.9	15.13 ± 0.15
100.8	0.491 ± 0.157	342.2	15.29 ± 0.14
103.2	0.90 ± 0.20	366.7	15.08 ± 0.15
105.8	1.67 ± 0.13	391.1	15.19 ± 0.13
108.2	2.68 ± 0.22	440	15.03 ± 0.16
110.5	3.32 ± 0.14	490	15.26 ± 0.08
113.0	4.59 ± 0.18	539	14.87 ± 0.11
115.6	5.26 ± 0.16	589	14.52 ± 0.14
125.5	6.96 ± 0.15	637	14.30 ± 0.12
135.5	8.23 ± 0.13	688	14.21 ± 0.27
145.1	9.40 ± 0.12	736	14.65 ± 0.14
155.0	10.15 ± 0.12	787	14.13 ± 0.15
174.7	11.86 ± 0.10	885	13.14 ± 0.14
194.5	12.86 ± 0.11	985	12.90 ± 0.15
213.7	13.64 ± 0.15	1131	11.55 ± 0.13
233.7	14.51 ± 0.13	1279	10.64 ± 0.11
252.9	15.22 ± 0.13	1478	9.40 ± 0.13
272.7	15.29 ± 0.12		

Electron-impact single ionization cross sections for Ni⁶⁺. Uncertainties are one-standard-deviation relative only, while the absolute uncertainty is about $\pm 10\%$ at 90% confidence level for a typical point near the peak cross section. Reference: L.J. Wang *et al.*, J. Phys. B **21**, 2117 (1988).

Energy (eV)	σ (10^{-18} cm 2)	Energy (eV)	σ (10^{-18} cm 2)
116.1	-0.099 \pm 0.158	342.2	9.92 \pm 0.09
120.8	-0.096 \pm 0.125	391.1	9.84 \pm 0.13
125.5	-0.043 \pm 0.134	440	9.87 \pm 0.13
130.8	0.500 \pm 0.102	490	9.89 \pm 0.10
133.2	1.24 \pm 0.15	539	9.82 \pm 0.07
135.5	1.28 \pm 0.11	589	9.58 \pm 0.07
140.4	2.56 \pm 0.10	637	9.58 \pm 0.06
145.1	3.23 \pm 0.15	688	9.44 \pm 0.06
155.0	4.35 \pm 0.17	736	9.69 \pm 0.08
164.7	5.21 \pm 0.14	787	9.77 \pm 0.12
174.7	5.98 \pm 0.13	885	9.42 \pm 0.08
194.5	7.14 \pm 0.13	985	8.90 \pm 0.18
219.2	8.16 \pm 0.16	1083	8.41 \pm 0.06
243.6	9.13 \pm 0.13	1183	8.07 \pm 0.06
268.1	9.70 \pm 0.17	1327	7.35 \pm 0.07
292.6	10.04 \pm 0.12	1478	6.81 \pm 0.05

Electron-impact single ionization cross sections for Ni⁷⁺. Uncertainties are one-standard-deviation relative only, while the absolute uncertainty is about $\pm 10\%$ at 90% confidence level for a typical point near the peak cross section. Reference: L.J. Wang *et al.*, J. Phys. B 21, 2117 (1988).

Energy (eV)	σ (10^{-18} cm 2)	Energy (eV)	σ (10^{-18} cm 2)
145.1	0.03 ± 0.22	391.1	6.78 ± 0.09
155.0	0.14 ± 0.20	415.7	7.17 ± 0.13
159.7	0.37 ± 0.27	440	6.98 ± 0.13
164.7	0.51 ± 0.21	465	7.16 ± 0.15
169.9	1.38 ± 0.25	490	7.12 ± 0.13
174.7	1.86 ± 0.20	539	7.06 ± 0.13
174.7	2.49 ± 0.22	589	7.07 ± 0.12
179.4	2.75 ± 0.20	637	7.09 ± 0.11
184.5	3.11 ± 0.14	688	6.92 ± 0.10
194.5	3.93 ± 0.13	736	7.07 ± 0.09
204.3	4.58 ± 0.20	787	6.98 ± 0.13
214.3	5.10 ± 0.13	837	6.99 ± 0.08
233.7	5.69 ± 0.14	885	6.66 ± 0.13
252.9	6.02 ± 0.13	934	6.48 ± 0.13
272.7	6.50 ± 0.13	985	6.58 ± 0.12
292.6	6.43 ± 0.26	1083	6.21 ± 0.11
316.9	6.82 ± 0.11	1183	5.94 ± 0.10
342.2	6.81 ± 0.15	1327	5.43 ± 0.11
366.7	6.87 ± 0.11	1478	5.13 ± 0.08

Electron-impact single ionization cross sections for Ni⁸⁺. Uncertainties are one-standard-deviation relative only, while the absolute uncertainty is about $\pm 10\%$ at 90% confidence level for a typical point near the peak cross section. Reference: L.J. Wang *et al.*, J. Phys. B **21**, 2117 (1988).

Energy (eV)	σ (10^{-18} cm 2)	Energy (eV)	σ (10^{-18} cm 2)
135.5	0.04 \pm 0.19	366.7	4.37 \pm 0.13
145.1	0.12 \pm 0.10	391.1	4.38 \pm 0.10
155.0	0.09 \pm 0.14	415.7	4.59 \pm 0.08
164.7	0.15 \pm 0.11	440	4.43 \pm 0.10
174.7	0.24 \pm 0.12	465	4.61 \pm 0.11
184.5	0.19 \pm 0.13	490	4.52 \pm 0.12
194.5	0.26 \pm 0.13	539	4.45 \pm 0.11
199.5	0.74 \pm 0.12	589	4.44 \pm 0.11
204.3	1.37 \pm 0.13	637	4.58 \pm 0.10
209.2	1.58 \pm 0.12	688	4.57 \pm 0.09
214.3	1.78 \pm 0.12	736	4.51 \pm 0.11
224.0	2.22 \pm 0.11	787	4.44 \pm 0.09
233.7	2.67 \pm 0.12	837	4.50 \pm 0.11
243.6	3.13 \pm 0.12	885	4.69 \pm 0.15
252.9	3.13 \pm 0.09	934	4.62 \pm 0.11
263.1	3.54 \pm 0.14	985	4.41 \pm 0.12
272.7	3.61 \pm 0.12	1083	4.17 \pm 0.15
292.6	3.71 \pm 0.13	1183	4.03 \pm 0.16
316.9	4.01 \pm 0.15	1327	3.83 \pm 0.06
342.2	4.24 \pm 0.14	1478	3.71 \pm 0.08

Electron-impact single ionization cross sections for Ni¹²⁺. Uncertainties are one-standard-deviation relative only, while the absolute uncertainty is about $\pm 10\%$ at 90% confidence level for a typical point near the peak cross section. Reference: L.J. Wang *et al.*, J. Phys. B 21, 2117 (1988).

Energy (eV)	σ (10^{-18} cm 2)	Energy (eV)	σ (10^{-18} cm 2)
303.3	-0.023 \pm 0.038	736	0.680 \pm 0.034
327.5	0.025 \pm 0.038	787	0.747 \pm 0.028
352.2	0.101 \pm 0.029	837	0.734 \pm 0.032
371.7	0.058 \pm 0.028	860	0.813 \pm 0.029
391.1	0.072 \pm 0.029	885	0.877 \pm 0.031
410.8	0.206 \pm 0.050	910	0.946 \pm 0.028
431.0	0.327 \pm 0.037	934	0.971 \pm 0.029
451	0.427 \pm 0.040	959	0.928 \pm 0.037
470	0.404 \pm 0.040	985	0.912 \pm 0.023
490	0.465 \pm 0.053	1034	0.994 \pm 0.023
515	0.536 \pm 0.039	1083	0.940 \pm 0.021
539	0.538 \pm 0.036	1183	0.961 \pm 0.028
564	0.605 \pm 0.034	1279	0.940 \pm 0.028
589	0.656 \pm 0.032	1379	0.881 \pm 0.020
637	0.638 \pm 0.032	1478	0.898 \pm 0.021
688	0.674 \pm 0.040		

Electron-impact single ionization cross sections for Ni¹⁴⁺. Uncertainties are one-standard-deviation relative only, while the absolute uncertainty is about $\pm 10\%$ at 90% confidence level for a typical point near the peak cross section. Reference: L.J. Wang *et al.*, J. Phys. B 21, 2117 (1988).

Energy (eV)	σ (10^{-18} cm 2)	Energy (eV)	σ (10^{-18} cm 2)
440	0.016 \pm 0.027	910	0.443 \pm 0.033
490	0.129 \pm 0.035	934	0.508 \pm 0.019
589	0.238 \pm 0.029	985	0.532 \pm 0.019
688	0.275 \pm 0.024	1034	0.621 \pm 0.024
787	0.319 \pm 0.023	1083	0.604 \pm 0.046
812	0.306 \pm 0.019	1131	0.587 \pm 0.048
837	0.261 \pm 0.015	1183	0.582 \pm 0.043
860	0.331 \pm 0.018	1279	0.586 \pm 0.033
885	0.403 \pm 0.019	1379	0.514 \pm 0.035

Electron-impact single ionization cross sections for Kr⁴⁺. Uncertainties are one-standard-deviation relative only; absolute uncertainty at the two-standard-deviation level is approximately $\pm 12\%$. Reference: A.M. Howald *et al.*, unpublished (1985), ref. 27.

Energy (eV)	σ (10^{-18} cm 2)	Energy (eV)	σ (10^{-18} cm 2)
36.5	0.04 \pm 0.07	106.3	17.68 \pm 0.05
40.8	-0.07 \pm 0.08	111.0	17.90 \pm 0.07
41.5	0.12 \pm 0.06	116.2	17.88 \pm 0.06
42.5	0.14 \pm 0.10	121.0	18.17 \pm 0.06
46.5	0.56 \pm 0.08	125.6	18.50 \pm 0.06
47.4	0.73 \pm 0.09	130.9	18.57 \pm 0.07
51.4	0.72 \pm 0.06	135.9	18.78 \pm 0.04
56.2	0.87 \pm 0.06	145.5	18.97 \pm 0.06
58.1	0.83 \pm 0.09	151.1	18.77 \pm 0.12
59.1	0.83 \pm 0.09	155.4	18.66 \pm 0.08
60.0	0.76 \pm 0.09	165.7	18.15 \pm 0.05
61.8	1.05 \pm 0.06	175.3	17.40 \pm 0.08
64.4	2.40 \pm 0.06	184.5	17.05 \pm 0.09
65.2	4.38 \pm 0.10	195.5	16.96 \pm 0.04
66.4	4.73 \pm 0.05	220	16.38 \pm 0.07
68.0	6.18 \pm 0.10	225	16.65 \pm 0.08
69.0	7.65 \pm 0.11	244	16.20 \pm 0.06
70.1	7.68 \pm 0.08	255	15.74 \pm 0.07
71.7	9.24 \pm 0.06	269	15.91 \pm 0.06
72.1	10.06 \pm 0.11	274	14.98 \pm 0.06
73.8	10.94 \pm 0.08	294	15.04 \pm 0.02
76.3	11.87 \pm 0.05	319	14.04 \pm 0.06
77.9	12.45 \pm 0.09	344	13.21 \pm 0.04
79.9	13.73 \pm 0.10	394	12.34 \pm 0.08
81.5	14.34 \pm 0.06	443	11.99 \pm 0.06
84.0	15.31 \pm 0.09	493	11.10 \pm 0.04
86.2	16.44 \pm 0.05	593	10.42 \pm 0.04
87.8	16.27 \pm 0.09	692	9.65 \pm 0.04
89.8	16.24 \pm 0.09	842	8.48 \pm 0.03
91.5	16.59 \pm 0.07	997	7.76 \pm 0.02
94.1	16.14 \pm 0.09	1198	6.48 \pm 0.08
96.5	16.84 \pm 0.04	1240	6.96 \pm 0.05
99.8	17.56 \pm 0.12	1397	5.53 \pm 0.08
101.5	16.89 \pm 0.06	1500	6.40 \pm 0.03
103.5	17.39 \pm 0.11		

Kr⁷⁺ ionization cross section data: The second column lists the measured data with their absolute uncertainties. The third column gives data reduced by $9.25/\sqrt{E}$ (where E is in eV). Absolute uncertainties in the third column include the contribution from the uncertainties due to correction for space-charge modulation. Reference: D.C. Gregory and A.M. Howald, unpublished (1985).

Ionization cross sections (10^{-18} cm^2)

Energy (eV)	Measured data	Data after the correction for space-charge modulation
75.5	1.01 ± 0.21	-0.06 ± 0.22
85.3	1.48 ± 0.50	0.47 ± 0.50
95.2	1.11 ± 0.16	0.16 ± 0.17
96.4	0.98 ± 0.27	0.03 ± 0.28
106	0.71 ± 0.17	-0.19 ± 0.18
116	0.81 ± 0.14	-0.05 ± 0.15
125	0.96 ± 0.16	0.13 ± 0.17
136	1.72 ± 0.16	0.92 ± 0.17
145	3.24 ± 0.15	2.47 ± 0.16
154	3.45 ± 0.16	2.70 ± 0.17
157	4.51 ± 0.11	3.77 ± 0.12
160	4.98 ± 0.09	4.25 ± 0.10
165	5.12 ± 0.12	4.40 ± 0.13
171	5.32 ± 0.57	4.61 ± 0.57
175	5.29 ± 0.15	4.59 ± 0.16
183	5.48 ± 0.17	4.79 ± 0.18
195	6.16 ± 0.14	5.49 ± 0.15
213	6.57 ± 0.16	5.93 ± 0.17
221	7.61 ± 0.37	6.98 ± 0.37
232	6.73 ± 0.15	6.12 ± 0.16
243	7.74 ± 0.19	7.14 ± 0.19
251	6.83 ± 0.14	6.24 ± 0.15
271	7.37 ± 0.13	6.81 ± 0.14
291	8.04 ± 0.07	7.50 ± 0.08
309	8.21 ± 0.11	7.68 ± 0.12
329	8.50 ± 0.09	7.99 ± 0.10
341	8.38 ± 0.24	7.88 ± 0.24
349	8.68 ± 0.08	8.18 ± 0.09
368	8.65 ± 0.09	8.17 ± 0.10
389	8.94 ± 0.07	8.47 ± 0.08
420	8.90 ± 0.10	8.45 ± 0.10
454	9.12 ± 0.09	8.68 ± 0.09
488	9.35 ± 0.06	8.93 ± 0.07
495	9.48 ± 0.11	9.06 ± 0.11
538	9.57 ± 0.17	9.17 ± 0.17
587	9.48 ± 0.12	9.10 ± 0.12

(Continued)

Ionization cross sections (10^{-18} cm^2)

Energy (eV)	Measured data	Data after the correction for space-charge modulation
637	9.37 ± 0.09	9.00 ± 0.09
687	8.99 ± 0.12	8.64 ± 0.12
736	9.10 ± 0.11	8.76 ± 0.11
786	8.95 ± 0.11	8.62 ± 0.11
835	8.72 ± 0.08	8.40 ± 0.08
885	8.75 ± 0.08	8.44 ± 0.08
934	8.61 ± 0.07	8.31 ± 0.07
989	8.28 ± 0.07	7.98 ± 0.07
1090	7.97 ± 0.07	7.69 ± 0.07
1187	7.76 ± 0.07	7.49 ± 0.07
1284	7.59 ± 0.05	7.33 ± 0.05
1385	7.17 ± 0.06	6.92 ± 0.06
1485	6.95 ± 0.06	6.71 ± 0.06

Experimental electron-impact ionization cross sections for Kr⁸⁺. Uncertainties are one-standard-deviation relative only; absolute uncertainty of the curve is $\pm 8\%$ at 90% confidence level for a point near the peak of the curve. Reference: M.E. Bannister et al., Phys. Rev. A 38, 38 (1988).

Energy (eV)	σ (10^{-18} cm 2)	Energy (eV)	σ (10^{-18} cm 2)
124.7	0.03 \pm 0.09	331.1	3.70 \pm 0.05
134.5	0.06 \pm 0.09	350.8	3.87 \pm 0.04
144.4	-0.02 \pm 0.08	370.4	4.06 \pm 0.05
149.3	0.09 \pm 0.05	390.6	4.40 \pm 0.06
154.1	0.12 \pm 0.05	414.8	4.56 \pm 0.05
159.2	0.35 \pm 0.07	439.7	4.80 \pm 0.06
163.8	0.58 \pm 0.05	464.1	4.98 \pm 0.05
173.6	0.64 \pm 0.06	489.0	5.16 \pm 0.05
183.4	0.79 \pm 0.06	513.7	5.29 \pm 0.05
193.8	0.86 \pm 0.06	538.3	5.37 \pm 0.05
203.7	0.91 \pm 0.06	563.0	5.43 \pm 0.04
213.5	1.07 \pm 0.06	586.7	5.45 \pm 0.05
218.1	1.03 \pm 0.06	636.2	5.59 \pm 0.04
223.2	1.04 \pm 0.05	685.6	5.65 \pm 0.03
232.9	1.08 \pm 0.05	734.7	5.73 \pm 0.03
237.7	1.22 \pm 0.05	783.7	5.71 \pm 0.04
242.8	1.53 \pm 0.04	832.9	5.71 \pm 0.03
247.4	1.75 \pm 0.06	882.6	5.66 \pm 0.03
252.5	1.79 \pm 0.06	982.4	5.63 \pm 0.03
262.4	2.14 \pm 0.06	1081	5.46 \pm 0.05
272.3	2.48 \pm 0.06	1179	5.27 \pm 0.03
282.2	2.64 \pm 0.06	1277	5.03 \pm 0.03
291.9	2.98 \pm 0.06	1375	4.88 \pm 0.03
311.3	3.47 \pm 0.06		

Electron-impact single ionization cross sections for Kr⁹⁺. Uncertainties are one-standard-deviation relative only. Reference: D.C. Gregory, K. Rinn, and L.J. Wang, unpublished (1986).

Energy (eV)	σ (10^{-18} cm 2)	Energy (eV)	σ (10^{-18} cm 2)
208	-0.12 ± 0.16	792	3.54 ± 0.14
247	0.32 ± 0.16	893	3.46 ± 0.11
296	0.73 ± 0.17	994	3.55 ± 0.11
346	1.65 ± 0.17	1193	3.34 ± 0.13
396	2.48 ± 0.17	1293	3.64 ± 0.14
495	3.45 ± 0.15	1393	3.53 ± 0.12
594	3.84 ± 0.16	1492	3.13 ± 0.08
693	3.60 ± 0.14		

Electron-impact single ionization cross sections for Xe⁶⁺. Uncertainties are one-standard-deviation relative only. Reference: D.C. Gregory, K. Rinn, and L.J. Wang, unpublished (1986).

Energy (eV)	σ (10^{-18} cm 2)	Energy (eV)	σ (10^{-18} cm 2)
66.4	-0.16 ± 0.42	100.4	27.70 ± 0.59
69.3	0.26 ± 0.38	100.6	28.14 ± 0.28
72.3	0.38 ± 0.39	101.3	28.83 ± 0.29
74.0	-0.31 ± 0.46	101.3	27.95 ± 0.31
76.1	0.52 ± 0.39	101.8	30.82 ± 0.28
78.5	-0.04 ± 0.33	101.8	28.61 ± 0.33
79.7	0.77 ± 0.27	102.5	28.92 ± 0.35
80.9	1.71 ± 0.36	102.5	28.01 ± 0.30
82.2	4.01 ± 0.38	103.0	28.28 ± 0.22
83.5	4.78 ± 0.24	103.7	29.89 ± 0.30
84.6	6.32 ± 0.38	105.4	30.65 ± 0.32
85.7	7.83 ± 0.28	107.9	31.84 ± 0.30
86.1	8.30 ± 0.42	110.2	31.66 ± 0.35
87.2	11.67 ± 0.37	112.9	32.51 ± 0.33
88.2	11.15 ± 0.34	114.3	33.69 ± 0.32
89.5	11.48 ± 0.36	114.9	33.33 ± 0.29
90.8	10.85 ± 0.26	115.4	33.66 ± 0.30
92.2	10.92 ± 0.35	115.6	34.65 ± 0.38
93.3	12.36 ± 0.38	116.1	36.01 ± 0.29
93.6	11.29 ± 0.36	116.7	36.91 ± 0.48
94.2	12.30 ± 0.43	117.2	38.70 ± 0.29
94.8	13.45 ± 0.40	117.5	38.92 ± 0.34
95.4	15.33 ± 0.28	117.8	40.00 ± 0.36
95.8	16.43 ± 0.23	118.4	40.40 ± 0.29
96.0	15.83 ± 0.28	119.3	39.83 ± 0.55
96.5	15.80 ± 0.34	120.2	40.35 ± 0.30
97.1	16.65 ± 0.30	120.2	38.60 ± 0.55
97.8	18.75 ± 0.30	121.2	37.74 ± 0.32
98.2	20.02 ± 0.24	122.0	37.89 ± 0.28
98.4	21.15 ± 0.28	122.7	38.79 ± 0.14
98.8	24.98 ± 0.28	123.7	38.63 ± 0.28
99.5	26.13 ± 0.29	124.7	38.69 ± 0.28
100.0	25.91 ± 0.28	125.5	38.26 ± 0.27

Electron-impact double ionization cross sections for Xe⁶⁺. Uncertainties are one-standard-deviation relative only; absolute uncertainty is $\pm 8\%$ at good confidence level. Reference: A.M. Howald *et al.*, Phys. Rev. Lett. **56**, 1675 (1986).

Energy (eV)	σ (10^{-18} cm 2)	Energy (eV)	σ (10^{-18} cm 2)
144	0.03 ± 0.24	491	2.85 ± 0.09
194	0.55 ± 0.18	591	2.80 ± 0.15
218	1.13 ± 0.31	640	2.95 ± 0.15
244	1.42 ± 0.15	691	2.95 ± 0.15
267	1.99 ± 0.18	742	2.86 ± 0.15
292	2.26 ± 0.12	841	2.52 ± 0.15
342	2.52 ± 0.13	988	2.21 ± 0.15
392	2.82 ± 0.13		

Electron-impact triple ionization cross sections for Xe⁶⁺. Uncertainties are one-standard-deviation relative only; absolute uncertainty is $\pm 12\%$ at good confidence level. Reference: A.M. Howald *et al.*, Phys. Rev. Lett. **56**, 1675 (1986).

Energy (eV)	σ (10^{-18} cm 2)	Energy (eV)	σ (10^{-18} cm 2)
293	0.0	692	0.143 ± 0.010
392	0.01 ± 0.01	742	0.166 ± 0.008
426	0.026 ± 0.01	792	0.196 ± 0.007
458	0.07 ± 0.01	843	0.221 ± 0.009
493	0.10 ± 0.012	892	0.247 ± 0.008
525	0.098 ± 0.011	942	0.279 ± 0.008
559	0.122 ± 0.011	995	0.289 ± 0.007
592	0.120 ± 0.010	1094	0.312 ± 0.010
643	0.140 ± 0.011	1194	0.321 ± 0.010

Experimental electron-impact ionization cross sections for Xe⁸⁺. Uncertainties are one-standard-deviation relative only; absolute uncertainty of the curve is $\pm 8\%$ at 90% confidence level for a point near the peak of the curve. Reference: M.E. Bannister et al., Phys. Rev. A 38, 38 (1988).

Energy (eV)	σ (10^{-18} cm 2)	Energy (eV)	σ (10^{-18} cm 2)
87.6	0.46 ± 0.54	243.1	9.47 ± 0.18
97.3	-0.02 ± 0.47	268.0	9.59 ± 0.22
111.8	0.38 ± 0.73	291.9	9.65 ± 0.23
121.1	1.06 ± 0.58	316.0	10.09 ± 0.19
129.4	2.36 ± 0.58	342.8	10.10 ± 0.16
138.2	2.94 ± 0.69	389.9	10.27 ± 0.12
145.8	2.79 ± 0.50	440.0	10.38 ± 0.12
153.4	2.46 ± 0.48	487.5	10.28 ± 0.13
162.1	2.50 ± 0.63	537.0	10.35 ± 0.12
170.0	3.18 ± 0.36	585.7	9.91 ± 0.11
180.0	3.13 ± 0.23	634.0	9.42 ± 0.13
181.7	2.94 ± 0.36	635.0	9.60 ± 0.08
185.0	5.00 ± 0.44	684.0	9.66 ± 0.07
189.7	5.20 ± 0.34	782.0	9.53 ± 0.11
195.0	5.58 ± 0.46	879.0	8.87 ± 0.13
199.2	5.93 ± 0.32	978.0	8.41 ± 0.12
204.0	6.96 ± 0.35	982.0	8.28 ± 0.15
209.0	7.44 ± 0.35	1081	7.25 ± 0.12
214.7	7.44 ± 0.29	1180	6.63 ± 0.09
219.7	7.95 ± 0.20	1278	6.23 ± 0.09
224.1	7.79 ± 0.27	1377	5.89 ± 0.12
234.0	8.91 ± 0.30	1476	5.77 ± 0.11

Cross section measurements for double ionization of Xe⁸⁺ by electron impact. Uncertainties are relative only at the equivalent of one-standard-deviation confidence level; absolute uncertainty for a point near the peak cross section is $\pm 8\%$ at 90% confidence level. Reference: D.W. Mueller *et al.*, Phys. Rev. A 39, 2381 (1989).

Energy (eV)	σ (10^{-18} cm 2)	Energy (eV)	σ (10^{-18} cm 2)
286	-0.013 \pm 0.065	688	0.311 \pm 0.032
335	0.008 \pm 0.059	698	0.310 \pm 0.030
383	0.021 \pm 0.048	720	0.354 \pm 0.031
411	0.082 \pm 0.032	754	0.349 \pm 0.030
420	0.033 \pm 0.046	768	0.367 \pm 0.026
431	0.146 \pm 0.046	784	0.387 \pm 0.027
440	0.158 \pm 0.044	817	0.410 \pm 0.031
450	0.163 \pm 0.043	833	0.406 \pm 0.029
460	0.099 \pm 0.031	854	0.445 \pm 0.036
470	0.134 \pm 0.043	882	0.454 \pm 0.023
479	0.096 \pm 0.040	884	0.510 \pm 0.010
490	0.156 \pm 0.040	931	0.515 \pm 0.031
509	0.167 \pm 0.041	980	0.547 \pm 0.029
527	0.222 \pm 0.038	984	0.599 \pm 0.028
547	0.262 \pm 0.041	1032	0.546 \pm 0.021
563	0.186 \pm 0.041	1082	0.579 \pm 0.030
577	0.214 \pm 0.030	1131	0.618 \pm 0.028
597	0.229 \pm 0.038	1180	0.567 \pm 0.020
612	0.227 \pm 0.038	1229	0.578 \pm 0.026
623	0.231 \pm 0.030	1278	0.566 \pm 0.016
646	0.242 \pm 0.031	1327	0.567 \pm 0.023
661	0.320 \pm 0.037	1376	0.517 \pm 0.012
668	0.272 \pm 0.036	1425	0.582 \pm 0.024
686	0.259 \pm 0.027	1476	0.567 \pm 0.016

Electron-impact single ionization cross sections for Ta⁸⁺. Uncertainties are one-standard-deviation relative only. Reference: D.C. Gregory and F.W. Meyer, unpublished (1988).

Energy (eV)	σ (10^{-18} cm 2)	Energy (eV)	σ (10^{-18} cm 2)
146	3.24 ± 4.2	437	20.1 ± 1.9
195	15.3 ± 2.4	486	20.8 ± 1.7
243	12.0 ± 2.0	582	18.1 ± 1.3
291	20.2 ± 1.8	680	16.4 ± 0.9
341	20.5 ± 1.7	777	15.9 ± 1.0
389	17.3 ± 1.6		

Single ionization cross sections for U^{10+} ions. Cross section uncertainties are relative only at the equivalent of one standard deviation for statistics; collision energy uncertainties range from ± 0.2 (at low energies) to ± 1 eV (at high energies). Absolute uncertainty for a point near the peak cross section is $\pm 8\%$ at the two-standard-deviation level. Reference: D.C. Gregory *et al.*, Phys. Rev. A **41**, 106 (1990).

Energy (eV)	σ (10^{-18} cm^2)	Energy (eV)	σ (10^{-18} cm^2)
115.4	0.38 ± 0.16	203.5	20.72 ± 0.11
120.3	-0.04 ± 0.16	213.3	21.29 ± 0.16
125.3	1.14 ± 0.19	223.9	21.46 ± 0.16
128.4	1.51 ± 0.17	233.0	21.79 ± 0.13
129.4	1.72 ± 0.17	242.6	21.69 ± 0.13
130.0	2.06 ± 0.15	252.4	21.32 ± 0.13
130.5	1.91 ± 0.16	272.3	21.62 ± 0.12
131.4	1.86 ± 0.16	292.5	21.22 ± 0.09
132.5	1.84 ± 0.14	317.5	20.47 ± 0.18
133.3	1.84 ± 0.14	343.4	19.85 ± 0.12
134.4	1.92 ± 0.14	367.0	18.88 ± 0.11
135.0	2.17 ± 0.20	392.0	17.89 ± 0.11
135.4	2.15 ± 0.16	416.0	17.10 ± 0.18
136.2	2.30 ± 0.13	440.7	16.85 ± 0.11
137.2	2.56 ± 0.16	465.0	16.58 ± 0.12
138.2	2.40 ± 0.21	489.9	16.15 ± 0.05
139.8	2.44 ± 0.15	539.3	15.63 ± 0.12
144.8	4.85 ± 0.11	588.4	15.05 ± 0.13
149.5	6.40 ± 0.21	637.4	14.39 ± 0.12
154.5	7.95 ± 0.15	687.4	13.99 ± 0.05
159.4	9.30 ± 0.23	735.8	13.81 ± 0.07
164.3	11.90 ± 0.15	784.9	13.23 ± 0.08
169.2	13.52 ± 0.17	883.1	12.66 ± 0.08
174.2	15.79 ± 0.09	981.9	11.91 ± 0.05
179.1	17.40 ± 0.13	1080	11.27 ± 0.05
183.9	18.20 ± 0.11	1179	10.48 ± 0.08
188.7	19.20 ± 0.28	1276	10.09 ± 0.05
193.9	19.98 ± 0.13	1396	9.08 ± 0.04
198.7	20.62 ± 0.15	1451	8.91 ± 0.06

Electron-impact double ionization cross sections for U^{10+} . Uncertainties listed are relative combining one standard deviation on counting statistics with uncertainties in the form factor. Total uncertainties are approximately $\pm 10\%$ at 90% confidence level for a typical point near the peak cross section. Note that the cross section is listed in units of 10^{-19} cm^2 . Reference: D.C. Gregory *et al.*, Phys. Rev. A 41, 106 (1990).

Energy (eV)	σ (10^{-19} cm^2)	Energy (eV)	σ (10^{-19} cm^2)
243.5	-0.61 \pm 0.22	526.7	23.73 \pm 0.26
292.3	-0.84 \pm 0.19	546.3	23.94 \pm 0.45
302.1	-0.79 \pm 0.19	565.9	24.08 \pm 0.22
311.9	-0.53 \pm 0.20	585.2	24.17 \pm 0.24
321.7	-0.38 \pm 0.19	609.6	24.32 \pm 0.28
331.4	0.42 \pm 0.18	634.2	23.88 \pm 0.24
341.2	1.61 \pm 0.21	658.7	24.71 \pm 0.22
350.7	3.82 \pm 0.17	687.6	24.28 \pm 0.09
360.7	5.68 \pm 0.16	707.5	24.46 \pm 0.21
370.4	7.98 \pm 0.16	732.2	24.83 \pm 0.21
380.1	9.95 \pm 0.16	781.4	24.52 \pm 0.25
389.9	12.22 \pm 0.18	830.2	25.11 \pm 0.21
404.3	15.23 \pm 0.17	879.1	24.67 \pm 0.28
419.0	17.36 \pm 0.19	928.0	25.11 \pm 0.21
433.7	18.94 \pm 0.25	980.5	24.88 \pm 0.19
448.2	20.18 \pm 0.27	1082	23.49 \pm 0.19
463.2	20.84 \pm 0.26	1180	23.45 \pm 0.18
477.6	21.92 \pm 0.28	1279	22.84 \pm 0.19
487.6	21.91 \pm 0.21	1378	23.10 \pm 0.20
507.1	22.67 \pm 0.24	1478	22.14 \pm 0.15

Single ionization cross sections for U¹³⁺ ions. Cross section uncertainties are relative only at the equivalent of one standard deviation for statistics; collision energy uncertainties range from ± 0.2 (at low energies) to ± 1 eV (at high energies). Absolute uncertainty for a point near the peak cross section is $\pm 9\%$ at the two-standard-deviation level. Reference: D.C. Gregory *et al.*, Phys. Rev. A **41**, 106 (1990).

Energy (eV)	σ (10^{-18} cm 2)	Energy (eV)	σ (10^{-18} cm 2)
186.8	0.00 ± 0.10	588.6	8.23 ± 0.05
197.0	0.19 ± 0.13	613.1	8.06 ± 0.06
206.2	1.22 ± 0.11	637.8	7.92 ± 0.06
215.9	1.74 ± 0.08	662.5	7.94 ± 0.06
226.0	2.37 ± 0.09	667.1	7.93 ± 0.05
235.6	2.86 ± 0.08	672.0	7.68 ± 0.05
245.3	3.87 ± 0.07	673.9	7.58 ± 0.04
245.7	4.04 ± 0.11	676.9	7.84 ± 0.05
255.1	4.55 ± 0.06	687.0	7.65 ± 0.04
264.9	5.18 ± 0.05	698.6	7.66 ± 0.04
274.6	5.51 ± 0.06	711.3	7.80 ± 0.06
284.6	6.07 ± 0.05	723.4	7.59 ± 0.04
294.4	6.23 ± 0.05	736.1	7.58 ± 0.05
294.7	6.47 ± 0.10	760.8	7.50 ± 0.04
304.1	6.66 ± 0.05	785.4	7.50 ± 0.06
313.9	6.79 ± 0.07	794.6	7.38 ± 0.03
323.9	7.13 ± 0.07	804.8	7.53 ± 0.05
333.5	7.72 ± 0.07	807.6	7.14 ± 0.03
343.9	7.86 ± 0.09	809.6	7.16 ± 0.03
353.2	8.08 ± 0.07	814.8	7.49 ± 0.05
363.1	7.82 ± 0.08	824.4	7.46 ± 0.05
372.6	8.11 ± 0.07	834.3	7.49 ± 0.07
382.3	8.12 ± 0.08	844.1	7.40 ± 0.04
392.6	8.26 ± 0.06	859.0	7.15 ± 0.04
401.9	8.08 ± 0.08	883.5	7.11 ± 0.05
411.8	8.40 ± 0.07	907.9	6.90 ± 0.04
421.6	8.38 ± 0.07	932.6	6.96 ± 0.05
431.3	8.56 ± 0.08	935.8	6.83 ± 0.05
441.6	8.50 ± 0.07	957.3	6.85 ± 0.03
450.8	8.72 ± 0.08	982.0	6.48 ± 0.04
461.1	8.66 ± 0.08	985.3	6.66 ± 0.05
470.7	8.75 ± 0.08	1084	6.23 ± 0.04
480.6	8.83 ± 0.08	1182	6.01 ± 0.03
491.0	8.73 ± 0.13	1281	5.87 ± 0.04
510.0	8.70 ± 0.06	1281	5.59 ± 0.04
529.0	8.67 ± 0.08	1379	5.58 ± 0.03
549.4	8.61 ± 0.06	1478	5.34 ± 0.03
569.1	8.44 ± 0.05		

Electron-impact double ionization cross sections for U¹³⁺. Uncertainties are typical relative uncertainties, which combine one standard deviation on counting statistics with uncertainties in the form factor. Total uncertainties are approximately $\pm 10\%$ at 90% confidence level for a typical point near the peak cross section. Note that the cross section is listed in units of 10^{-19} cm^2 . Reference: D.C. Gregory *et al.*, Phys. Rev. A **41**, 106 (1990).

Energy (eV)	σ (10^{-19} cm^2)	Energy (eV)	σ (10^{-19} cm^2)
487.8	-0.08 \pm 0.15	766.7	6.02 \pm 0.11
500.6	0.08 \pm 0.13	776.5	6.37 \pm 0.11
510.4	0.00 \pm 0.14	784.4	6.63 \pm 0.08
520.2	-0.18 \pm 0.12	795.9	6.86 \pm 0.11
530.1	0.13 \pm 0.15	805.7	6.98 \pm 0.14
538.4	0.13 \pm 0.09	815.6	7.28 \pm 0.17
549.7	0.47 \pm 0.14	825.5	7.23 \pm 0.11
559.6	0.60 \pm 0.16	835.5	7.28 \pm 0.13
569.3	0.81 \pm 0.11	845.5	7.59 \pm 0.16
579.1	1.03 \pm 0.16	855.4	8.01 \pm 0.15
589.1	1.56 \pm 0.14	865.3	8.05 \pm 0.13
598.7	1.73 \pm 0.14	875.0	8.26 \pm 0.13
608.7	1.83 \pm 0.18	885.6	8.46 \pm 0.10
618.5	2.43 \pm 0.14	894.8	8.81 \pm 0.14
628.4	3.03 \pm 0.14	904.8	8.75 \pm 0.13
638.8	2.85 \pm 0.22	914.7	9.05 \pm 0.13
648.3	3.08 \pm 0.20	924.4	8.90 \pm 0.13
658.1	3.60 \pm 0.12	934.3	8.81 \pm 0.12
667.9	3.74 \pm 0.17	944.3	8.76 \pm 0.12
677.9	4.24 \pm 0.13	954.2	9.01 \pm 0.15
688.3	4.30 \pm 0.04	964.1	9.61 \pm 0.22
697.5	4.67 \pm 0.13	974.0	9.54 \pm 0.13
707.3	5.15 \pm 0.13	984.5	9.58 \pm 0.12
717.3	5.17 \pm 0.13	1083	9.79 \pm 0.13
727.0	5.36 \pm 0.15	1182	10.07 \pm 0.12
736.8	5.56 \pm 0.14	1281	10.57 \pm 0.09
746.9	5.85 \pm 0.11	1380	10.81 \pm 0.10
756.7	6.07 \pm 0.11	1479	10.78 \pm 0.08

Single ionization cross sections for U¹⁶⁺ ions. Cross section uncertainties are relative only at the equivalent of one standard deviation for statistics; collision energy uncertainties range from ± 0.2 (at low energies) to ± 1 eV (at high energies). Absolute uncertainty for a point near the peak cross section is $\pm 10\%$ at the two-standard-deviation level. Reference: D.C. Gregory *et al.*, Phys. Rev. A 41, 106 (1990).

Energy (eV)	σ (10^{-18} cm 2)	Energy (eV)	σ (10^{-18} cm 2)
292.2	0.02 ± 0.10	533.1	3.11 ± 0.03
341.1	0.16 ± 0.09	538.1	3.03 ± 0.05
351.4	0.16 ± 0.08	543.0	3.04 ± 0.06
361.3	0.10 ± 0.08	548.0	3.04 ± 0.06
371.1	0.11 ± 0.08	552.7	3.14 ± 0.04
380.8	0.21 ± 0.09	557.7	3.17 ± 0.04
390.2	0.52 ± 0.06	562.5	3.08 ± 0.03
399.7	0.89 ± 0.08	567.6	3.30 ± 0.03
410.1	1.22 ± 0.06	572.3	3.21 ± 0.04
419.8	1.58 ± 0.08	577.4	3.31 ± 0.03
429.7	1.86 ± 0.09	587.4	3.14 ± 0.06
439.4	2.08 ± 0.06	597.0	3.29 ± 0.05
444.3	2.09 ± 0.07	606.8	3.29 ± 0.05
449.2	2.31 ± 0.08	616.6	3.26 ± 0.05
453.8	2.35 ± 0.08	626.4	3.46 ± 0.06
458.6	2.17 ± 0.07	646.1	3.45 ± 0.05
464.3	2.47 ± 0.05	665.8	3.35 ± 0.07
469.1	2.58 ± 0.03	688.2	3.45 ± 0.03
474.3	2.53 ± 0.04	709.9	3.43 ± 0.05
478.9	2.62 ± 0.04	734.5	3.68 ± 0.08
484.1	2.68 ± 0.03	783.8	3.63 ± 0.07
489.2	2.65 ± 0.03	832.5	3.68 ± 0.07
494.0	2.77 ± 0.03	881.7	3.53 ± 0.10
489.9	2.71 ± 0.03	979.7	3.59 ± 0.06
503.7	2.80 ± 0.06	1082	3.45 ± 0.05
508.7	2.82 ± 0.06	1180	3.33 ± 0.06
513.5	2.87 ± 0.04	1279	3.22 ± 0.05
518.3	2.83 ± 0.04	1378	3.22 ± 0.04
523.2	3.20 ± 0.03	1476	3.09 ± 0.05
528.3	3.03 ± 0.03		

Cross sections for production of ion fragments in electron impact dissociation of H₃O⁺ and D₃O⁺. Error bars are one standard deviation based on counting statistics. Reference: P.A. Schulz *et al.*, J. Chem Phys. **85**, 3386 (1986).

Energy (eV)	σ (10 ⁻¹⁸ cm ²)	Energy (eV)	σ (10 ⁻¹⁸ cm ²)
$e + D_3O^+ \rightarrow D_2O^+$			
45.3	55.6 ± 12.0	16.5	0.29 ± 0.86
94.9	69.9 ± 7.8	21.7	3.18 ± 0.51
194	66.6 ± 5.1	26.7	3.85 ± 0.57
293	61.5 ± 3.2	31.9	4.12 ± 0.41
492	54.5 ± 2.4	36.7	4.94 ± 0.56
692	46.4 ± 2.4	46.6	6.14 ± 0.39
995	37.2 ± 2.5	56.4	6.06 ± 0.46
		66.4	6.47 ± 0.39
		76.3	7.07 ± 0.21
$e + H_3O^+ \rightarrow OH^+$			
11.7	3.3 ± 9.2	81.5	7.50 ± 0.39
16.8	44.9 ± 7.8	86.4	7.68 ± 0.15
26.8	41.5 ± 5.8	91.2	7.19 ± 0.23
36.7	36.5 ± 6.9	96.6	7.44 ± 0.09
46.6	44.2 ± 3.9	122	8.19 ± 0.21
56.4	44.5 ± 4.2	146	8.34 ± 0.17
66.3	35.3 ± 2.5	171	8.13 ± 0.17
76.4	38.9 ± 3.1	196	7.92 ± 0.14
86.1	42.4 ± 2.8	221	7.45 ± 0.12
96.7	37.0 ± 2.2	245	7.54 ± 0.11
146	35.6 ± 1.7	296	6.86 ± 0.08
196	30.2 ± 1.2		
246	31.5 ± 0.9		
296	29.1 ± 0.6		
394	24.1 ± 0.9		
494	24.0 ± 0.7		
594	20.8 ± 0.7		
694	19.3 ± 0.7		
794	17.1 ± 0.6		
894	16.9 ± 0.6		
998	15.2 ± 0.5		

Cross sections for production of ion fragments in electron impact dissociation and ionization of CD_4^+ . Error bars are one standard deviation based on counting statistics. Cross sections for the process of interest are small compared to the background apparent cross section. Reference: D.C. Gregory *et al.*, unpublished (1989), ref. 39.

Energy (eV)	σ (10^{-18} cm^2)	Energy (eV)	σ (10^{-18} cm^2)
$e + \text{CD}_4^+ \rightarrow \text{CD}_3^+$		$e + \text{CD}_4^+ \rightarrow \text{CD}_4^{2+}$	
8.7	$1308. \pm 242$	8.8	16.3 ± 6.1
13.4	$463. \pm 142$	13.6	18.6 ± 4.7
17.6	$450. \pm 76$	15.6	12.4 ± 3.6
17.9	$521. \pm 79$	28.2	5.80 ± 0.77
27.1	$236. \pm 43$	47.4	4.02 ± 0.49
36.2	$165. \pm 28$	77.2	3.61 ± 0.62
45.4	$160. \pm 20$	96.7	1.93 ± 0.55

$\text{CD}_4^+ \rightarrow \text{CD}_2^+$ dissociation cross section data: The second column lists the measured data with their absolute uncertainties. The third column gives data with a functional form ($294 \times 10^{-18} E^{-1/2}$, where E is the energy in eV) subtracted to approximate the cross section for dissociation of a ground-energy molecule. Absolute uncertainties in the third column include the uncertainty in the correction, assuming that the functional form used was correct. Reference: D.C. Gregory *et al.*, unpublished (1989), ref. 39.

Electron energy (eV)	Ionization cross sections $\sigma (10^{-18} \text{ cm}^2)$	
	Measured data	Data after correction
4.0	140.6 ± 19.3	-6.4 ± 21.3
5.6	126.6 ± 13.8	2.4 ± 15.8
6.7	119.7 ± 10.7	6.1 ± 12.8
8.5	134.8 ± 11.3	34.0 ± 12.9
10.5	166.1 ± 10.9	75.4 ± 12.3
12.4	169.4 ± 7.8	85.9 ± 9.4
13.3	166.1 ± 7.6	85.5 ± 9.1
16.3	147.8 ± 12.8	75.0 ± 13.6
18.2	108.0 ± 4.9	39.1 ± 6.5
23.0	78.0 ± 6.0	16.7 ± 7.1
27.7	85.0 ± 4.1	29.1 ± 5.4
37.2	75.1 ± 2.4	26.9 ± 3.8
46.8	71.7 ± 3.8	28.7 ± 4.6
70.6	62.8 ± 2.3	27.8 ± 3.2
94.6	61.3 ± 1.8	31.1 ± 2.6
95.9	52.4 ± 1.4	22.4 ± 2.3
145.8	48.5 ± 1.5	24.2 ± 2.1
194.8	42.3 ± 1.0	21.2 ± 1.6
243.4	40.1	21.3
292.5	39.1	21.9

$\text{CD}_4^+ \rightarrow \text{CD}^+$ dissociation cross section data: The second column lists the measured data with their absolute uncertainties. The third column gives data with a functional form ($400 \times 10^{-18}/E$, where E is the energy in eV) subtracted to approximate the cross section for dissociation of a ground-energy molecule. Absolute uncertainties in the third column include the uncertainty in the correction, assuming that the functional form used was correct. Reference: D.C. Gregory *et al.*, unpublished (1989), ref. 39.

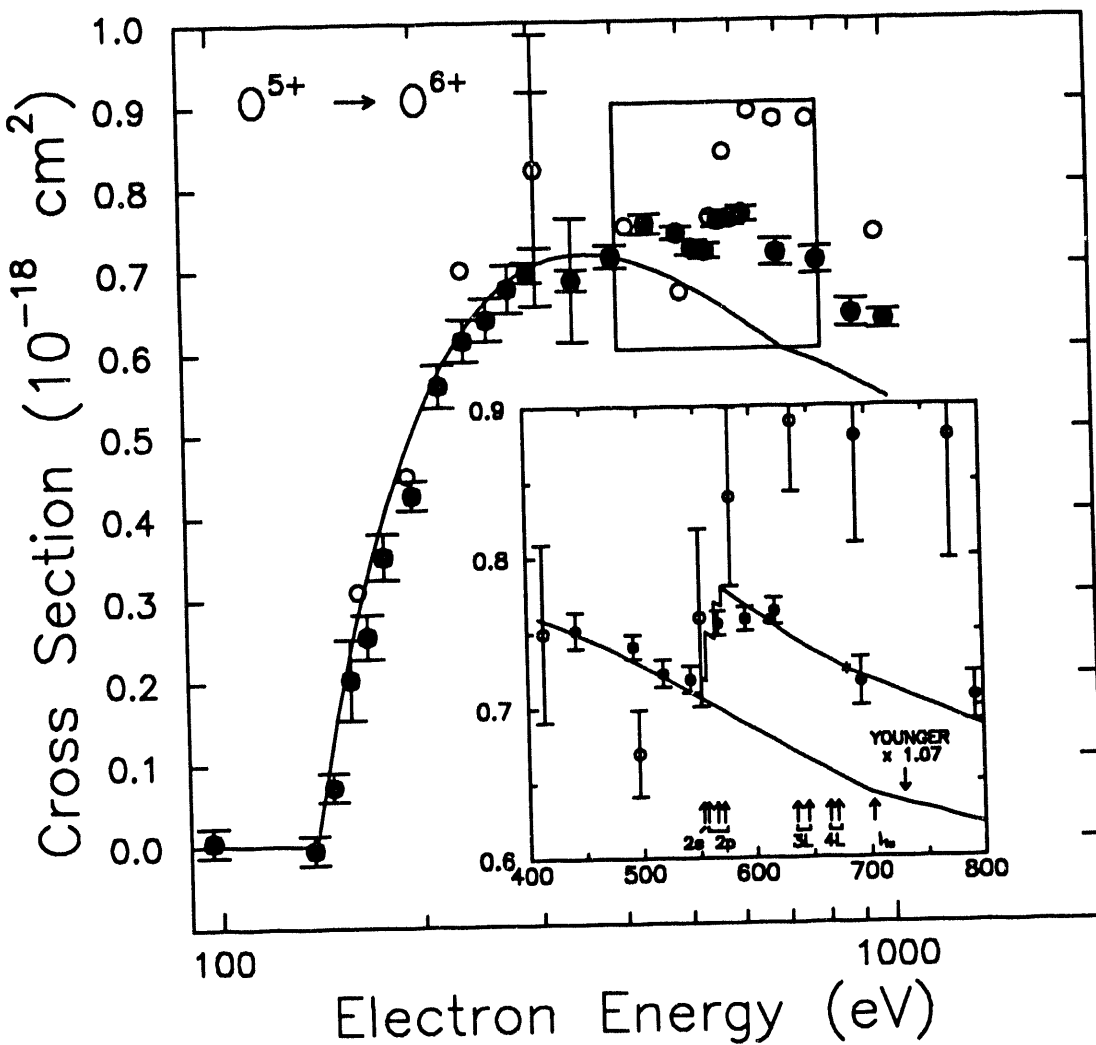
Electron energy (eV)	Ionization cross sections $\sigma (10^{-18} \text{ cm}^2)$	
	Measured data	Data after correction
4.1	103.2 ± 18.0	5.6 ± 20.6
5.0	78.2 ± 16.3	-1.8 ± 18.3
6.9	61.0 ± 10.0	3.0 ± 11.7
8.7	59.0 ± 14.0	13.0 ± 14.8
10.6	79.0 ± 11.0	41.3 ± 11.7
12.4	74.4 ± 7.6	42.1 ± 8.3
14.3	92.8 ± 6.4	64.8 ± 7.0
16.2	122.5 ± 5.4	97.8 ± 6.0
17.5	115.2 ± 4.8	92.3 ± 5.4
17.9	116.0 ± 7.6	93.7 ± 7.9
22.4	106.2 ± 5.2	88.3 ± 5.5
24.8	93.0 ± 2.6	76.9 ± 3.1
27.1	99.2 ± 4.1	84.4 ± 4.4
29.4	91.1 ± 2.0	77.5 ± 2.4
31.6	91.7 ± 3.5	79.0 ± 3.7
33.9	86.7 ± 1.6	74.9 ± 2.0
36.3	90.2 ± 1.5	79.2 ± 1.9
45.3	90.0 ± 1.5	81.2 ± 1.8
54.6	90.1 ± 2.1	82.8 ± 2.2
63.8	85.5 ± 1.2	79.2 ± 1.4
72.8	84.9 ± 1.0	79.4 ± 1.2
82.0	80.8	75.9
91.3	78.4	74.0
137	68.0	65.1
183	64.7	62.5
229	55.5	53.8
275	55.2	53.7

$\text{CD}_4^+ \rightarrow \text{C}^+$ dissociation cross section data: The second column lists the measured data with their absolute uncertainties. The third column gives data with a functional form $36 \times 10^{-18} E^{-1/2}$, where E is the energy in eV, subtracted to approximate the cross section for dissociation of a ground-energy molecule. Absolute uncertainties in the third column include the uncertainty in the correction, assuming that the functional form used was correct. Reference: D.C. Gregory *et al.*, unpublished (1989), ref. 39.

Electron energy (eV)	Ionization cross sections $\sigma (10^{-18} \text{ cm}^2)$	
	Measured data	Data after correction
6.5	16.9 ± 3.0	2.7 ± 3.4
8.4	12.8 ± 2.3	0.4 ± 2.7
9.3	9.3 ± 3.0	-2.6 ± 3.3
11.2	15.4 ± 2.3	4.1 ± 2.6
13.0	20.1 ± 2.9	10.0 ± 3.1
14.0	28.3 ± 2.5	18.6 ± 2.7
16.0	35.6 ± 3.3	26.5 ± 3.5
17.7	37.4 ± 2.0	28.8 ± 2.2
21.1	32.2 ± 3.0	24.3 ± 3.1
27.5	33.0 ± 1.7	26.1 ± 1.9
36.9	31.1 ± 1.2	25.1 ± 1.4
46.2	30.0 ± 1.1	24.7 ± 1.3
52.1	27.2 ± 1.1	22.2 ± 1.2
70.1	28.2 ± 1.9	23.9 ± 2.0
95.0	28.9 ± 0.7	25.2 ± 0.8
121.5	26.0 ± 1.1	22.7 ± 1.2
146.0	24.6 ± 0.6	21.6 ± 0.7
194.8	22.3 ± 0.4	19.7 ± 0.5
243.5	19.3 ± 0.4	17.0 ± 0.5
292.6	18.7 ± 0.4	16.6 ± 0.5

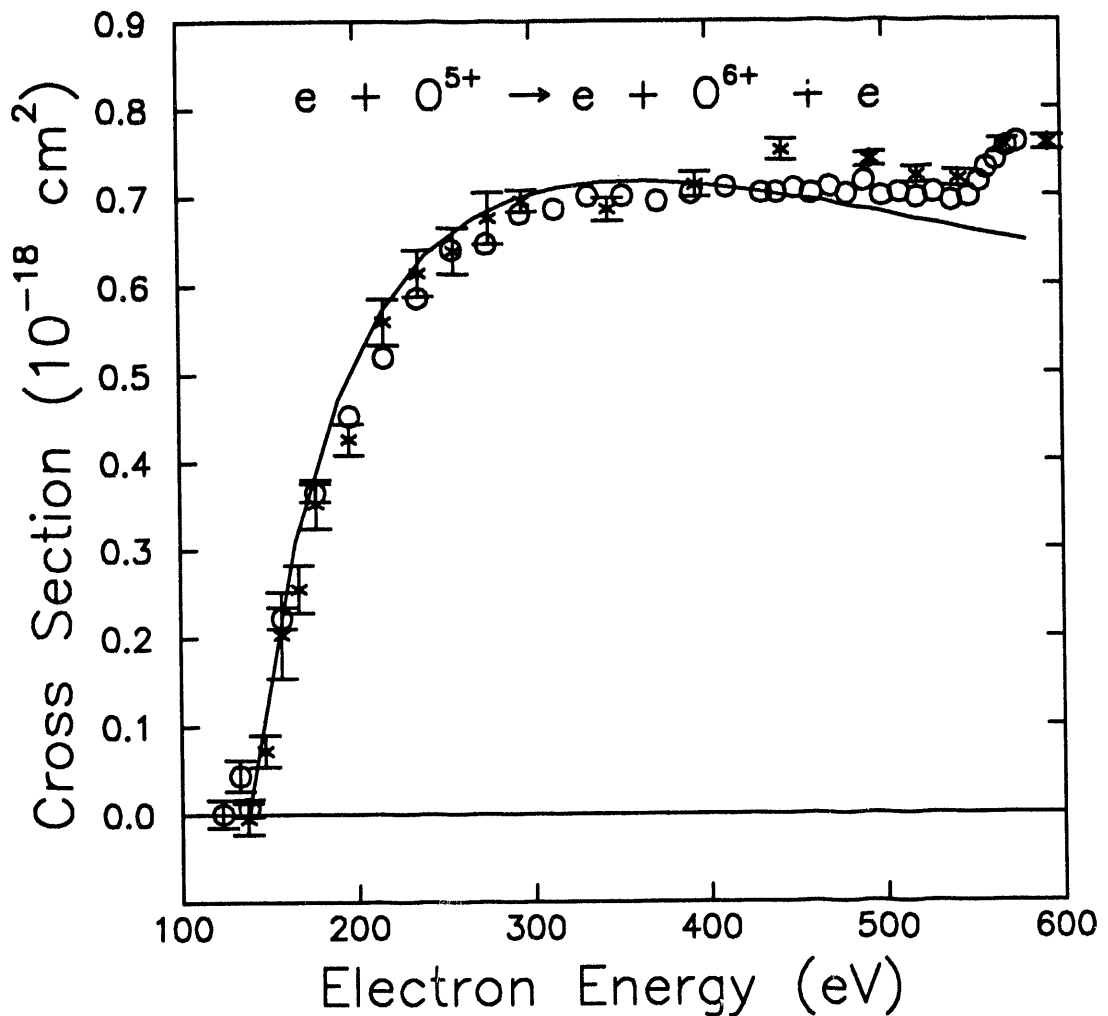
FIGURES

ORNL-DWG 92-5759

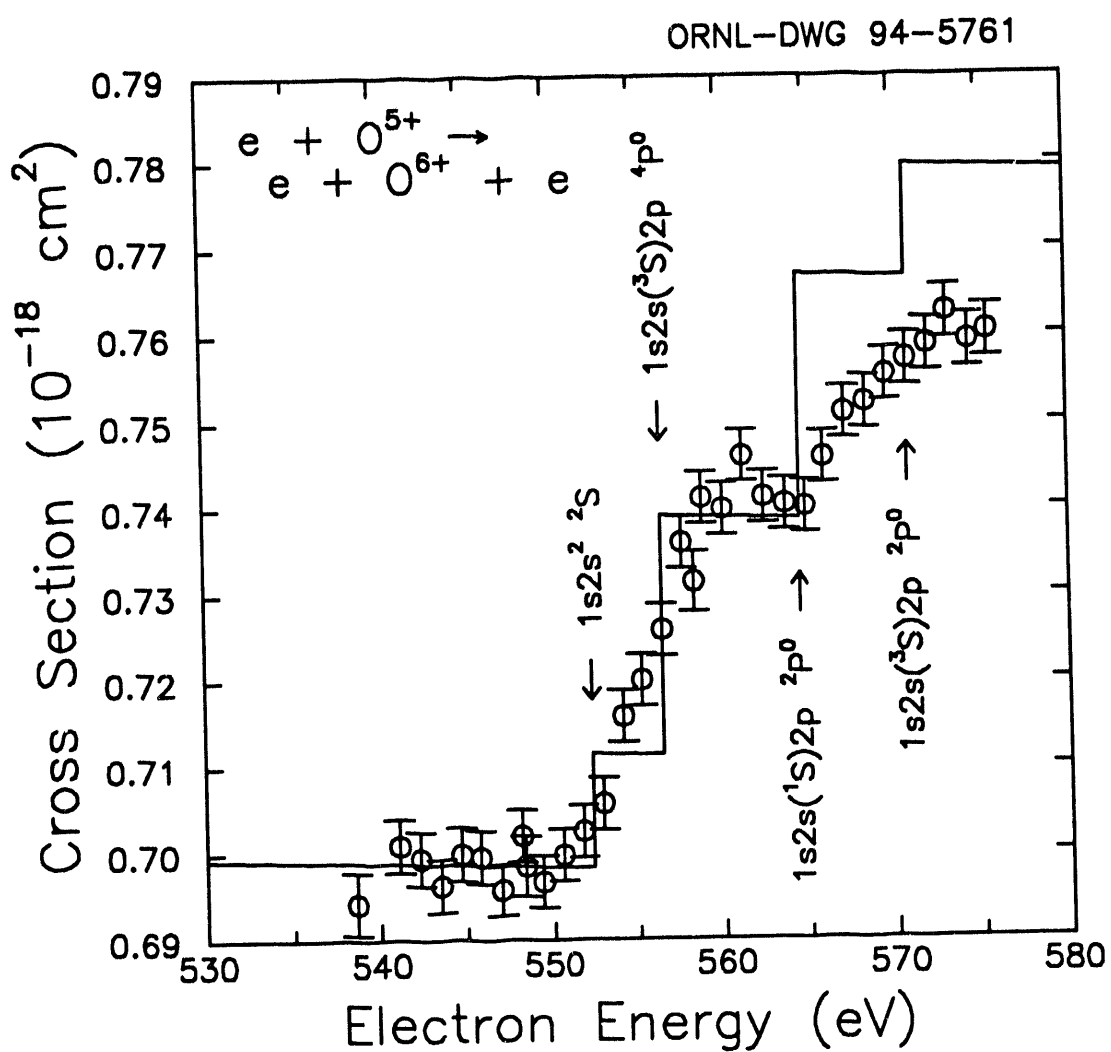


Electron-impact ionization of O^{5+} . Solid points are present experiment [D. H. Crandall *et al.*, Phys. Rev. A 34, 1757 (1986)] with relative uncertainties at one standard deviation except outer bars on point at 344 eV which are absolute uncertainty at 90%-confidence level. Open circles are previous experimental results with one-standard-deviation relative uncertainties. Solid curve is a distorted wave (DW) direct ionization calculation by Younger. The inset shows the excitation-autoionization region in greater detail with Younger's DW direct ionization multiplied by 1.07 to obtain the best fit to the data between 400 and 550 eV. The inset includes Henry's calculation for $1s^2 2s \rightarrow \Sigma, 1s 2s 2l$ excitation as a solid line added to the renormalized DW calculations. Actual excitation calculations are indicated by "X" on the figure.

ORNL-DWG 94-5760

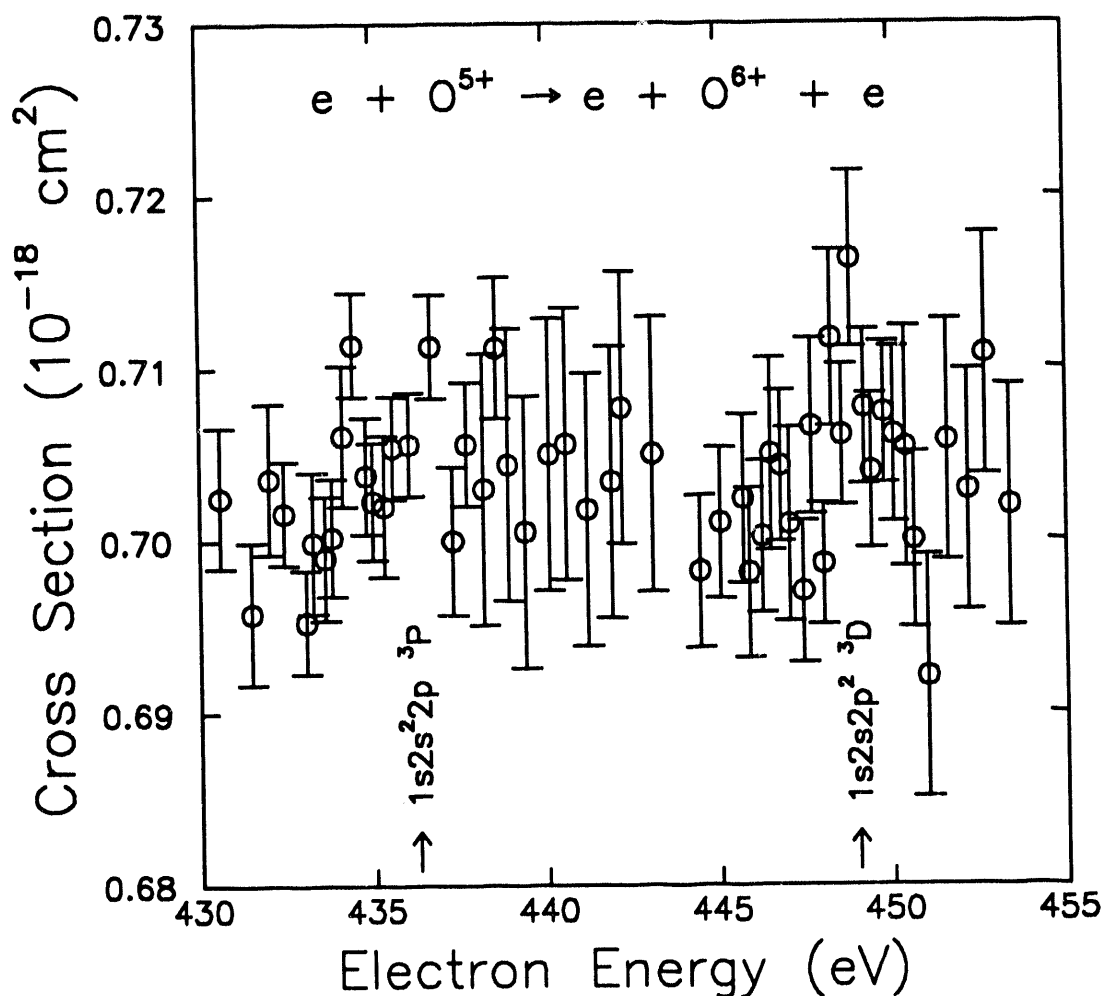


Cross section vs. interaction energy for electron-impact ionization of O^{5+} . The circles are present results [K. Rinn *et al.*, Phys. Rev. A 36, 595 (1987)] with one-standard-deviation relative uncertainties shown where larger than the symbol. The crosses are previous experimental results with typical relative uncertainties. Several distorted-wave calculations are represented by one curve since on the scale of this figure the theoretical results are indistinguishable.



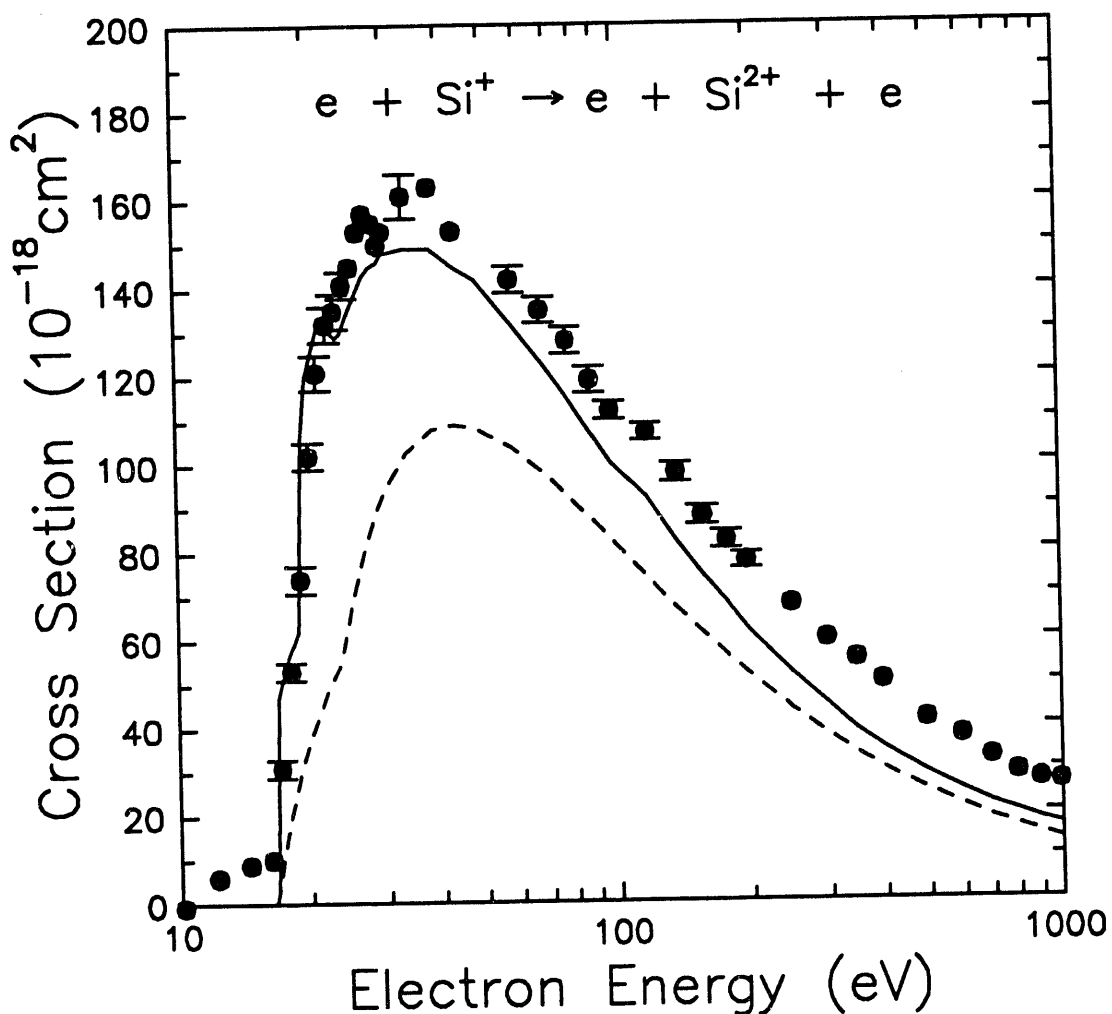
Ionization of O^{5+} . Energy range from 530-580 eV in more detail [K. Rinn *et al.*, Phys. Rev. A 36, 595 (1987)]. The onsets of the transitions leading to excitation-autoionization are marked. The transition strengths are based on excitation calculations by Henry.

ORNL-DWG 94-5762



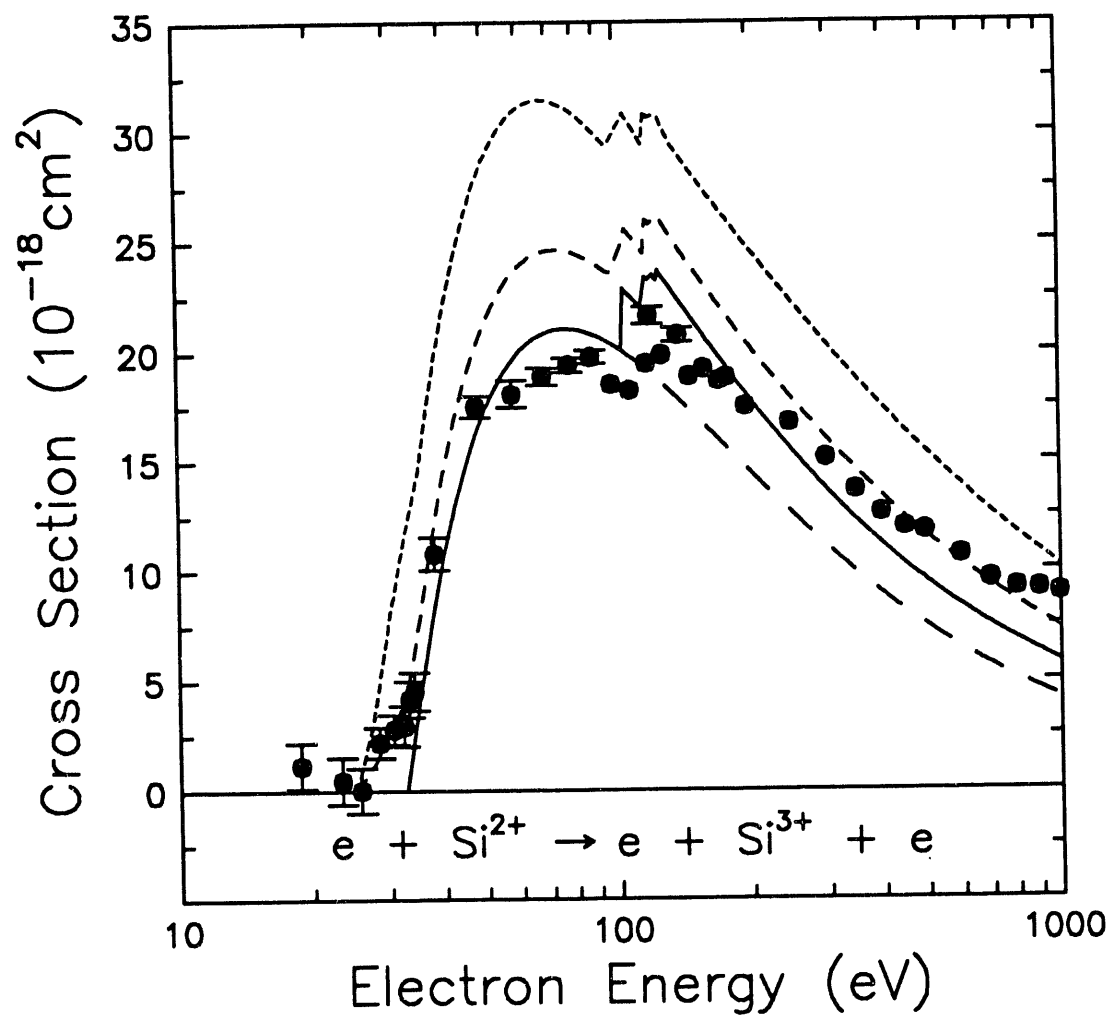
Ionization of O^{5+} . Energy range from 430-455 eV [K. Rinn *et al.*, Phys. Rev. A 36, 595 (1987)]. For reasons of clarity these results have been omitted from the previous two figures. Plotted uncertainties are one-standard-deviation relative only. The energies for two levels which could lead to the resonant excitation auto-double ionization (READI) process in this range are indicated.

ORNL-DWG 94-5763



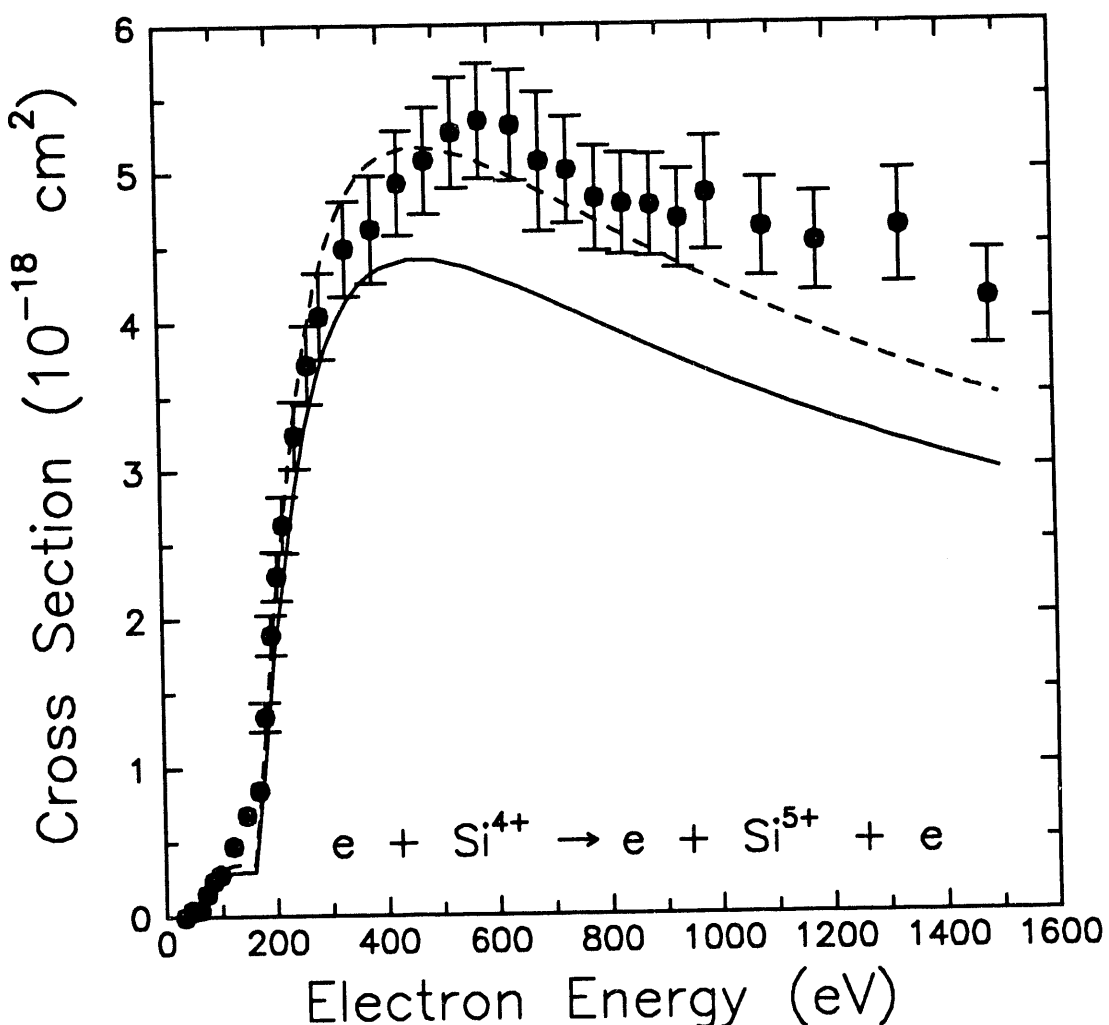
Absolute cross section vs. electron energy for electron-impact single ionization of Si^+ . The solid circles represent the measured cross sections [N. Djurić *et al.*, Phys. Rev. A 47, 4786 (1993)] and the error bars represent total relative uncertainties at a 90%-confidence level. The solid line is a distorted-wave (DW) calculation for total ionization while the dashed line is a DW calculation for direct ionization only.

ORNL-DWG 92-13472



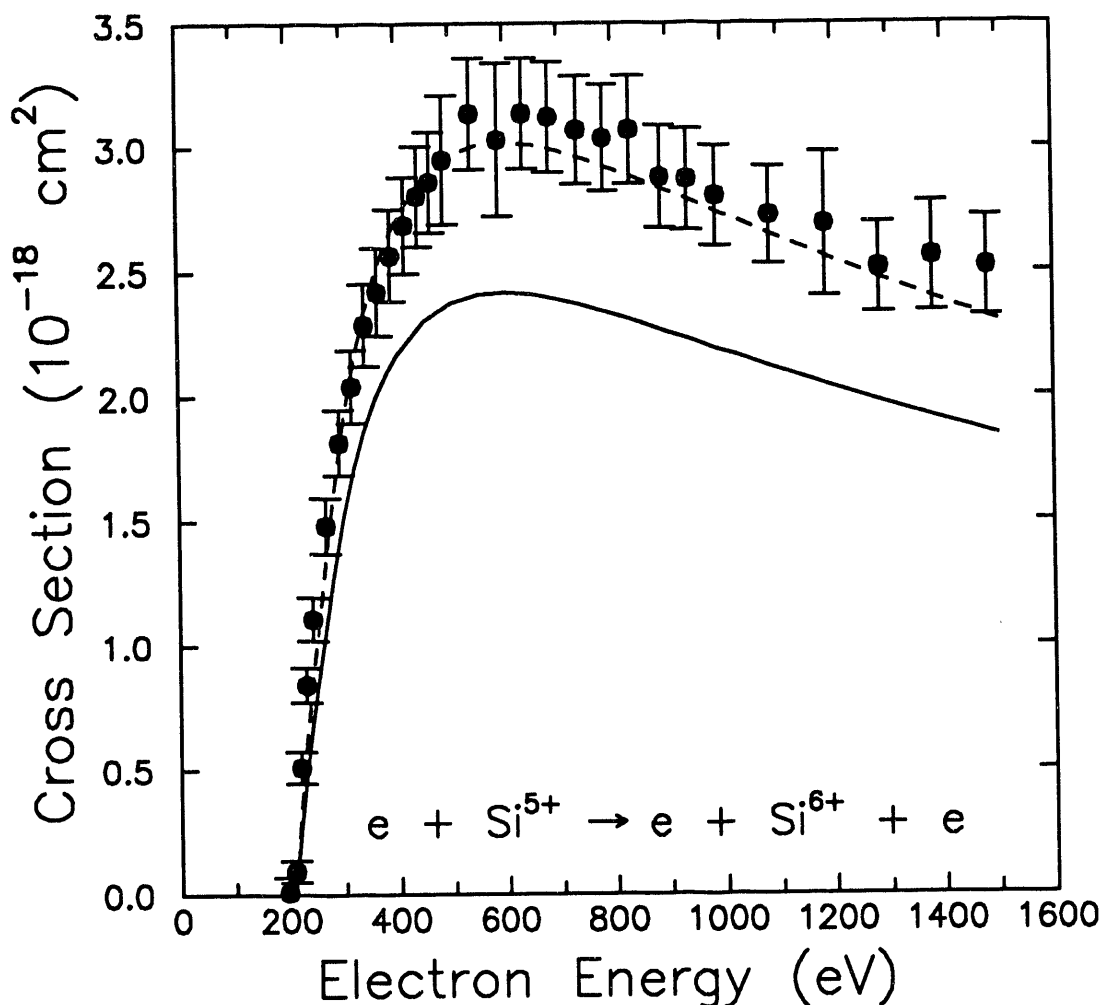
Absolute cross section vs. electron energy for electron-impact single ionization of Si^{2+} . The solid circles represent the measured cross sections [N. Djurić *et al.*, Phys. Rev. A 47, 4786 (1993)] and the error bars represent total relative uncertainties at a 90%-confidence level. The solid and long dashed lines are distorted-wave (DW) calculations for total ionization and direct ionization only, respectively, for the $3s^2$ ground configuration. The short dashed line is a DW calculation for total ionization of the $3s3p$ metastable configuration. The medium dashed line represents a DW calculation for total ionization assuming a mix of 65% ground state ions and 35% metastable ions.

ORNL-DWG 92-13474



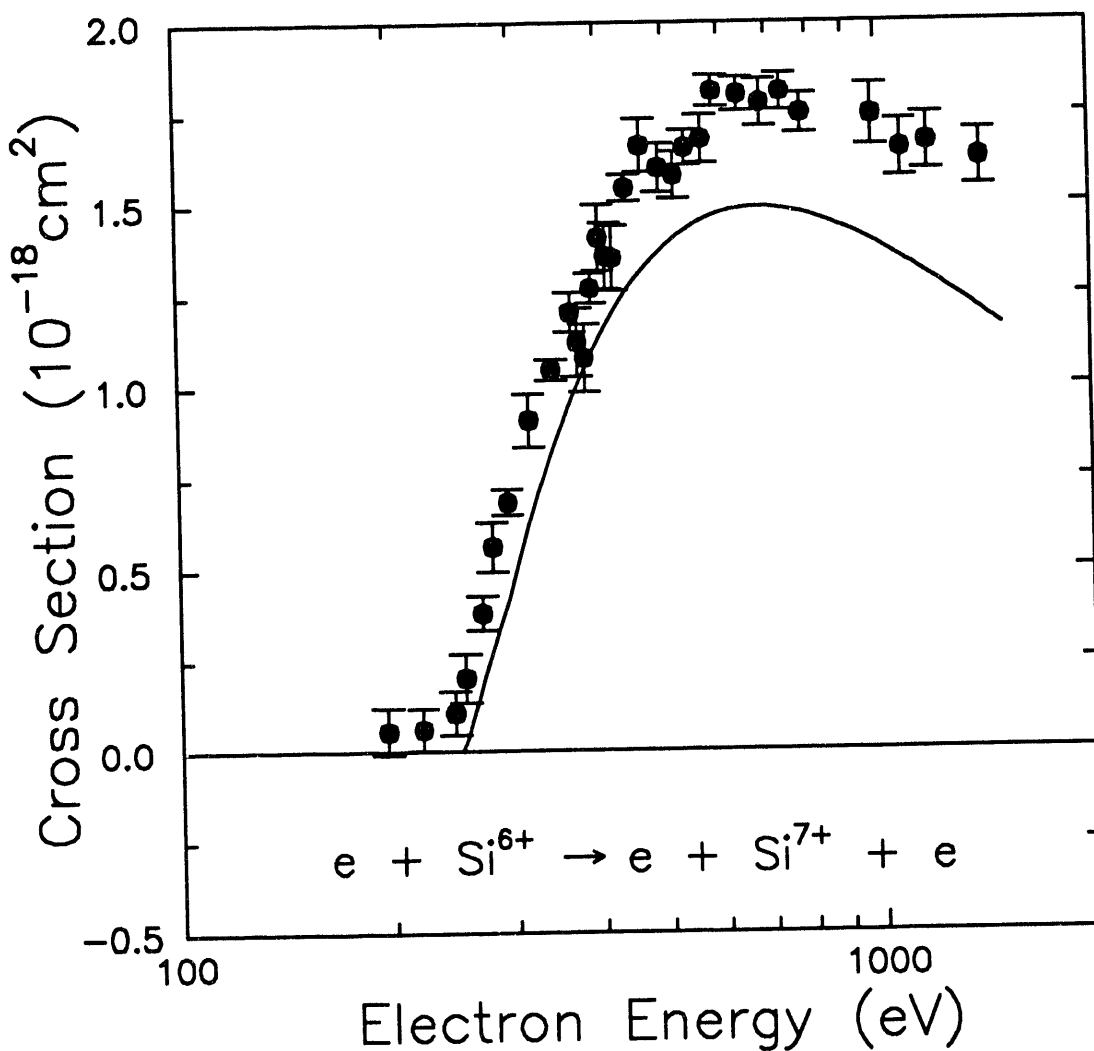
Absolute cross sections for electron-impact single ionization of Si^{4+} as a function of incident electron energy. The solid circles represent the measured cross sections [J. S. Thompson *et al.*, Phys. Rev. A, to be published (August 1994)]. The error bars represent absolute uncertainties at the 90%-confidence level. The solid line represents the Lotz cross section with 5% of the incident ion beam in the $(1s^2 2s^2 2p^5 3s)$ metastable state. The dashed line is the Lotz cross section times 1.17.

ORNL-DWG 92-13475



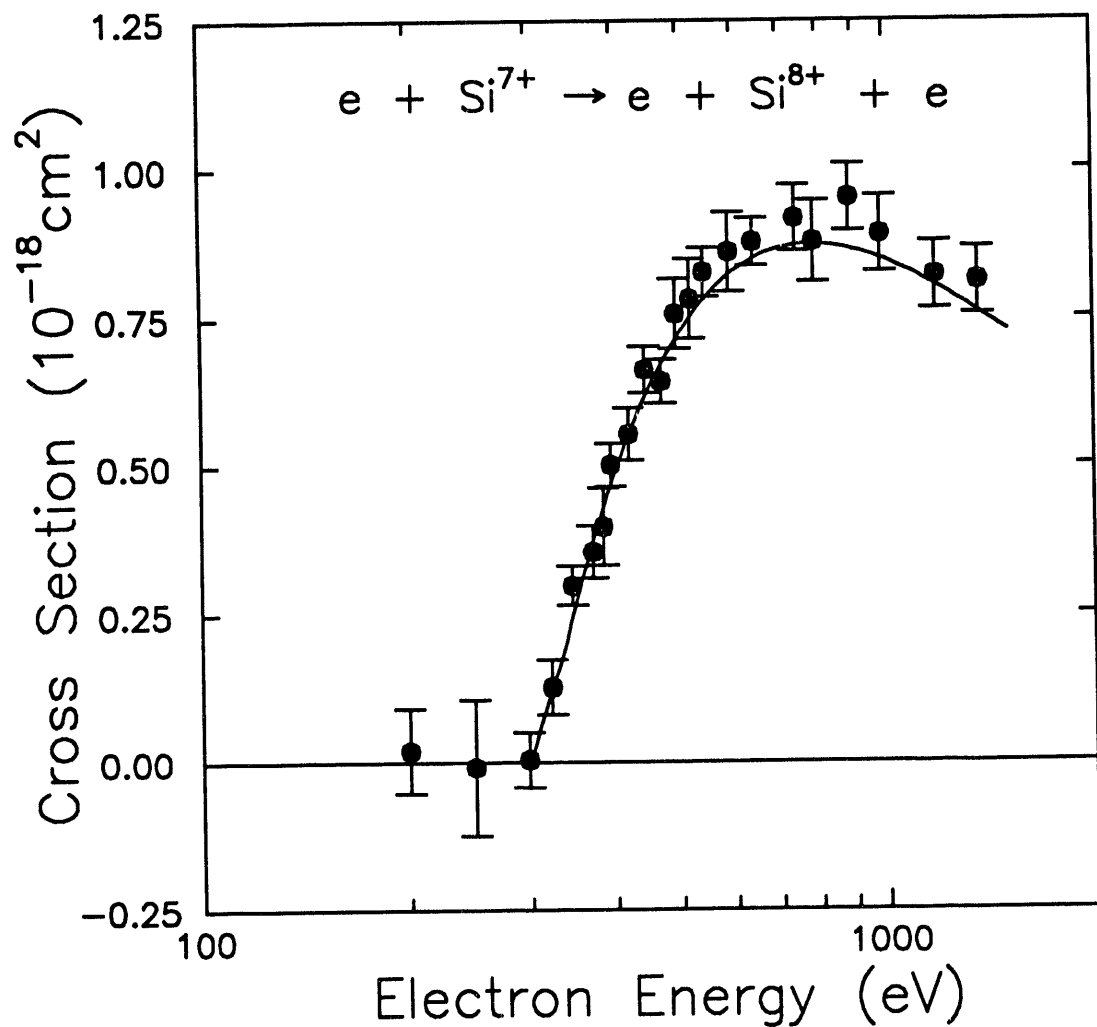
Absolute cross sections for electron-impact single ionization of Si^{5+} as a function of incident electron energy. The solid circles represent the measured cross sections [J. S. Thompson *et al.*, Phys. Rev. A, to be published (August 1994)]. The error bars represent absolute uncertainties at the 90%-confidence level. The solid line represents the Lotz cross section. The dashed line is the Lotz cross section times 1.25.

ORNL-DWG 92-13476



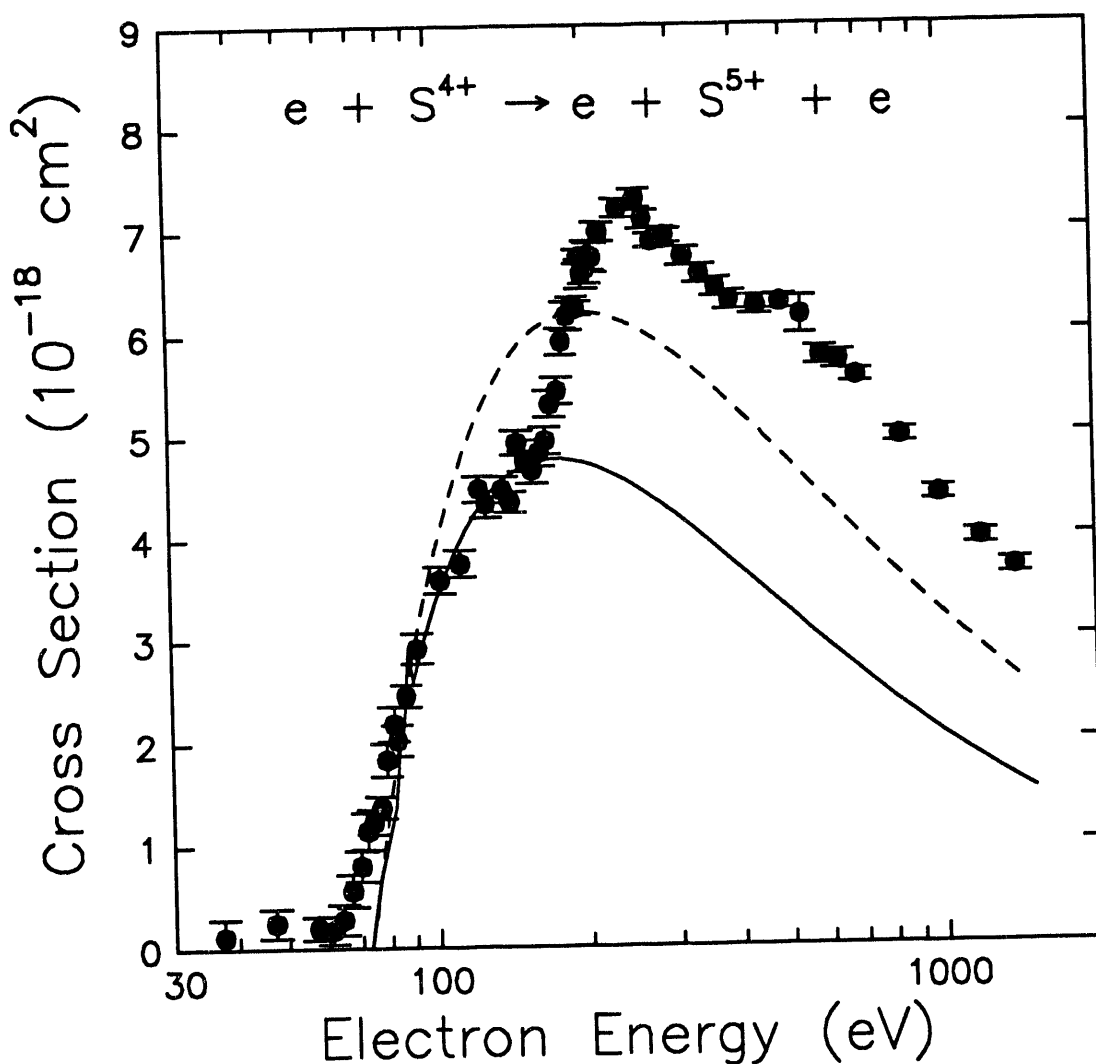
Absolute cross sections as a function of electron-impact energy for single ionization of Si^{6+} . The present experimental results are indicated by solid circles [P. A. Zeijlmans van Emmichoven *et al.*, Phys. Rev. A 47, 2888 (1993)]. Relative uncertainties are shown at the one-standard-deviation level. Results of distorted-wave calculations by Pindzola for direct ionization are indicated by the solid curve.

ORNL-DWG 92-13477



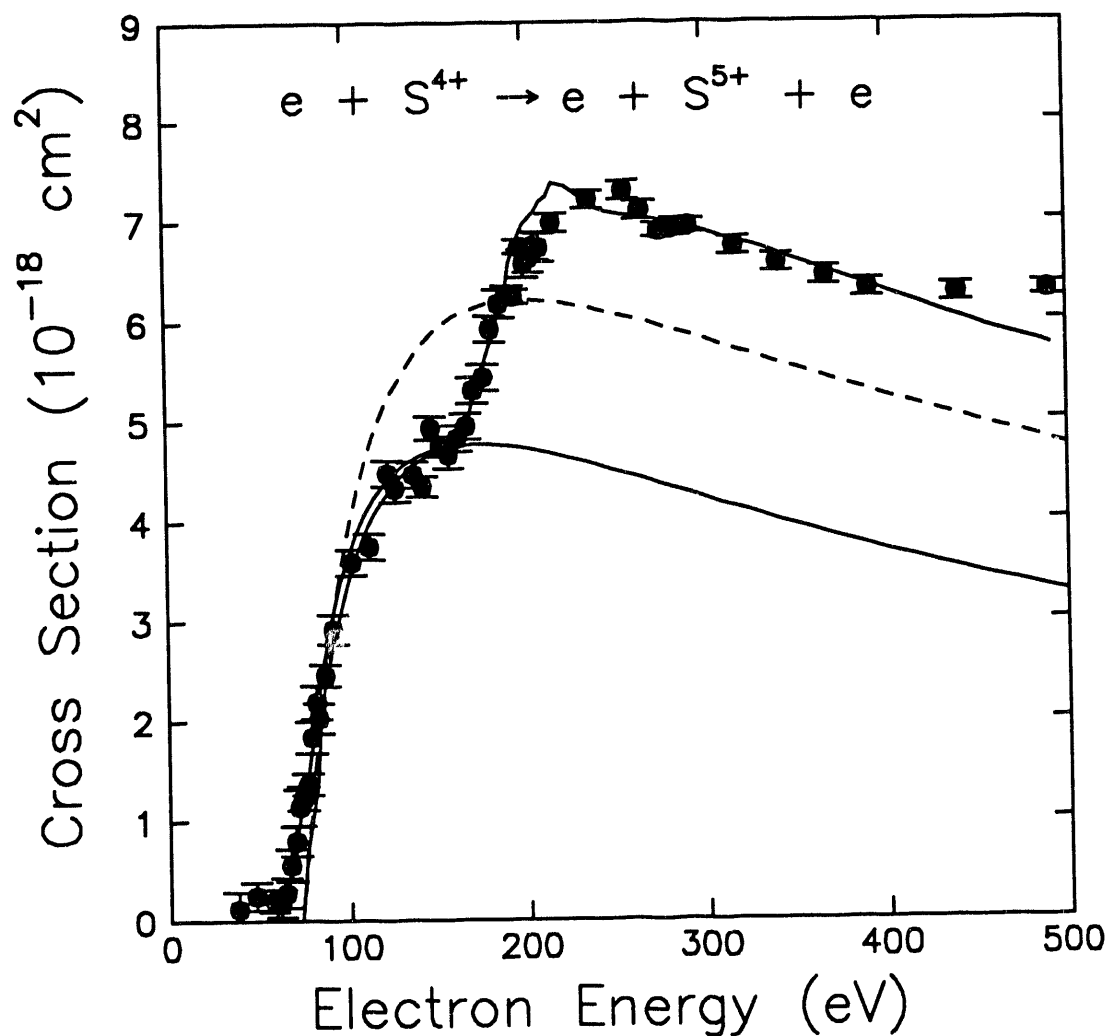
Absolute cross sections as a function of electron-impact energy for single ionization of Si^{7+} . The present experimental results are indicated by solid circles [P. A. Zeijlmans van Emmichoven *et al.*, Phys. Rev. A 47, 2888 (1993)]. Relative uncertainties are shown at the one-standard-deviation level. Results of distorted-wave calculations by Pindzola for direct ionization are indicated by the solid curve.

ORNL-DWG 94-5764

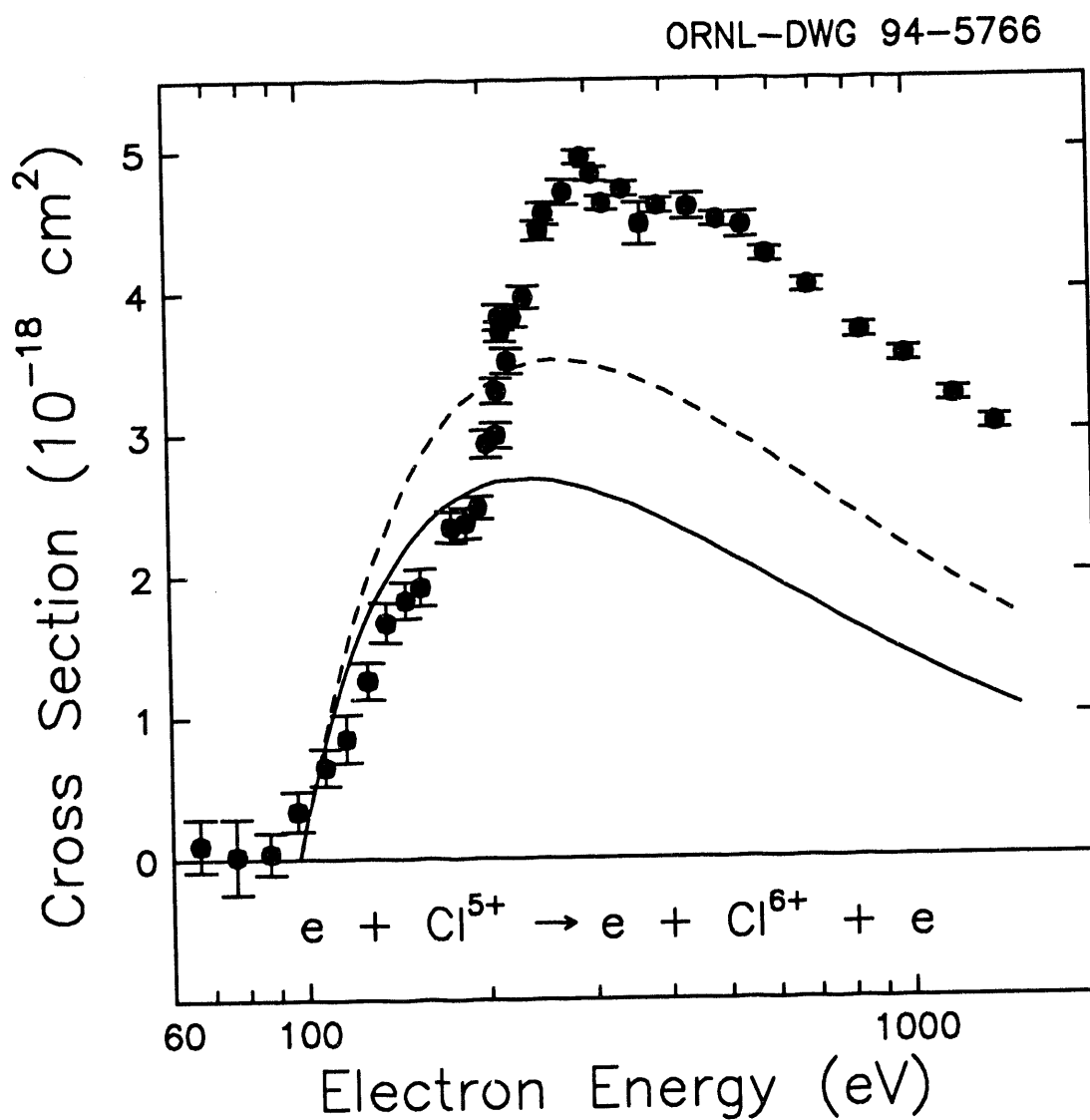


Cross sections for electron-impact ionization of S^{4+} . Experiment: •, present results [A. M. Howald *et al.*, Phys. Rev. A 33, 3779 (1986)]. Theory: - - -, Lotz semiempirical formula; —, distorted-wave result for Ar^{6+} scaled for S^{4+} . The change in slope near 160 eV in the experimental data is attributed to the onset of $2p-nl$ excitation-autoionization.

ORNL-DWG 94-5765

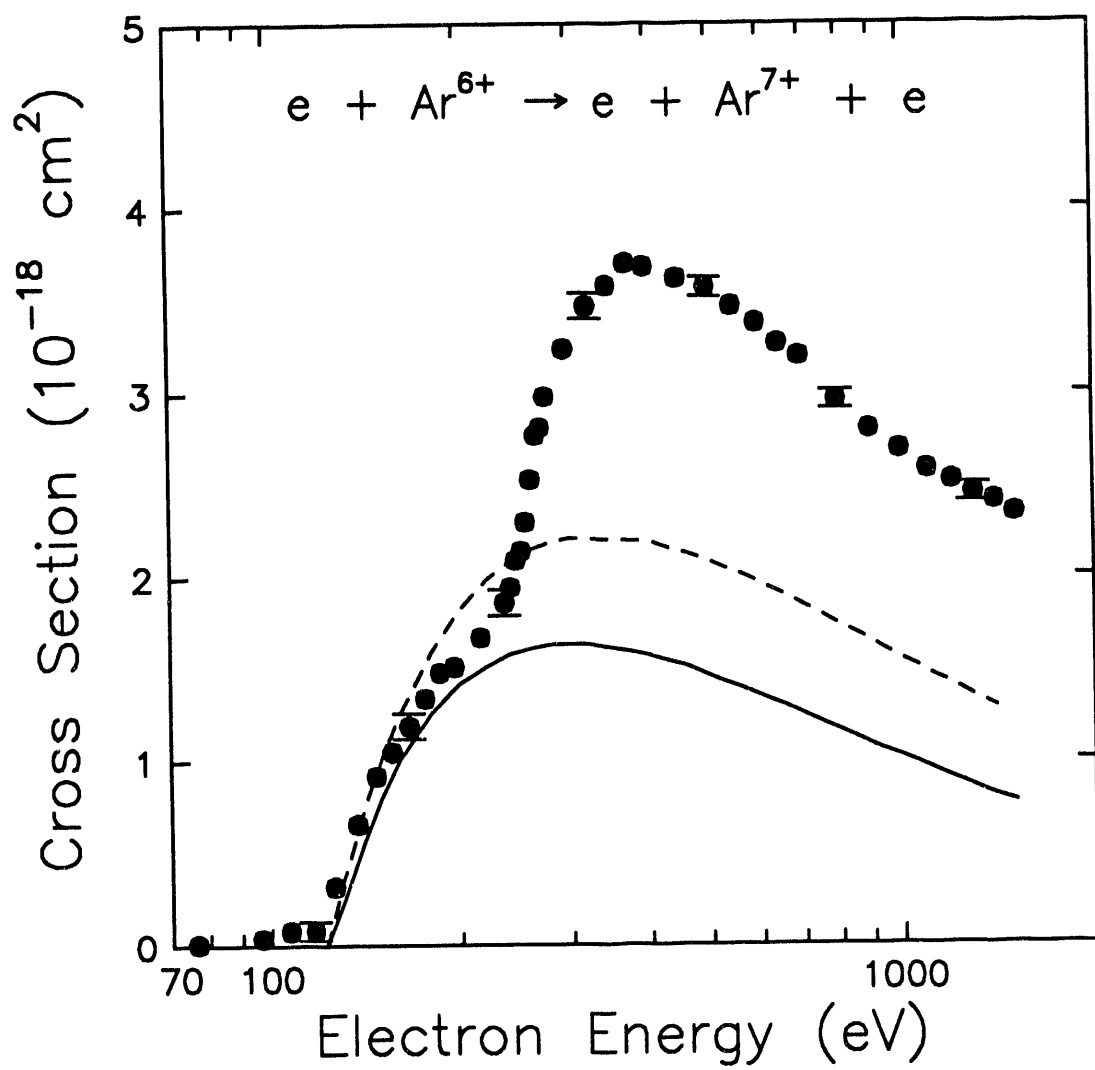


Low-energy cross sections for electron-impact ionization of S^{4+} . Experiment: •, present results [A. M. Howald *et al.*, Phys. Rev. A 33, 3779 (1986)]. Theory: - - -, Lotz semiempirical formula, — (lower), distorted-wave (DW) result for Ar^{5+} by Younger scaled for S^{4+} , — (upper), DW result by Griffin for metastable S^{4+} including excitation-autoionization.



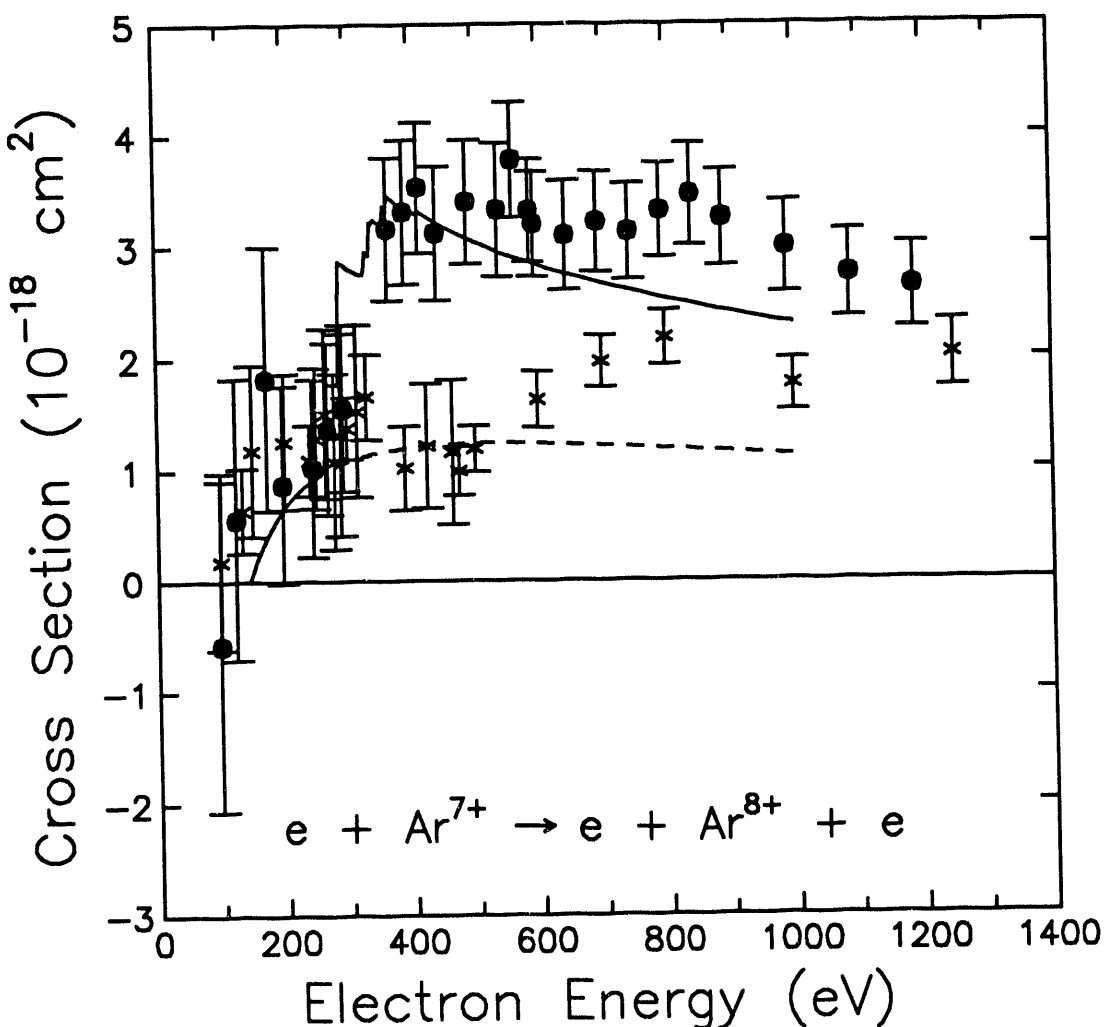
Cross sections for electron-impact ionization of Cl^{5+} . Experiment: •, present results [A. M. Howald *et al.*, Phys. Rev. A 33, 3779 (1986)]. Theory: - - -, Lotz semiempirical formula; —, distorted-wave result for Ar^{6+} by Younger scaled for Cl^{5+} . The change in slope near 200 eV in the experimental data is attributed to the onset of 2p-*nl* excitation-autoionization.

ORNL-DWG 94-5767



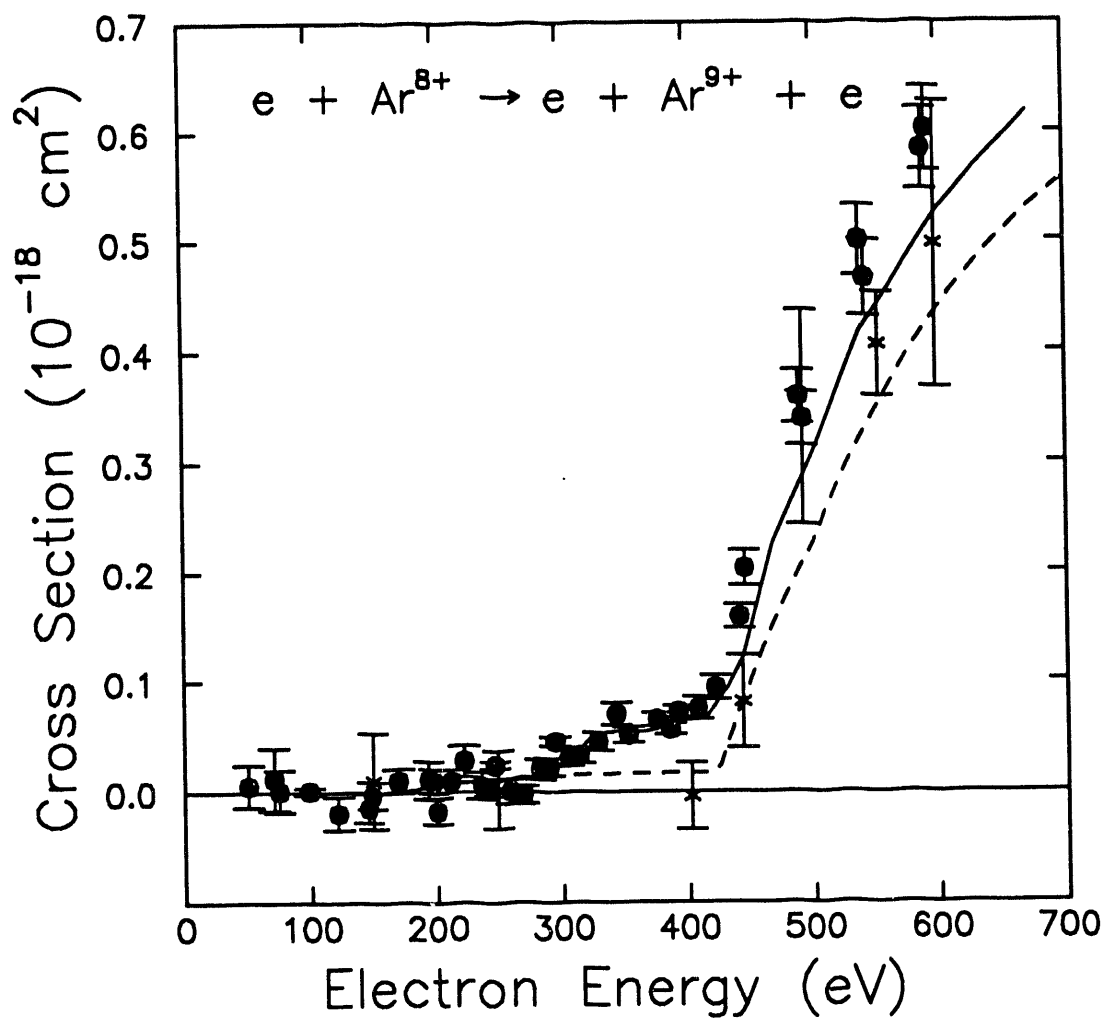
Cross sections for electron-impact ionization of Ar^{6+} . Experiment: •, present results [A. M. Howald *et al.*, Phys. Rev. A 33, 3779 (1986)]. Theory: - - -, Lotz semiempirical formula; —, distorted-wave calculation by Younger with exchange. The change in slope near 240 eV in the experimental data is attributed to the onset of 2p-*nl* excitation-autoionization.

ORNL-DWG 92-13478



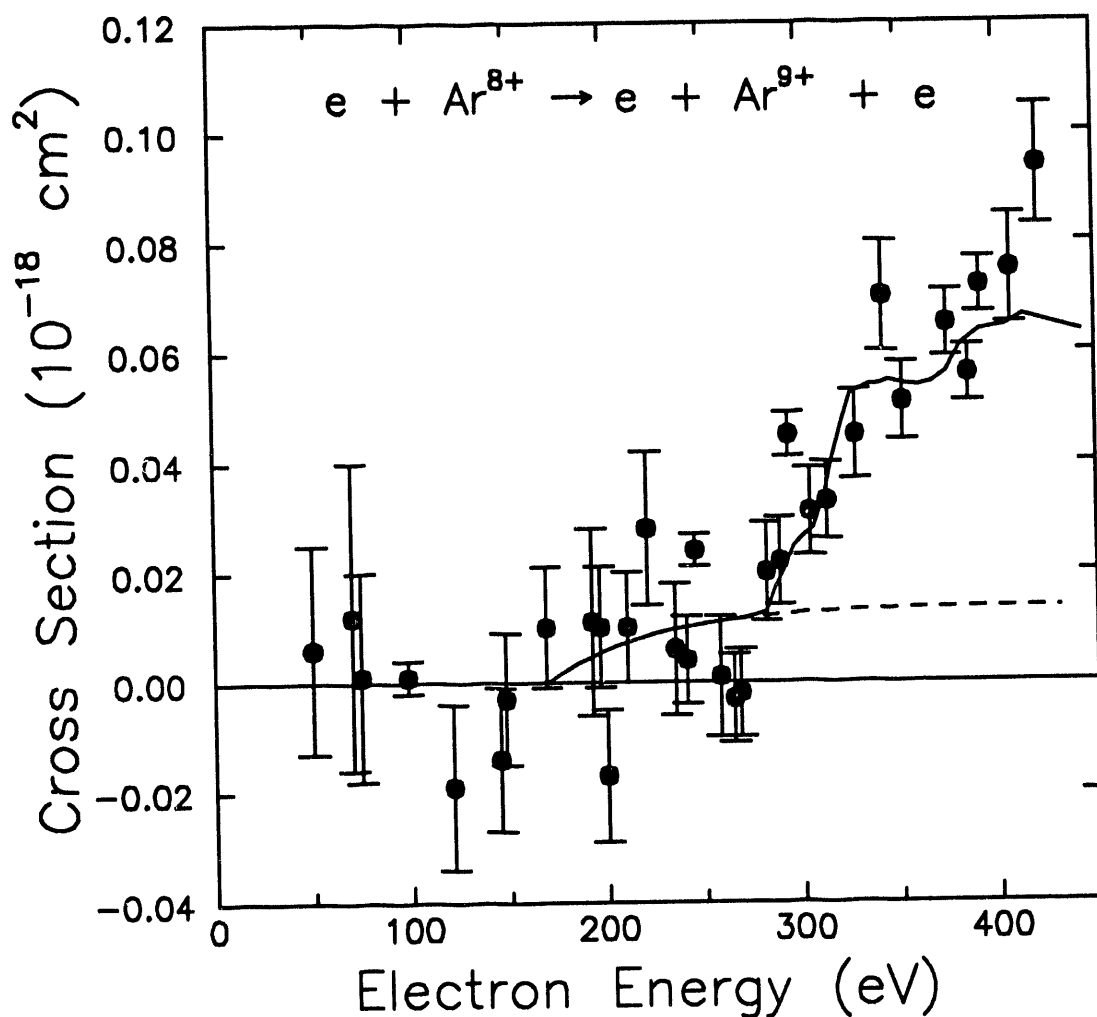
Ionization of Ar^{7+} . Cross sections near and above the direct-ionization threshold. Closed circles, present measurement with corrections for space-charge modulation and metastable ions [Y. Zhang *et al.*, Phys. Rev. A 45, 2929 (1992)]; crosses, measurements of Defrance *et al.*; solid line, distorted-wave calculations by Griffin *et al.* including excitation-autoionization from the ground state; short-dashed line, distorted-wave calculation with only 3s direct ionization.

ORNL-DWG 94-5768



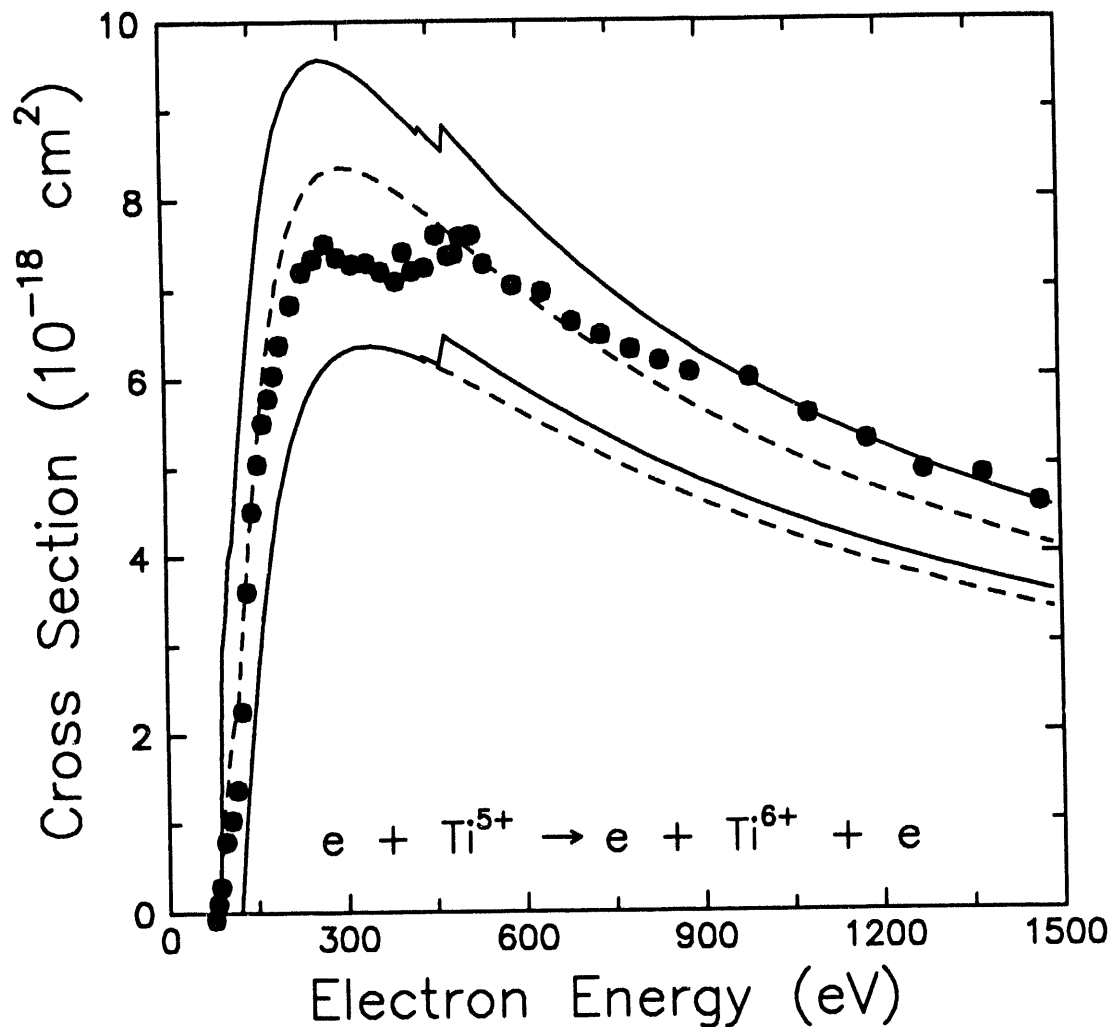
Total ionization cross sections for Ar⁸⁺. Solid circles, present measurements [Y. Zhang *et al.*, Phys. Rev. A **44**, 4368 (1991)]; crosses, previous measurements by Defrance *et al.*; dashed line, calculation for direct ionization using the Lotz formula; solid line, distorted wave calculation by Pindzola *et al.*. Both the Lotz and distorted-wave calculations assume 97% of the target ions in the ground configuration and 3% of the ions in the 2p⁵3s metastable configuration.

ORNL-DWG 92-13479



Ionization cross section for Ar^{8+} below the ground-configuration direct ionization threshold. Solid circles, present measurements [Y. Zhang *et al.*, Phys. Rev. A 44, 4368 (1991)]; dashed line, distorted-wave calculation of direct ionization by Pindzola *et al.*; solid line, distorted-wave calculation for total ionization. Both calculations assume 3% population fraction of metastable ions.

ORNL-DWG 94-5769



Electron-impact ionization cross section for Ti^{5+} . Solid points are the present measurements [S. J. Chantrenne *et al.*, Phys. Rev. A 41, 140 (1990)]; relative uncertainties at the one-standard-deviation level are smaller than the plotted points and have not been included in the graph. The two lower curves represent distorted-wave calculations for direct ionization only (dashed curve) and direct ionization plus excitation-autoionization (solid curve) assuming the ions are initially in the ground state. The two upper curves correspond to the same processes for 100% of the ions initially in the $3s^23p^43d$ metastable configuration.



AIIM

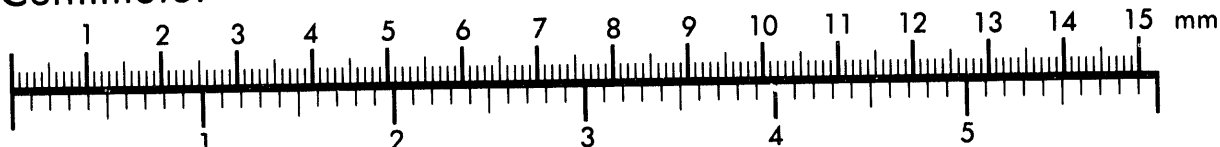
Association for Information and Image Management

1100 Wayne Avenue, Suite 1100

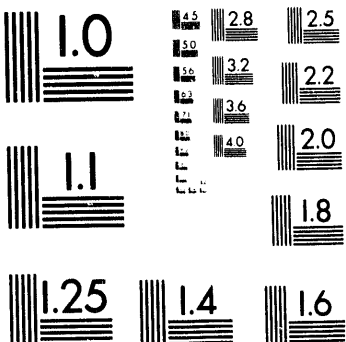
Silver Spring, Maryland 20910

301/587-8202

Centimeter

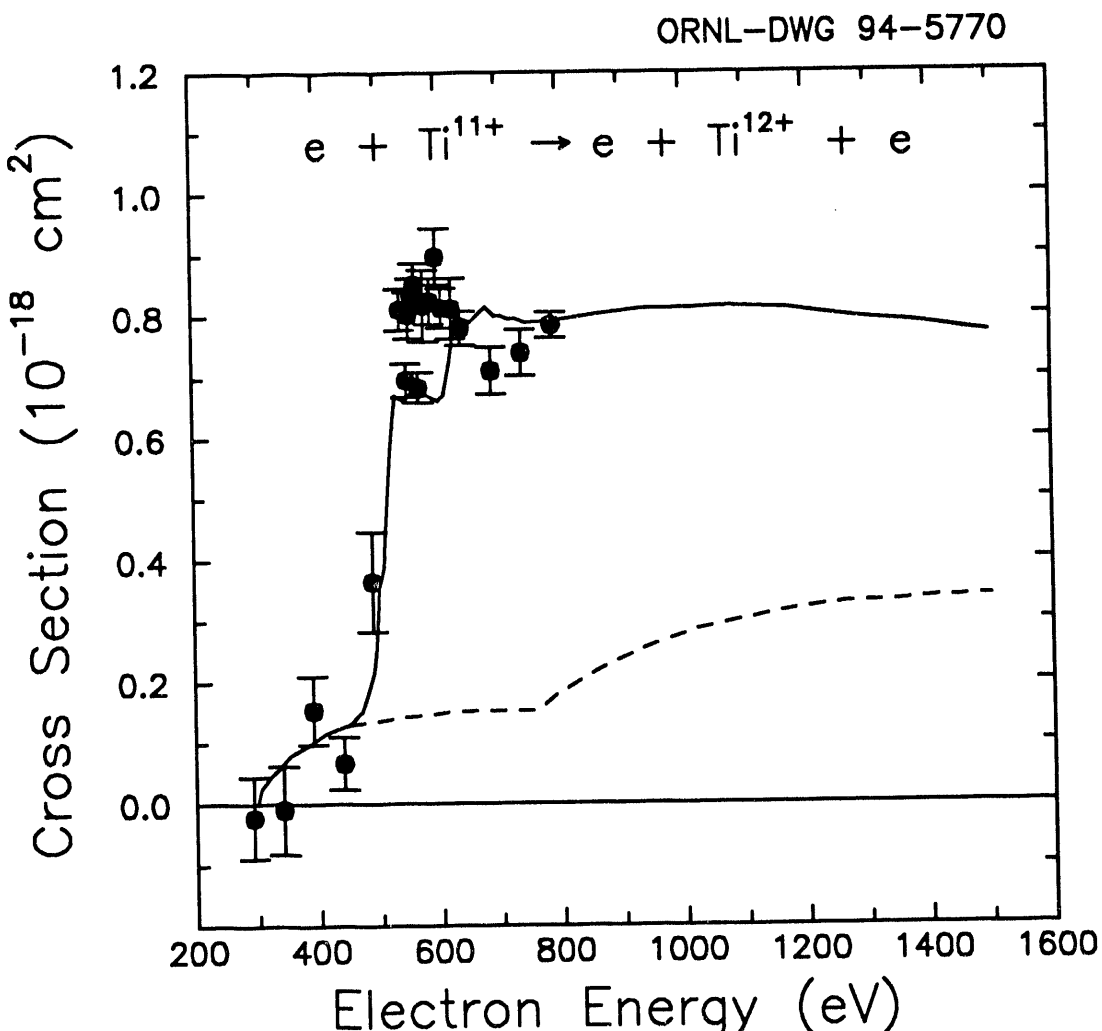


Inches



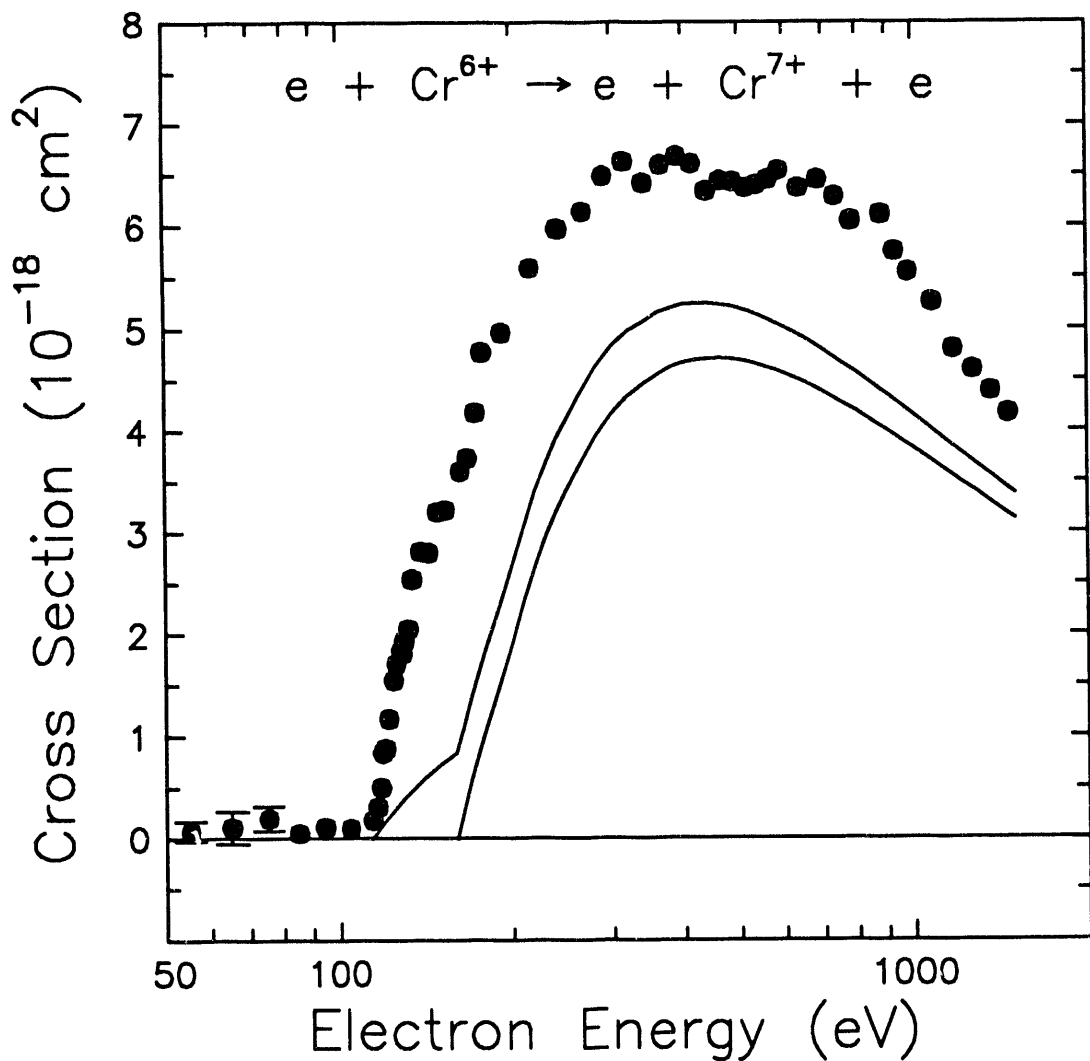
MANUFACTURED TO AIIM STANDARDS
BY APPLIED IMAGE, INC.

2 of 2



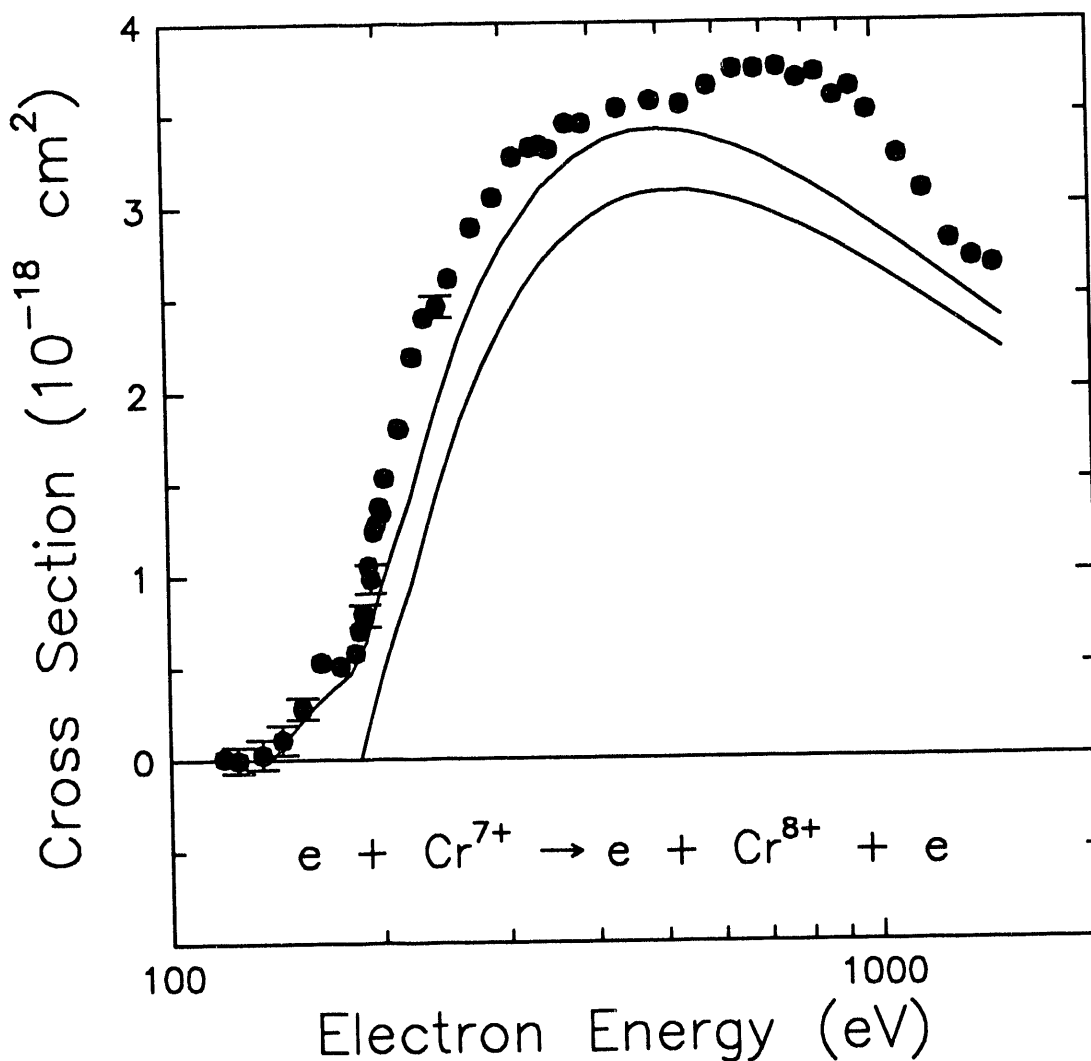
Electron-impact ionization cross section of Ti^{11+} . The solid points are the present data [D. C. Gregory *et al.*, Phys. Rev. A **41**, 6512 (1990)]; the dashed curve is a distorted-wave calculation for direct ionization only, while the solid curve includes excitation-autoionization (Griffin *et al.*). Uncertainties are relative at the one-standard-deviation level.

ORNL-DWG 94-5771



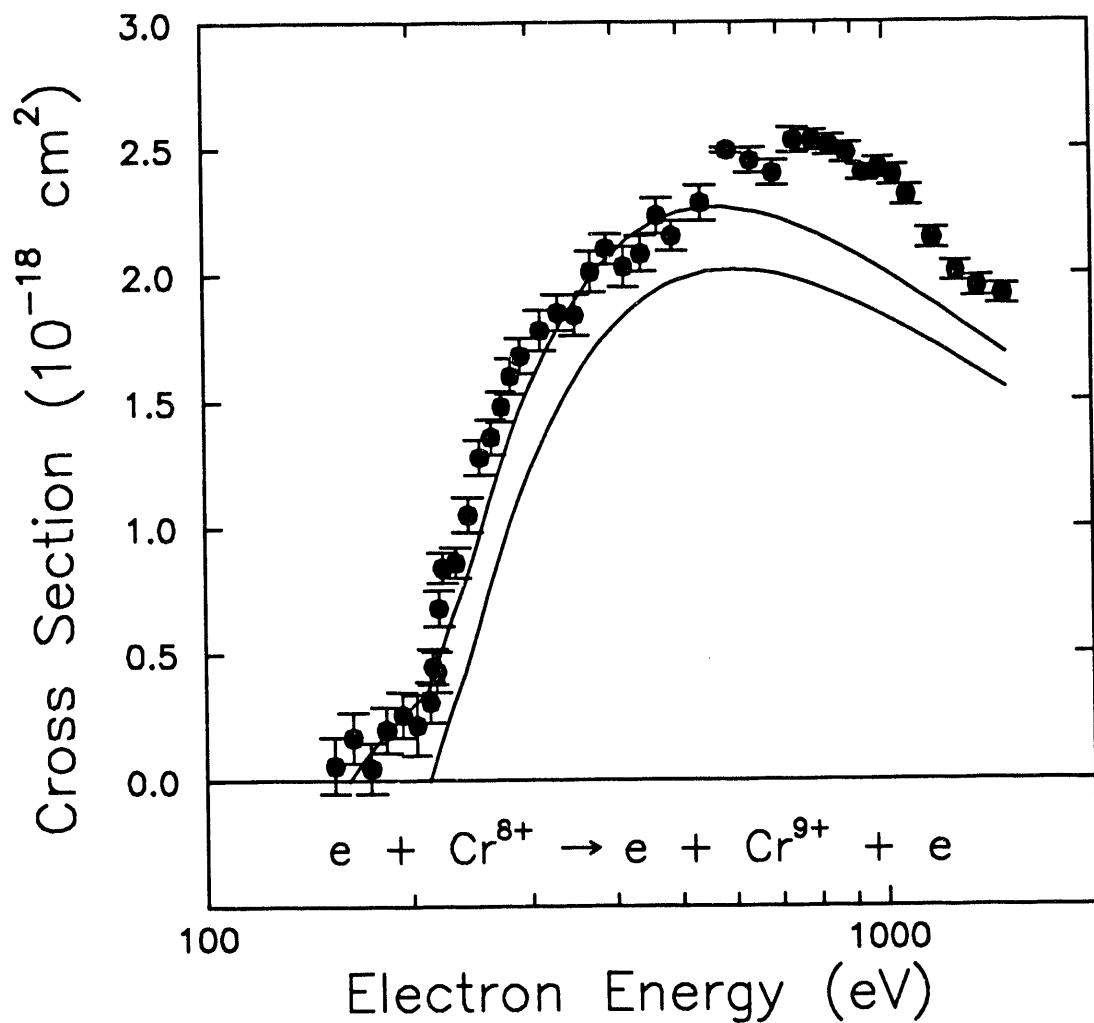
Electron-impact ionization cross section of Cr^{6+} . The closed circles are the present experiments [M. Sataka *et al.*, Phys. Rev. A 39, 2397 (1989)]; relative uncertainties for experimental data are plotted at the one-standard-deviation level where they are larger than the plotted circles. The solid curves are Lotz calculations for direct ionization from the ground- (lower curve) and metastable-state (upper curve) configurations.

ORNL-DWG 94-5772



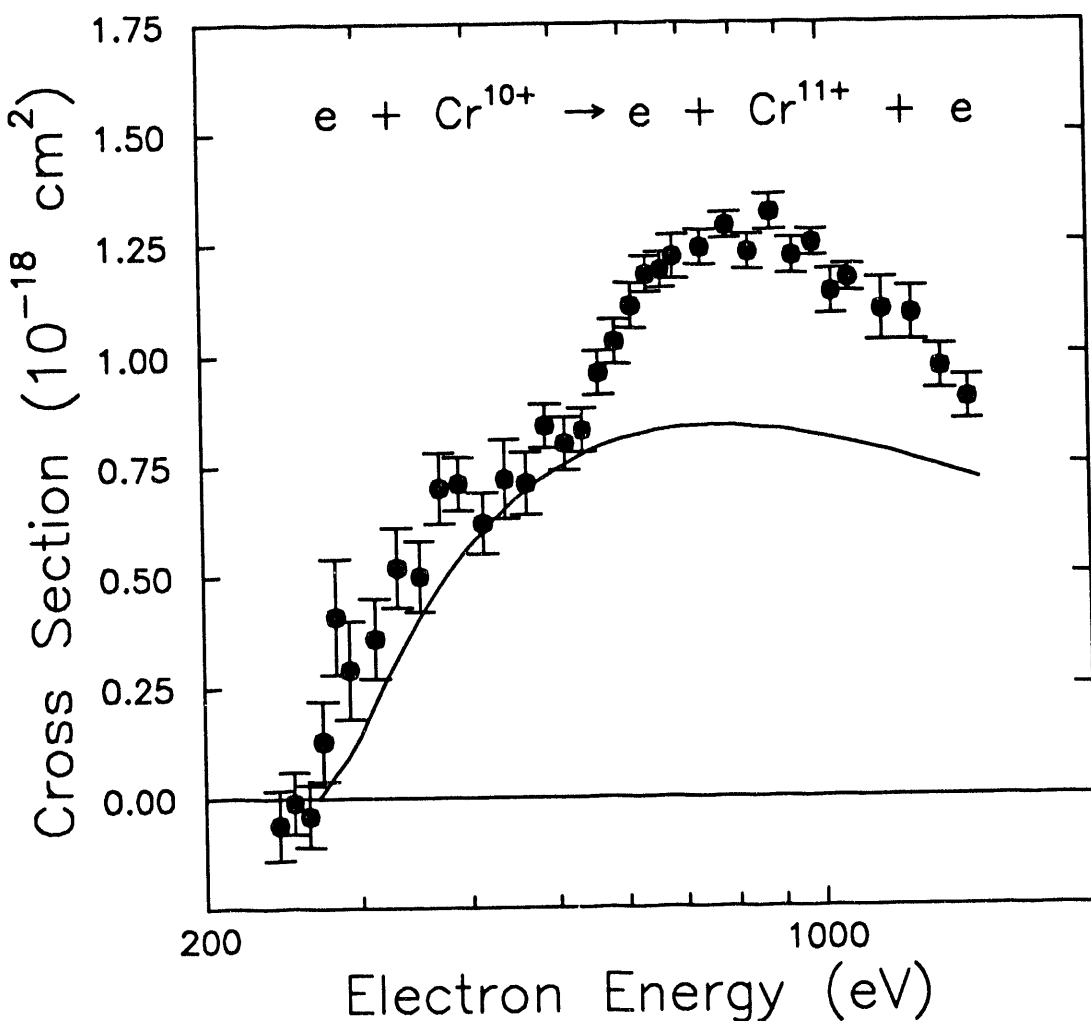
Electron-impact ionization cross section of Cr^{7+} . The closed circles are the present experiments [M. Sataka *et al.*, Phys. Rev. A 39, 2397 (1989)]; relative uncertainties for experimental data are plotted at the one-standard-deviation level where they are larger than the plotted circles. The solid curves are Lotz calculations for direct ionization from the ground- (lower curve) and metastable-state (upper curve) configurations.

ORNL-DWG 94-5773

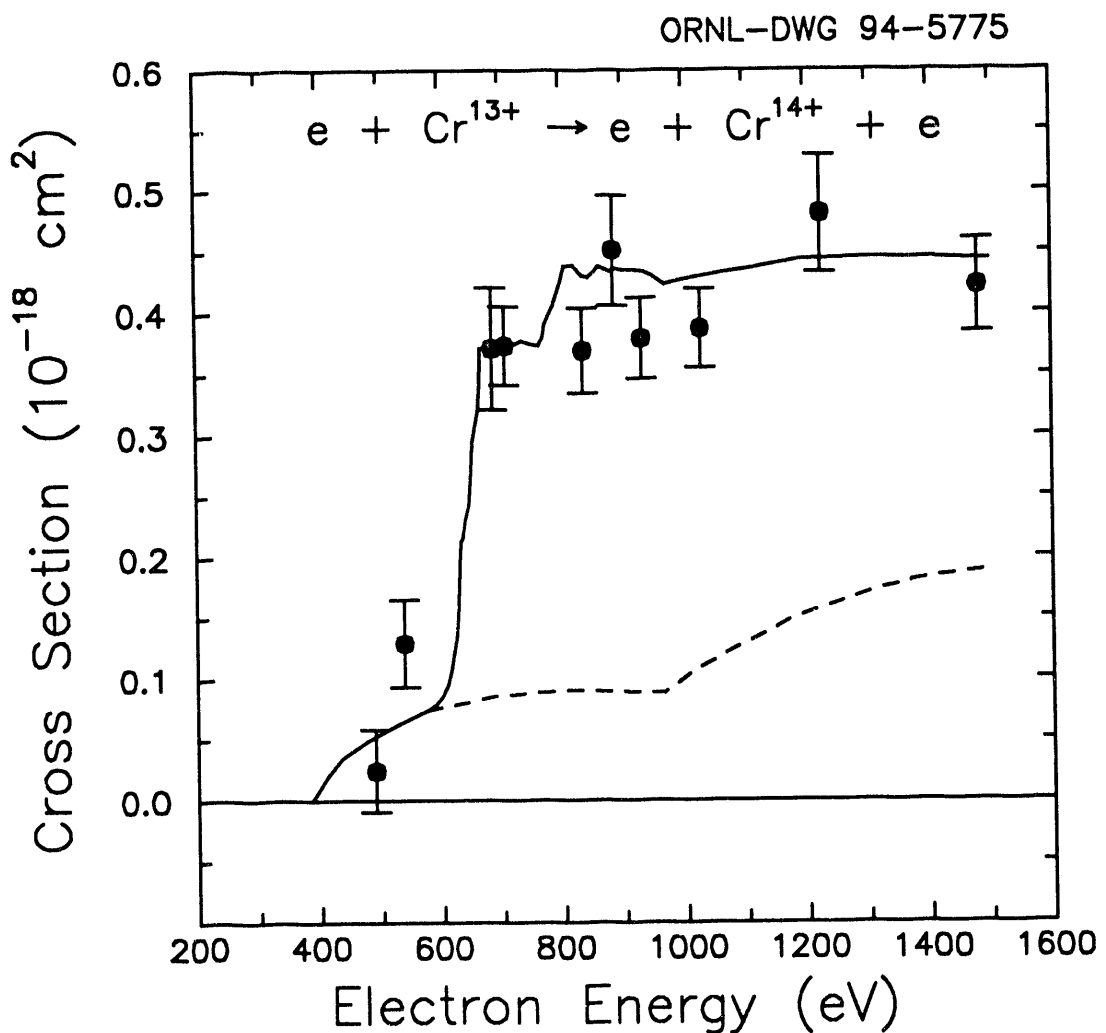


Electron-impact ionization cross section of Cr^{8+} . The closed circles are the present experiments [M. Sataka *et al.*, Phys. Rev. A 39, 2397 (1989)]; relative uncertainties for experimental data are plotted at the one-standard-deviation level. The solid curves are Lotz calculations for direct ionization from the ground- (lower curve) and metastable-state (upper curve) configurations.

ORNL-DWG 94-5774

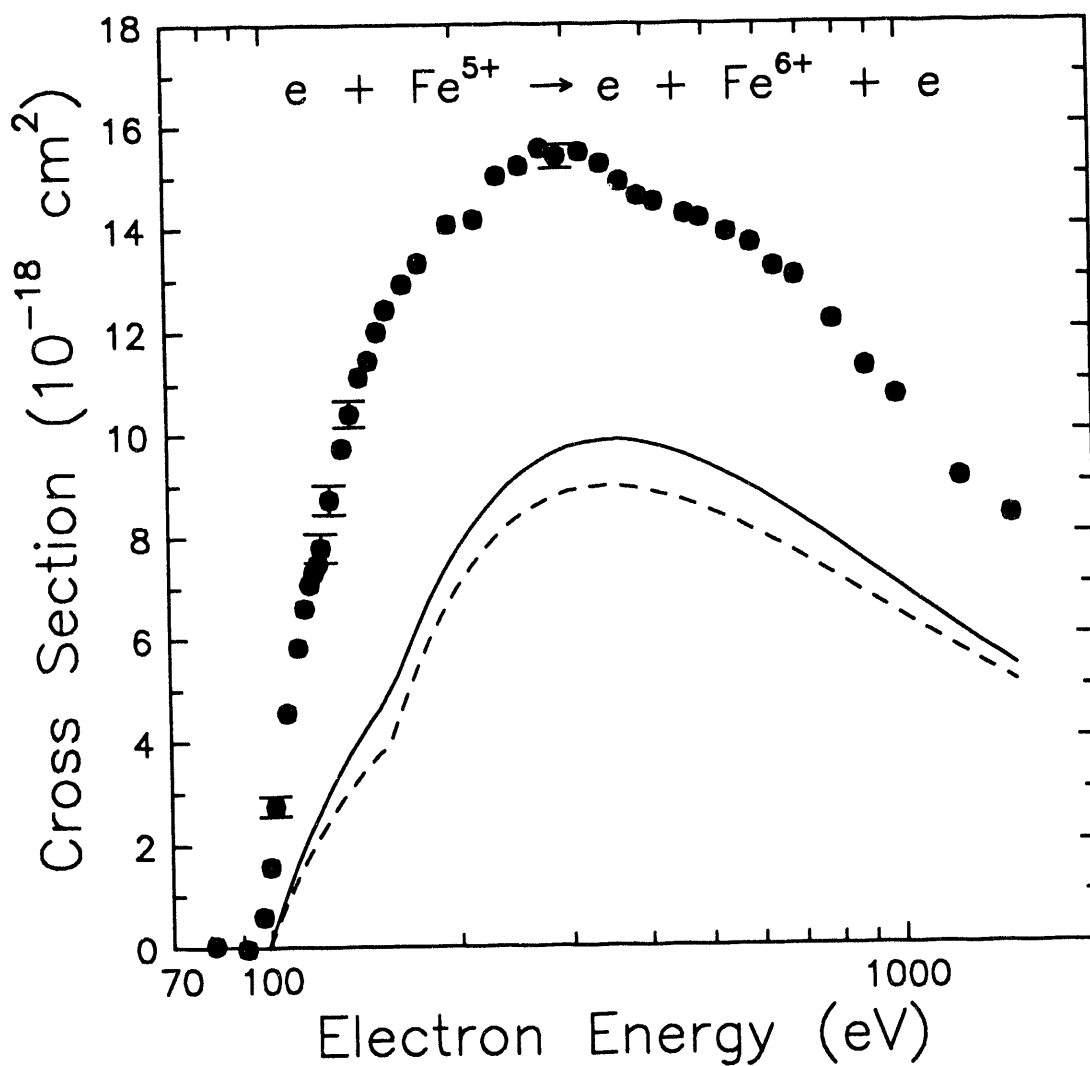


Electron-impact ionization cross section of Cr^{10+} . The closed circles are the present experiments [M. Sataka *et al.*, Phys. Rev. A **39**, 2397 (1989)]; relative uncertainties for experimental data are plotted at the one-standard-deviation level. The solid curve is a Lotz calculation for direct ionization from the ground-state configuration ($3s^2 3p^2$).



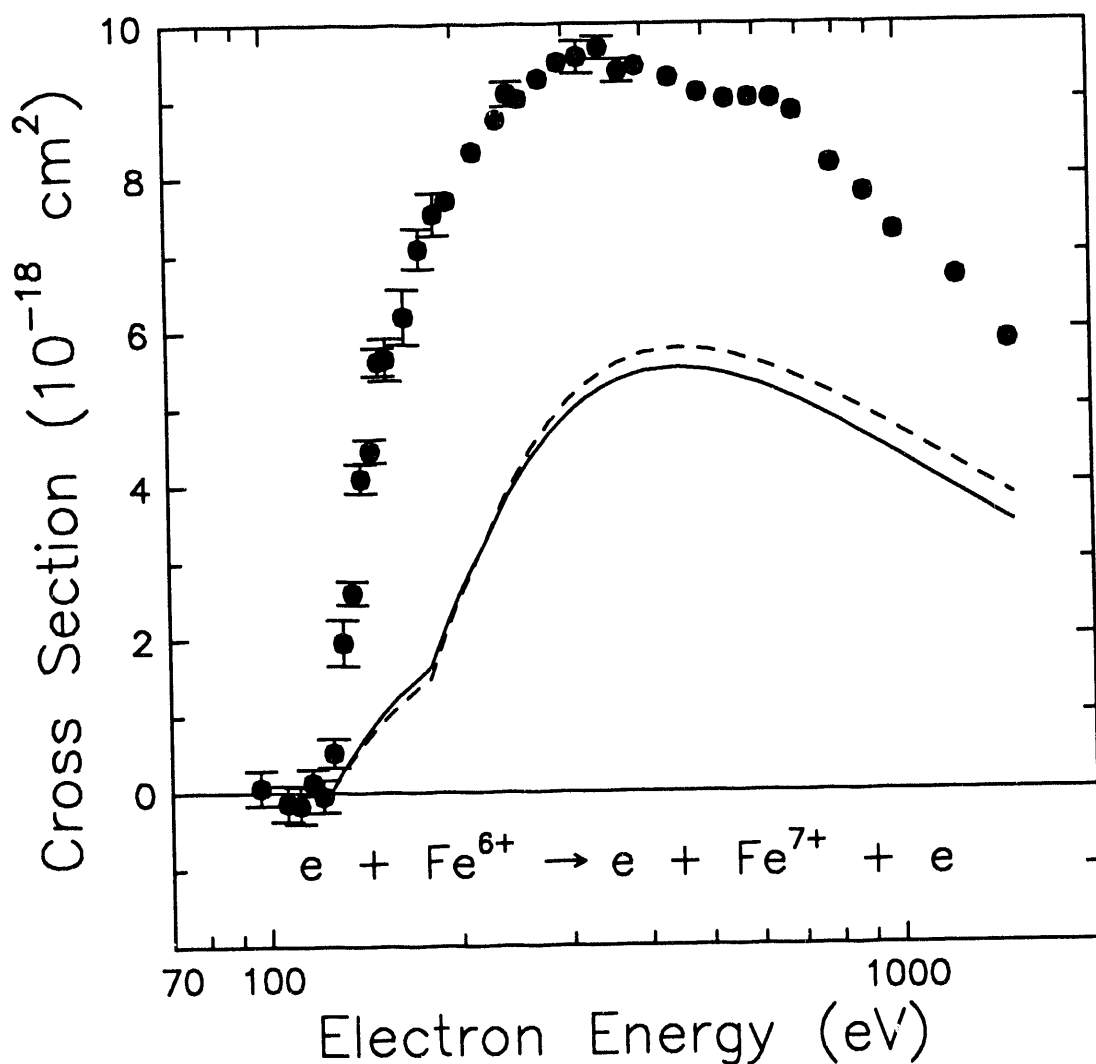
Electron-impact ionization cross section of Cr^{13+} . The solid points are the present data [D. C. Gregory *et al.*, Phys. Rev. A **41**, 6512 (1990)]; the dashed curve is a distorted-wave calculation for direct ionization only, while the solid curve includes excitation-autoionization (Griffin *et al.*). Uncertainties are relative at the one-standard-deviation level.

ORNL-DWG 94-5776

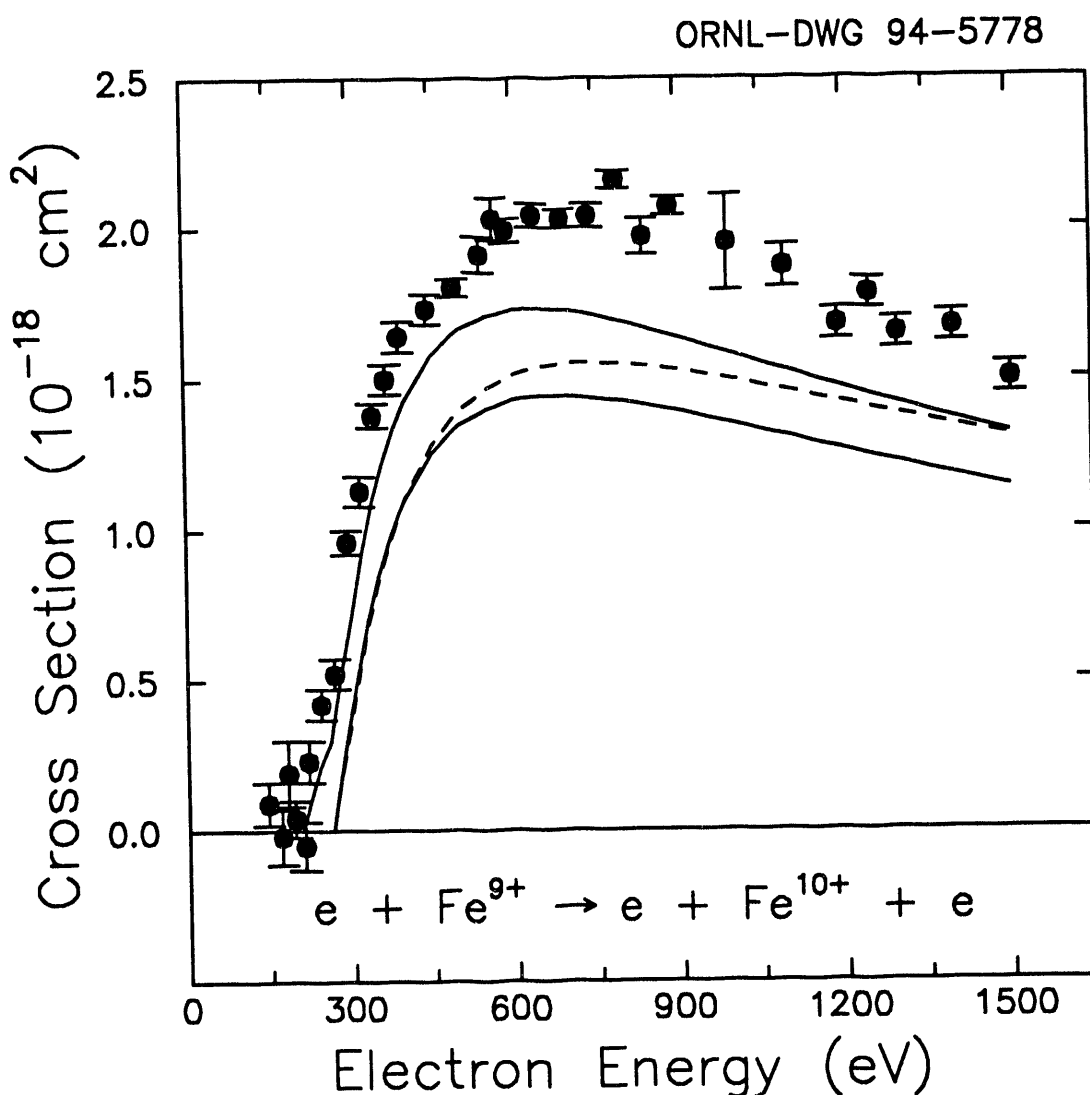


Cross section vs interaction energy for electron-impact ionization of Fe^{5+} . Solid circles are the present experimental data [D. C. Gregory *et al.*, Phys. Rev. A 34, 3657 (1986)], with one-standard-deviation relative uncertainties shown. The dashed curve is the cross section predicted by the semiempirical Lotz formula and the solid curve is a distorted-wave calculation by Younger, both based on direct ionization of 3d and 3p electrons.

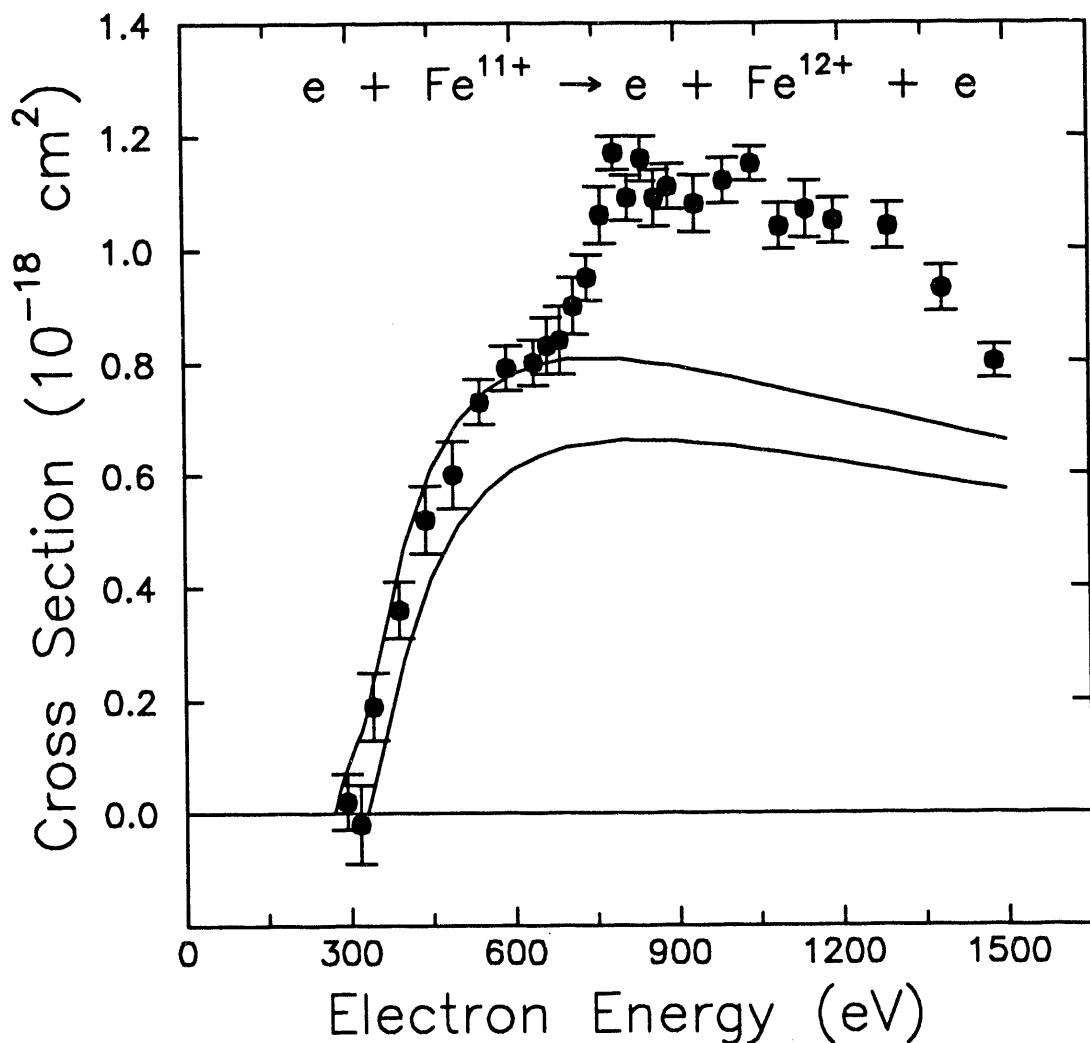
ORNL-DWG 94-5777



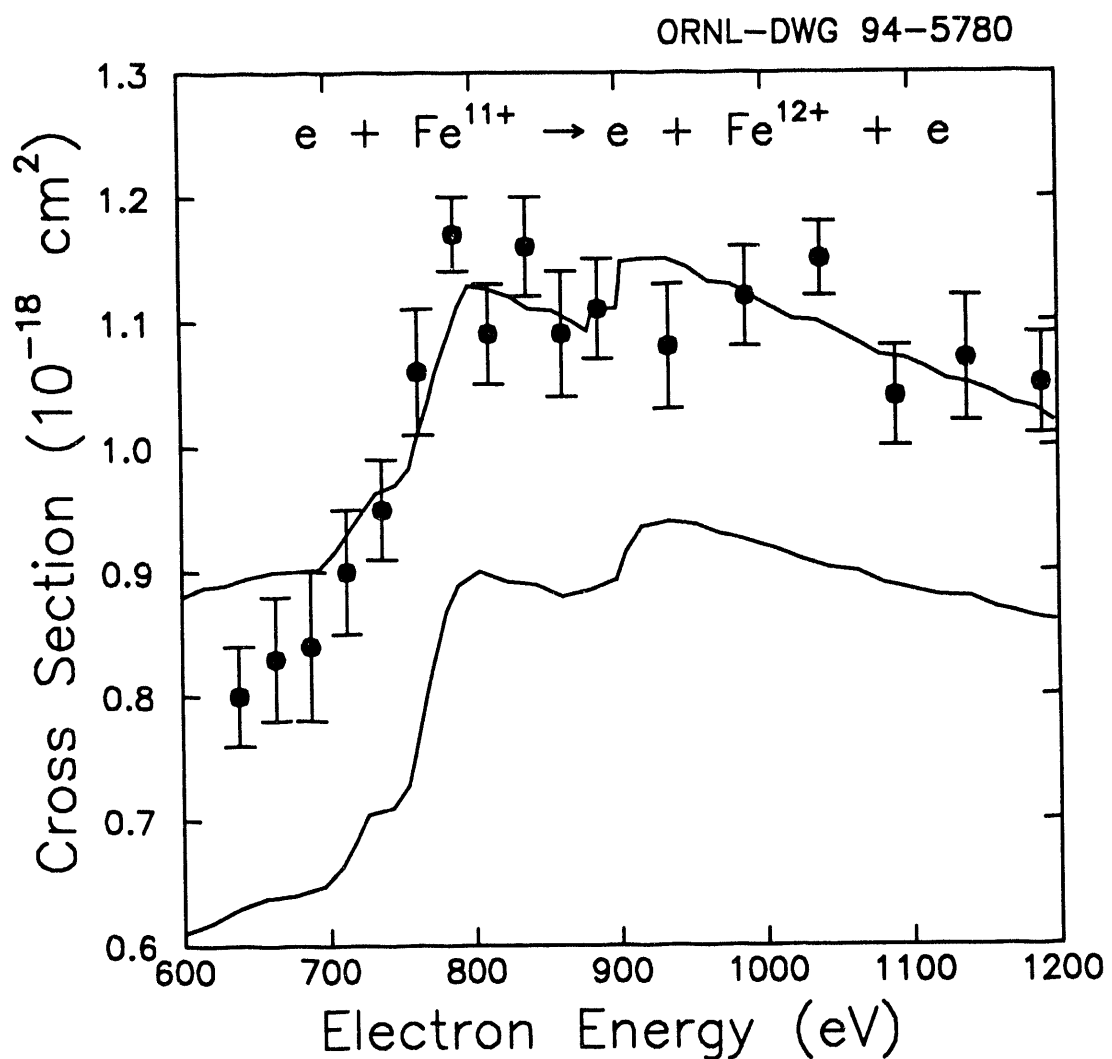
Cross section vs interaction energy for electron-impact ionization of Fe^{6+} . Solid circles are the present experimental data [D. C. Gregory *et al.*, Phys. Rev. A 34, 3657 (1986)], with representative uncertainties at the one-standard-deviation level shown. The solid curve is a distorted-wave calculation by Younger for direct ionization from the 3d, 3p and 3s subshells, and the dashed curve is from the Lotz formula for ionization from the same subshells.



Cross section vs interaction energy for electron-impact ionization of Fe^{9+} . Solid circles are the present experimental data [D. C. Gregory *et al.*, Phys. Rev. A 34, 3657 (1986)]. Relative uncertainties are shown at the one-standard-deviation level. The lower solid curve is a distorted-wave calculation by Younger for direct ionization of ground-state ions, while the upper solid curve is a similar calculation by Pindzola *et al.* for ions in the $3p^33d$ metastable state. The dashed curve is the prediction of the semiempirical Lotz formula for ionization of ground-state ions.

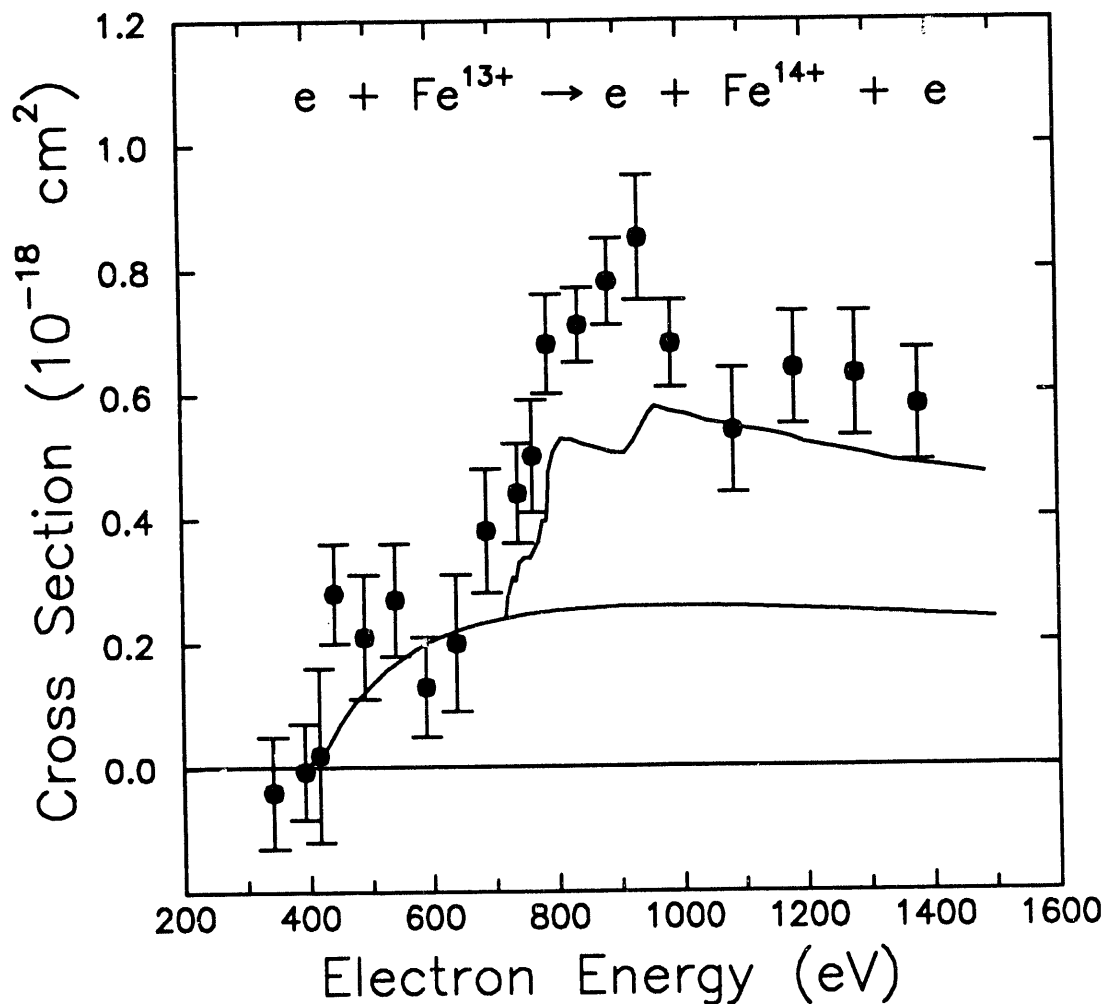


Cross section vs interaction energy for electron-impact ionization of Fe^{11+} . Solid points are the present data [D. C. Gregory *et al.*, Phys. Rev. A 35, 3256 (1987)]; plotted uncertainties are one-standard-deviation relative only. The solid curves are distorted-wave calculations for direct ionization of ground-state ($3s^23p^3$) ions (lower curve, by Younger) and of metastable ions in a $3s^23p^23d$ configuration (upper curve, by Pindzola *et al.*)



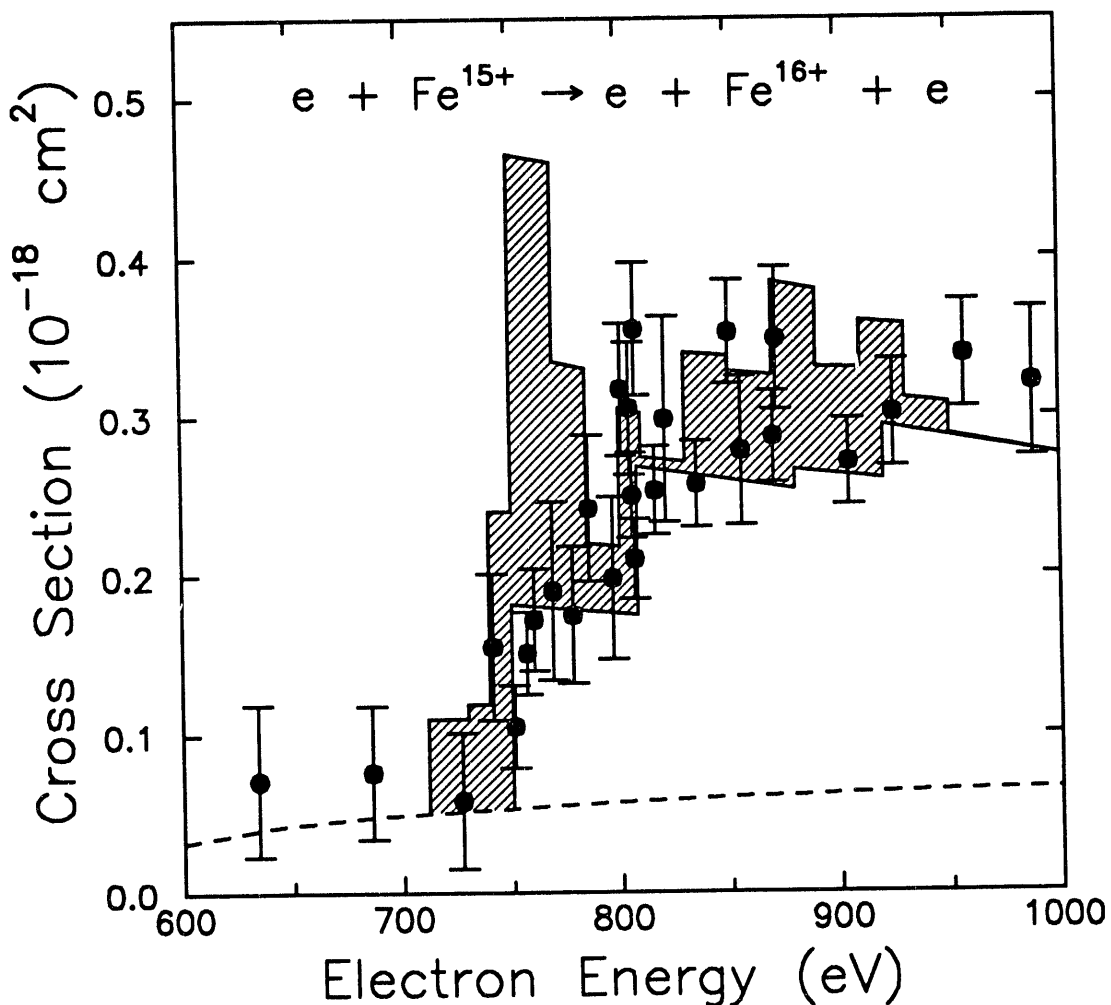
Electron-impact single ionization of Fe^{11+} . The experimental data [D. C. Gregory *et al.*, Phys. Rev. A 35, 3256 (1987)] are compared with distorted-wave calculations for total ionization, including direct ionization and excitation-autoionization effects. The calculations (from Pindzola *et al.*) include five transitions involving excitation of inner-shell 2p and 2s electrons. The lower curve is for initially ground-state ($3s^23p^3$) ions, and the upper curve is for metastable ($3s^23p^23d$) ions. Note that additional transitions at lower energies contribute to autoionization of metastable ions.

ORNL-DWG 94-5781



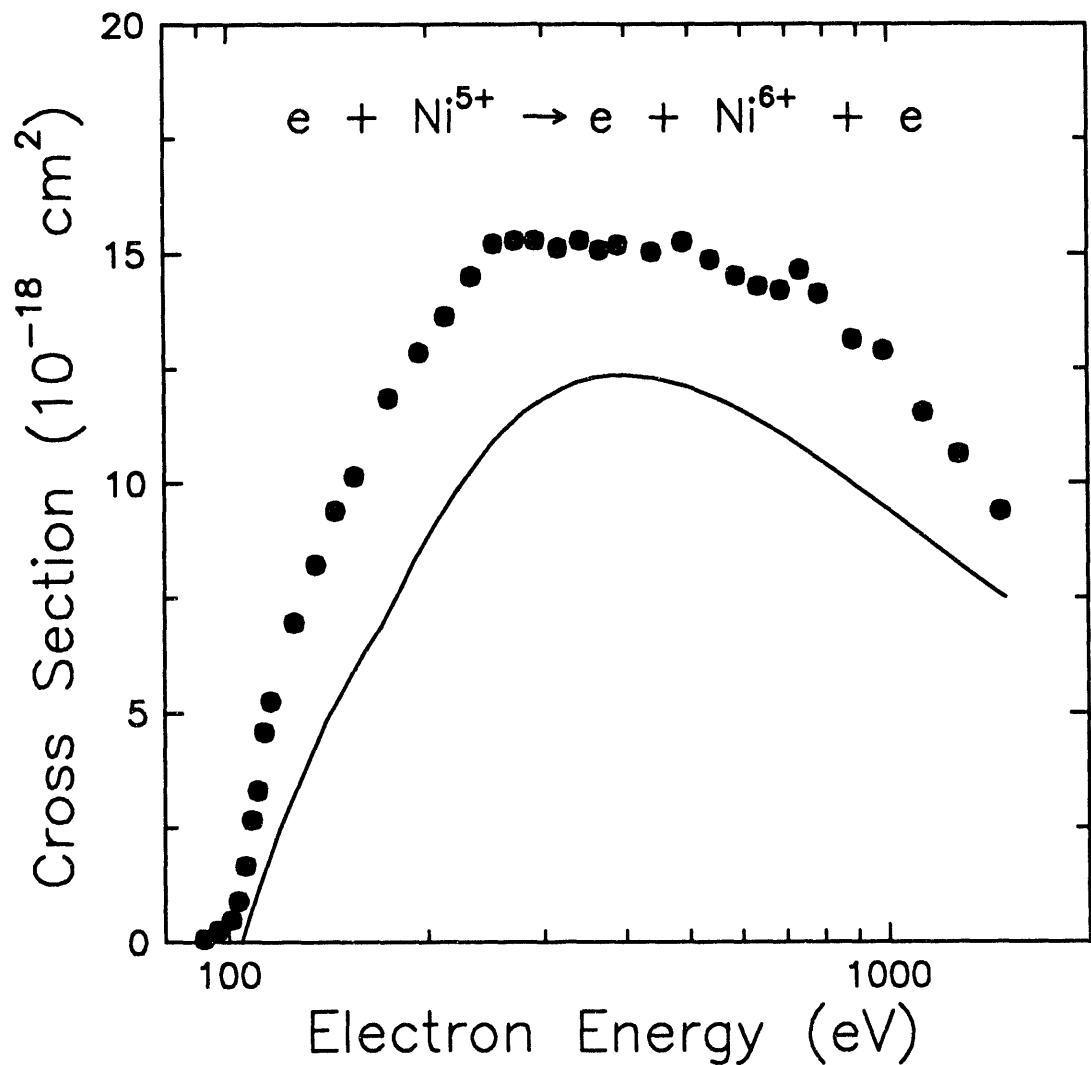
Electron-impact ionization of Fe^{13+} . The data [D. C. Gregory *et al.*, Phys. Rev. A 35, 3256 (1987)] are compared to distorted-wave calculations for direct ionization of ground-state ($3s^23p$) ions (lower curve, by Younger) and including the effects of excitation-autoionization (upper curve, by Pindzola *et al.*).

ORNL-DWG 94-5782



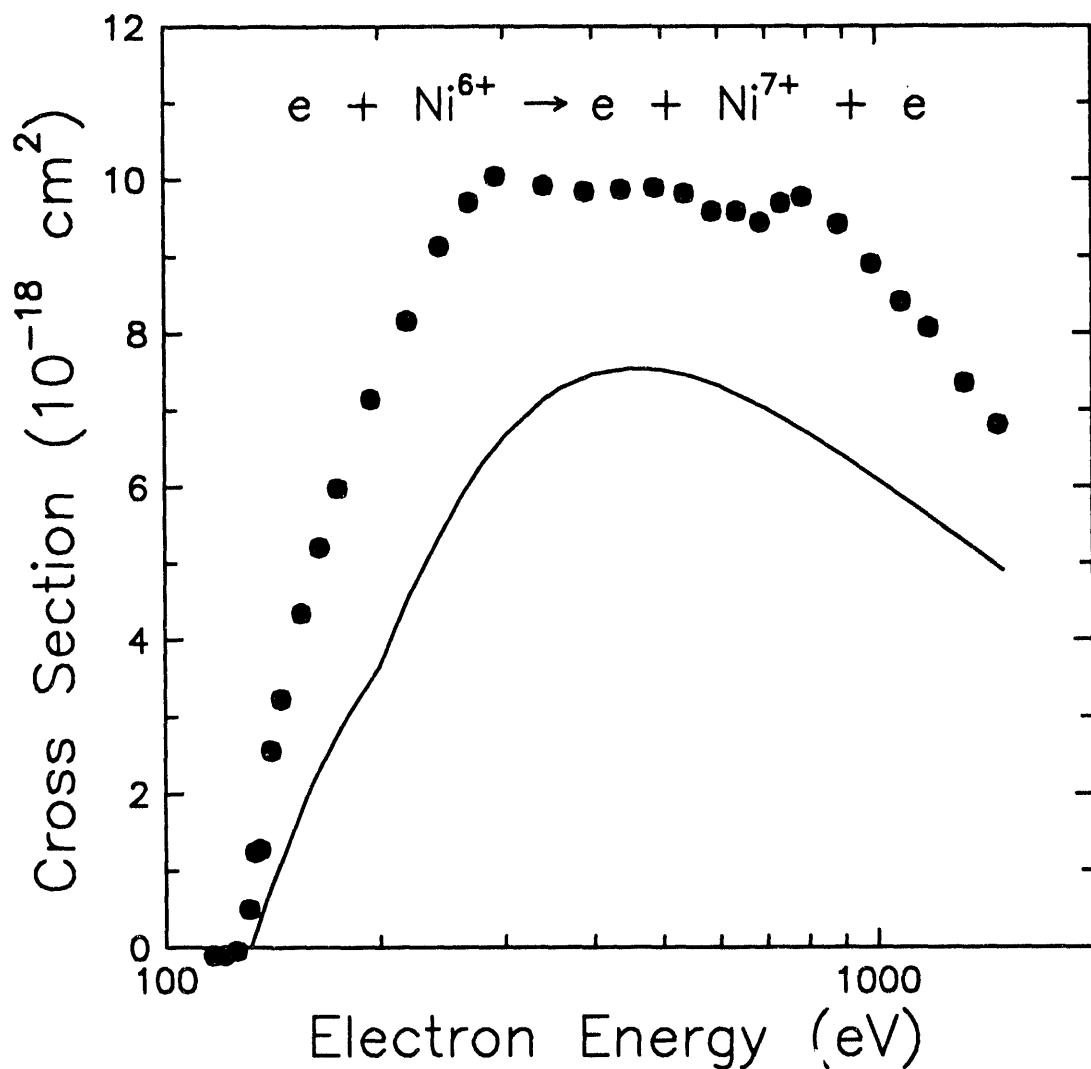
Electron-impact ionization of Fe^{15+} . Present data [D. C. Gregory *et al.*, Phys. Rev. A 35, 3256 (1987)] are compared to Lotz predictions for direct ionization (dashed curve), direct ionization added to distorted-wave calculations including excitation-autoionization (lower solid curve, from Mertz *et al.*), and calculations including resonant-excitation double autoionization (upper solid curve, LaGattuta and Hahn). The hatched region indicates the predicted cross-section enhancement due to resonant-excitation double autoionization (REDA).

ORNL-DWG 94-5783



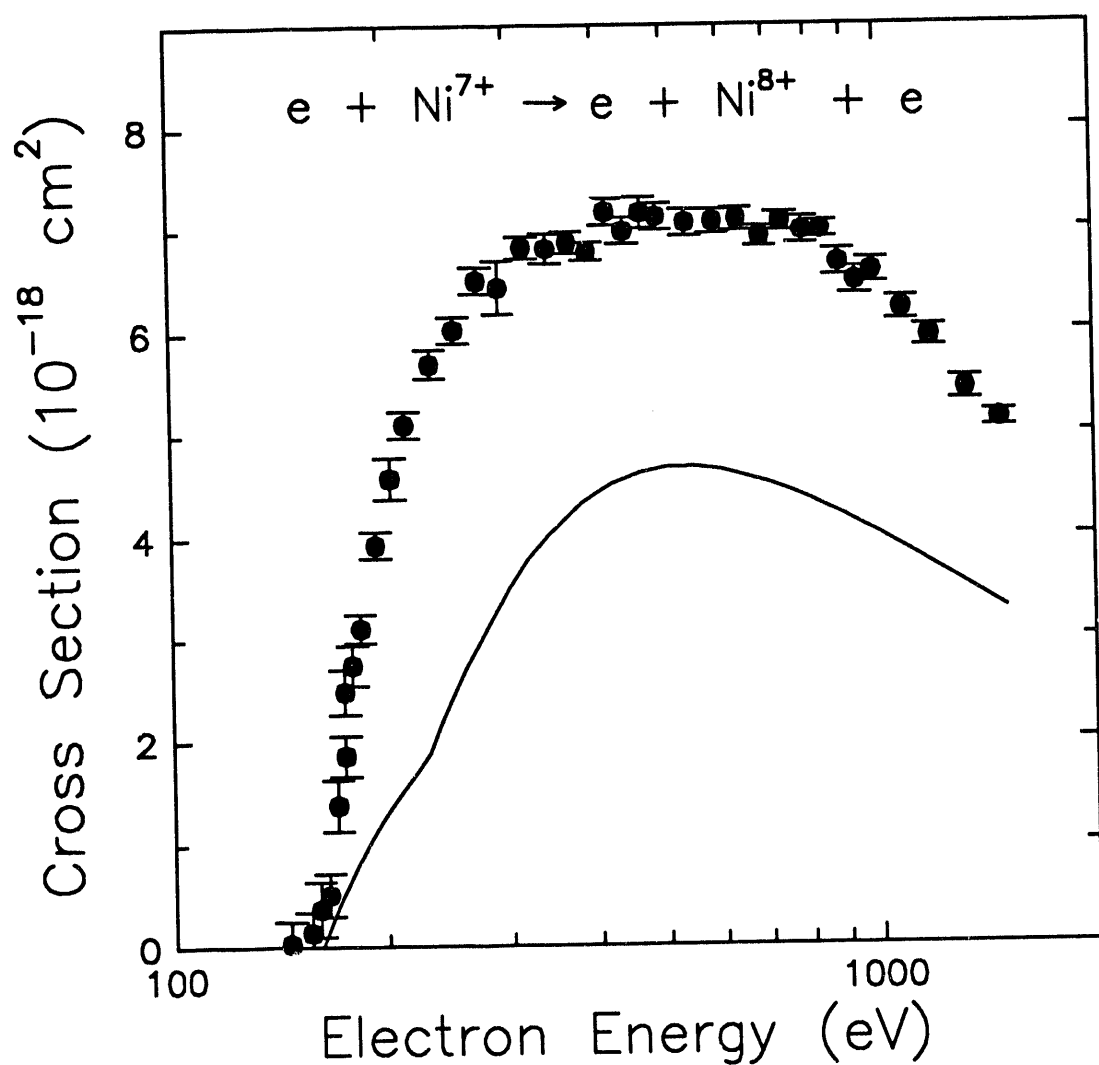
Cross sections for electron-impact single ionization of Ni^{5+} . Solid circles are the present data [L. J. Wang *et al.*, J. Phys. B 21, 2117 (1988)]; relative uncertainties at the one-standard-deviation level are smaller than the plotted points. The curve is a distorted-wave calculation for direct ionization by Buie and Pindzola.

ORNL-DWG 94-5784



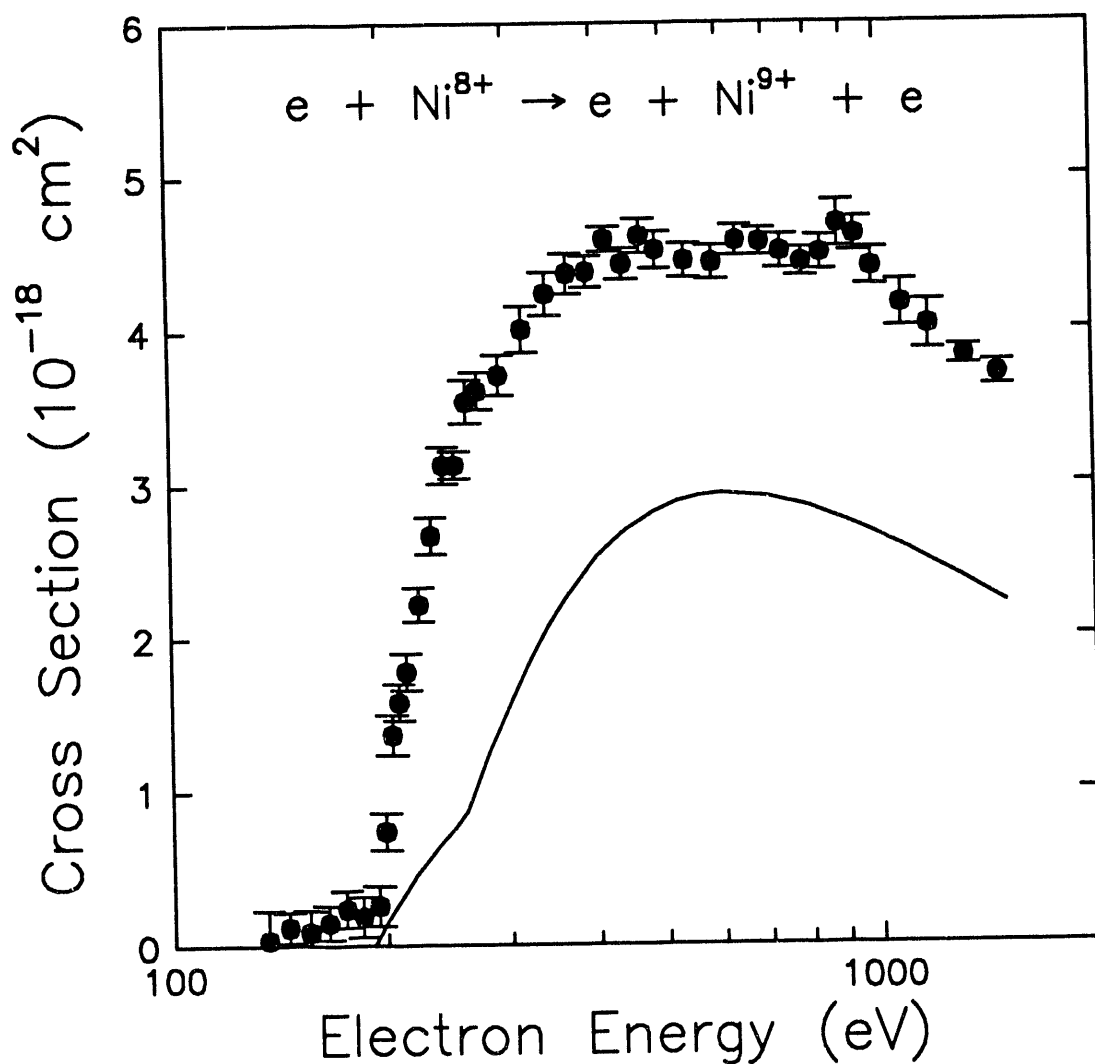
Cross sections for electron-impact single ionization of Ni^{6+} . Solid circles are the present data [L. J. Wang *et al.*, J. Phys. B 21, 2117 (1988)]; relative uncertainties at the one-standard-deviation level are smaller than the plotted points. The curve is a distorted-wave calculation for direct ionization by Buie and Pindzola.

ORNL-DWG 94-5785



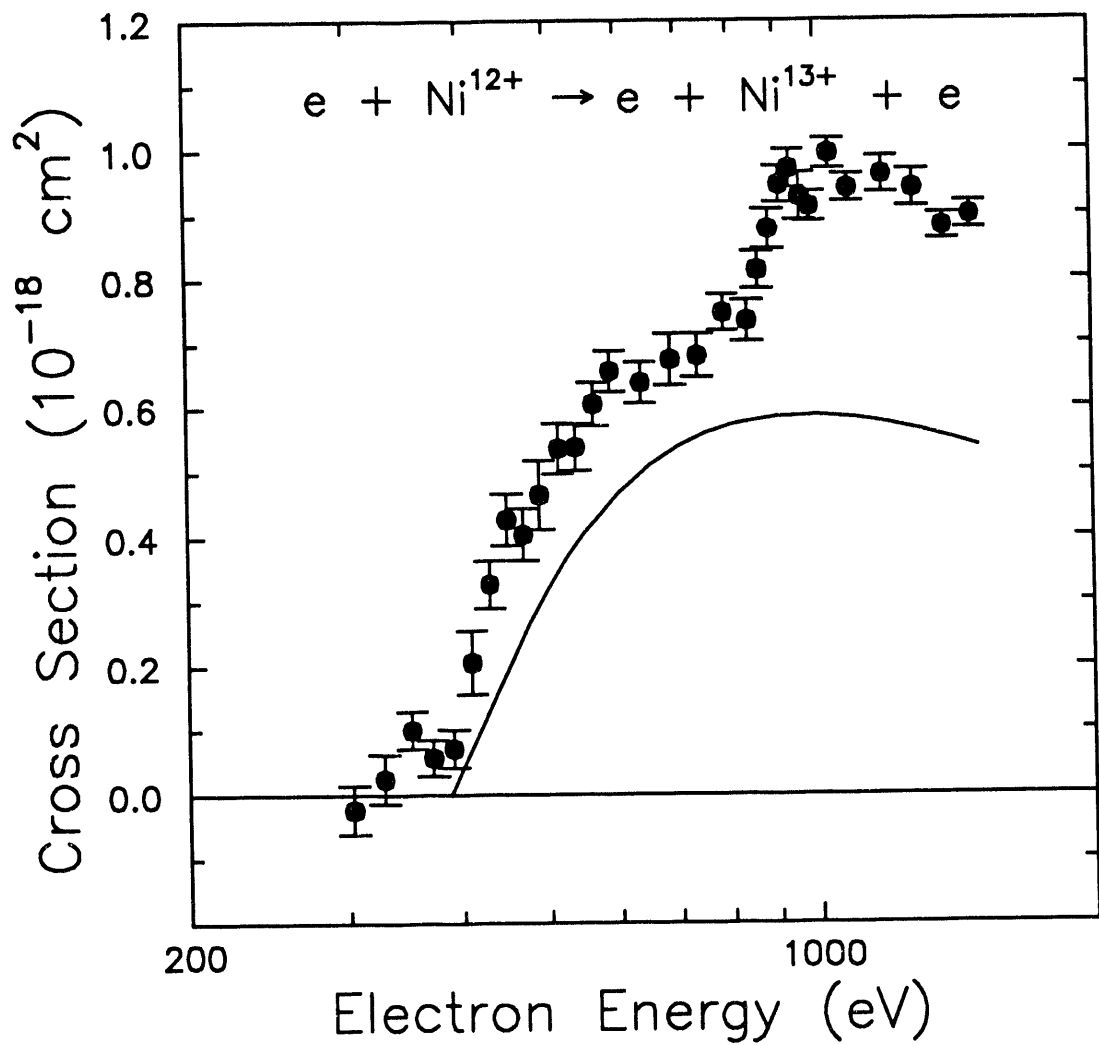
Cross sections for electron-impact single ionization of Ni^{7+} . Solid circles are the present data [L. J. Wang *et al.*, J. Phys. B 21, 2117 (1988)]; typical relative uncertainties are shown at the one-standard-deviation level. The curve is a distorted-wave calculation for direct ionization by Buie and Pindzola.

ORNL-DWG 94-5786



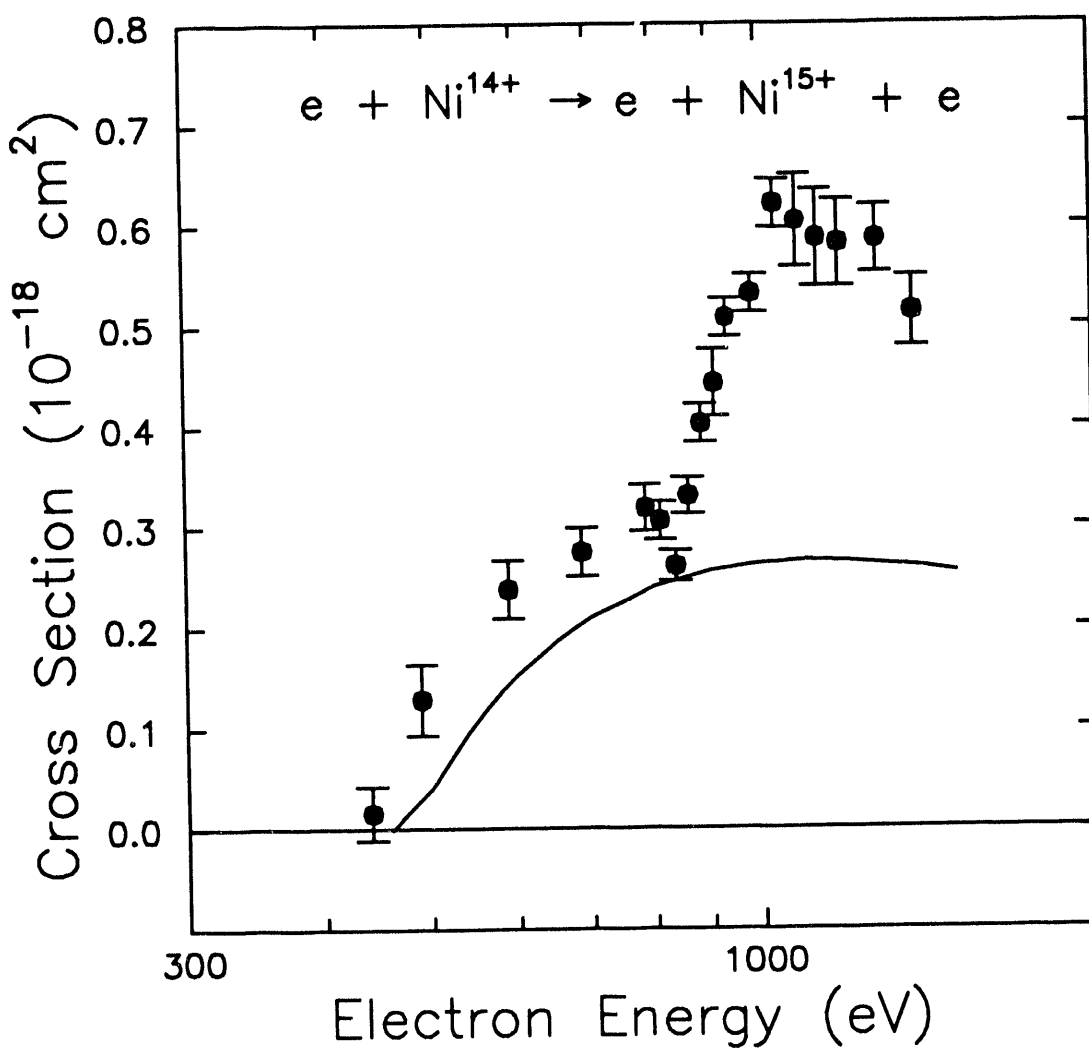
Cross sections for electron-impact single ionization of Ni^{8+} . Solid circles are the present data [L. J. Wang *et al.*, J. Phys. B 21, 2117 (1988)]; relative uncertainties are plotted at the one-standard-deviation level. The curve is a distorted-wave calculation for direct ionization by Buie and Pindzola.

ORNL-DWG 94-5787



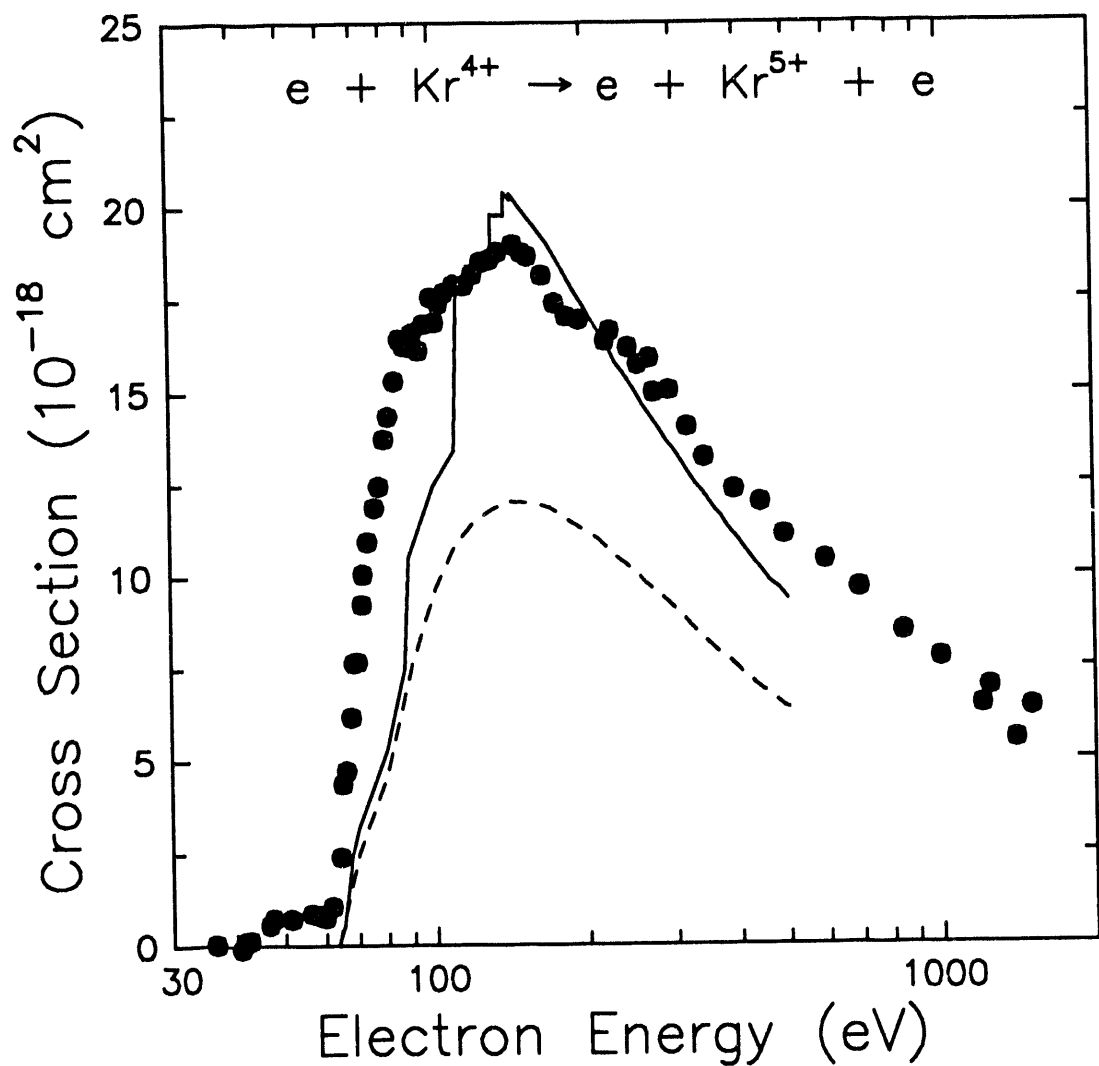
Cross sections for electron-impact single ionization of Ni^{12+} . Solid circles are the present data [L. J. Wang *et al.*, *J. Phys. B* **21**, 2117 (1988)]; relative uncertainties are plotted at the one-standard-deviation level. The curve is a distorted-wave calculation for direct ionization by Buie and Pindzola.

ORNL-DWG 94-5788



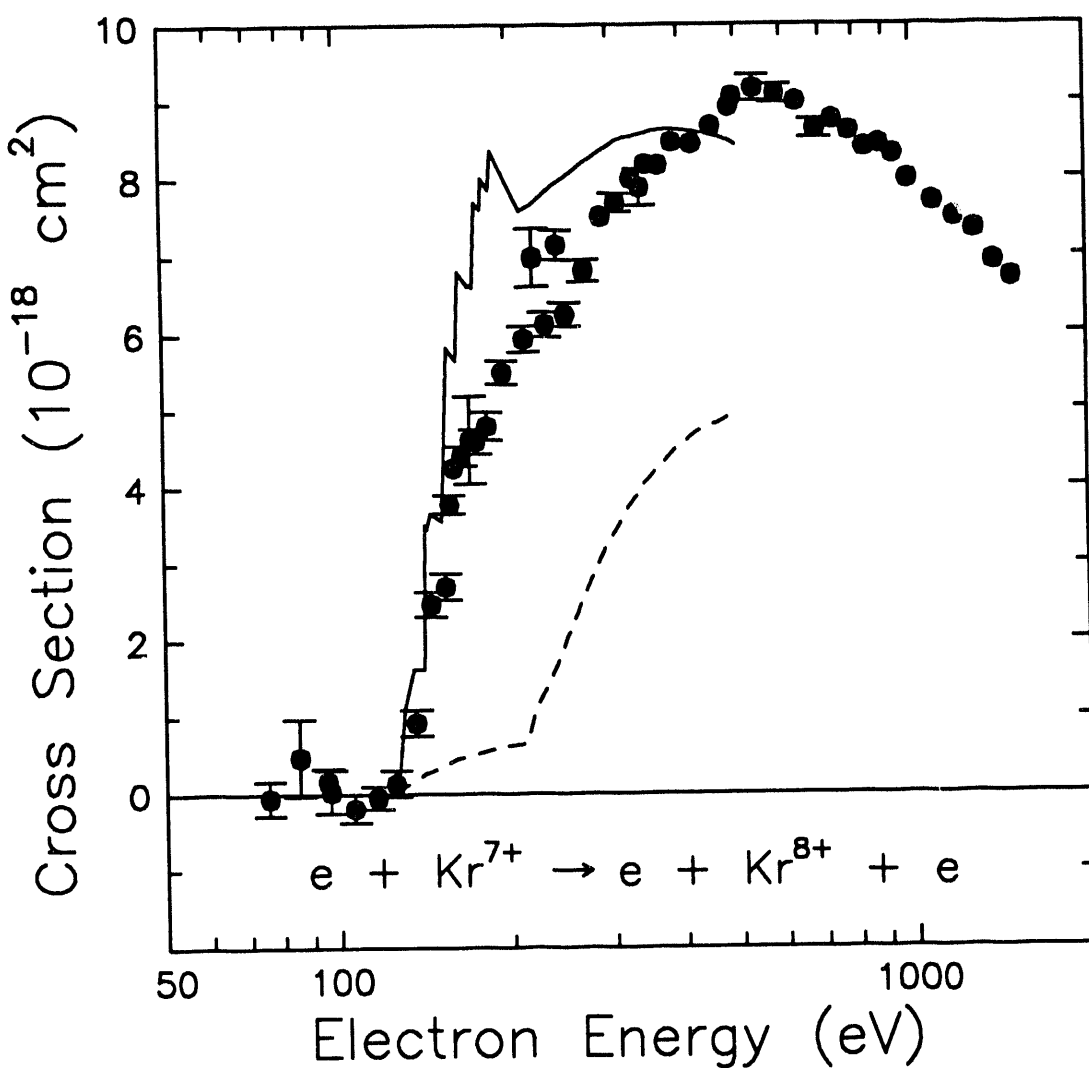
Cross sections for electron-impact single ionization of Ni^{14+} . Solid circles are the present data [L. J. Wang *et al.*, *J. Phys. B* **21**, 2117 (1988)]; relative uncertainties are plotted at the one-standard-deviation level. The curve is a distorted-wave calculation for direct ionization by Buie and Pindzola.

ORNL-DWG 92-13480



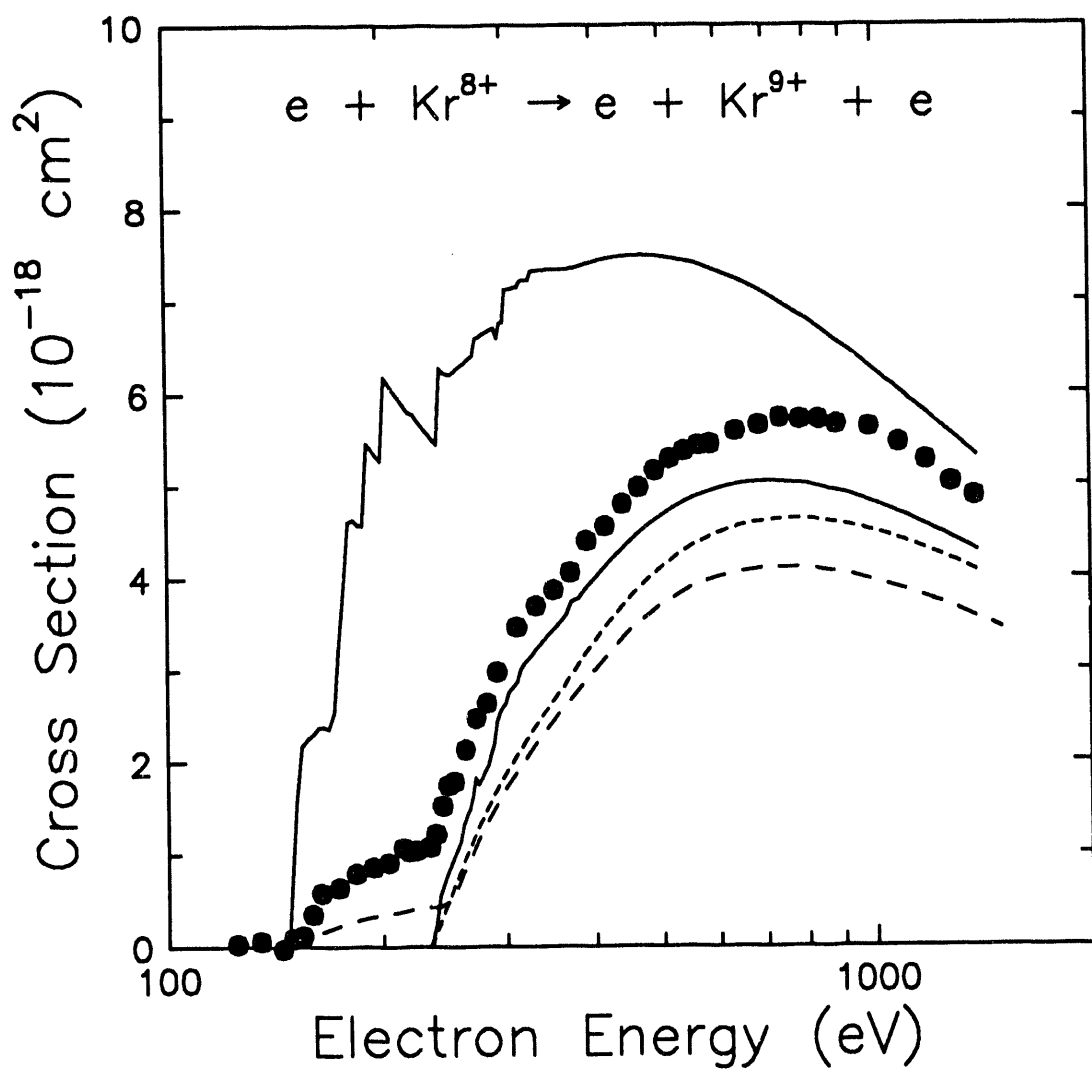
Electron-impact ionization of Kr^{4+} . Solid circles are the present data [A. M. Howald *et al.*, unpublished (1985)]. One-standard-deviation relative uncertainties are smaller than the plotted points. The below-threshold energy dependence of the cross section indicates the presence of a significant metastable component in the incident beam. The dashed curve is a distorted-wave calculation for direct ionization from the ground configuration; the solid curve includes excitation-autoionization effects (calculations from T. W. Gorczyca *et al.*, ref. 42).

ORNL-DWG 92-13481

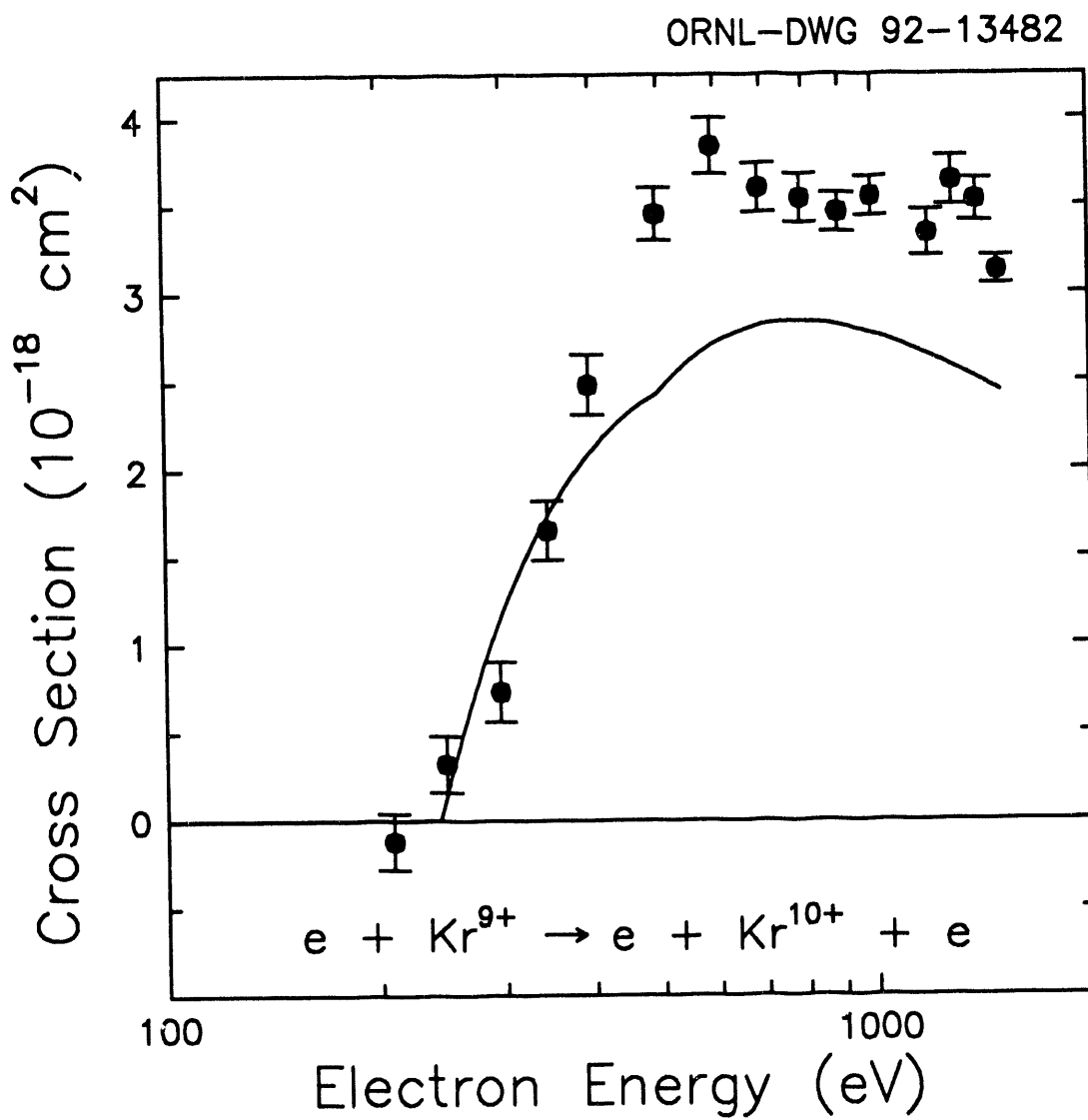


Electron-impact ionization of Kr^{7+} . Solid circles are the present data [D. C. Gregory and A. M. Howald, unpublished (1985)]. The below-threshold data has been "corrected" for what was assumed to be space-charge modulation effects; the correction is negligible above threshold. The dashed curve is a distorted-wave calculation for direct ionization; the solid curve includes excitation-autoionization effects (theory by T. W. Gorczyca *et al.*, ref. 42).

ORNL-DWG 94-5789

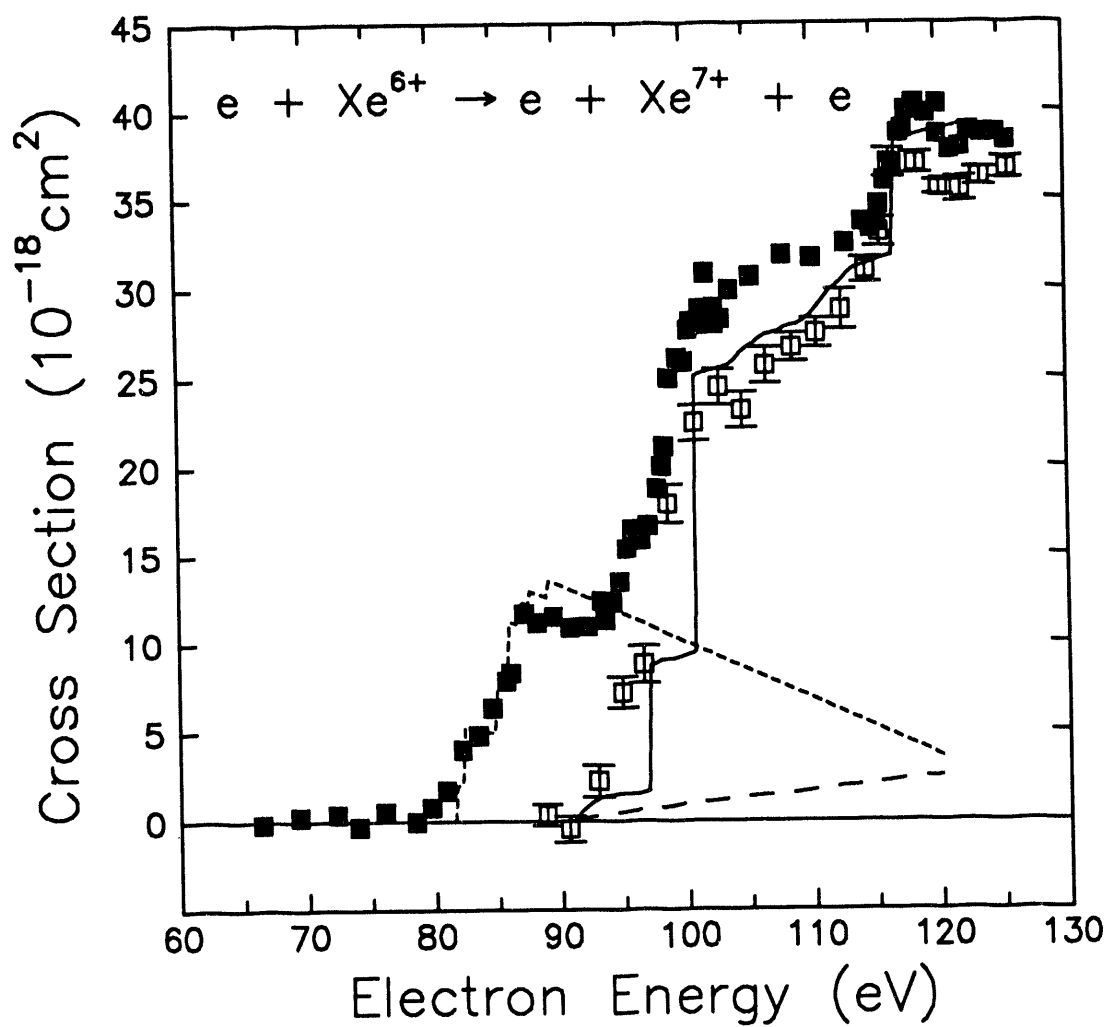


Single ionization of Kr^{8+} by electron impact. The points are the present data [M. E. Bannister *et al.*, Phys. Rev. A 38, 38 (1988)]; the dashed curves are CADW calculations of direct ionization from the ground (short-dash) and first-excited (long-dash) configurations; solid curves are CADW calculations for total ionization of ions in ground ($3d^{10}$, lower curve) and first-excited ($3d^94s$, upper curve) configurations. Relative uncertainties for the experimental data at the one-standard-deviation level are smaller than the symbol size.



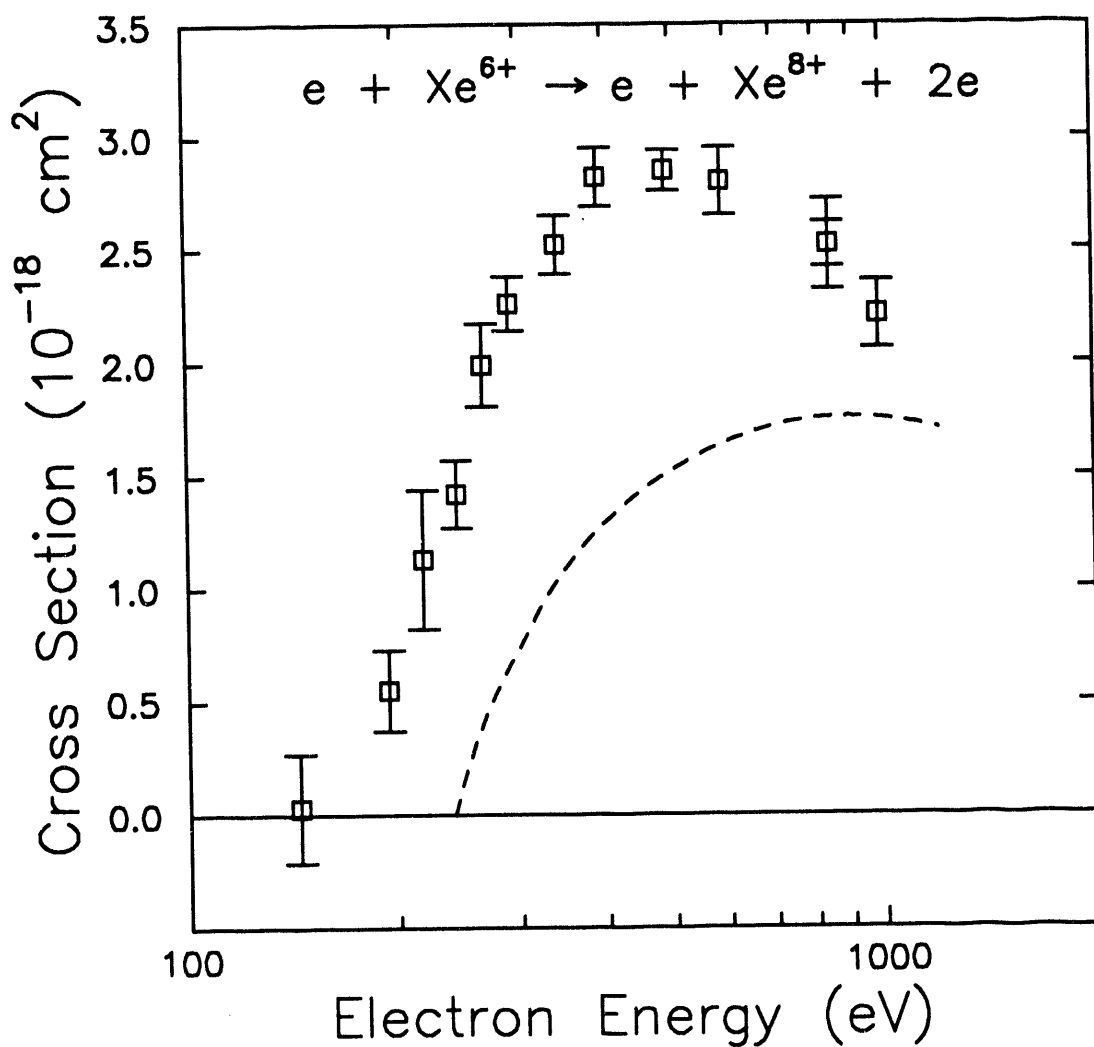
Electron-impact ionization of Kr^{9+} . The data [D. C. Gregory *et al.*, unpublished (1986)] are shown with one-standard-deviation relative uncertainties. The solid curve is a Lotz calculation for direct ionization from the 3d and 3p subshells.

ORNL DWG 94-5790



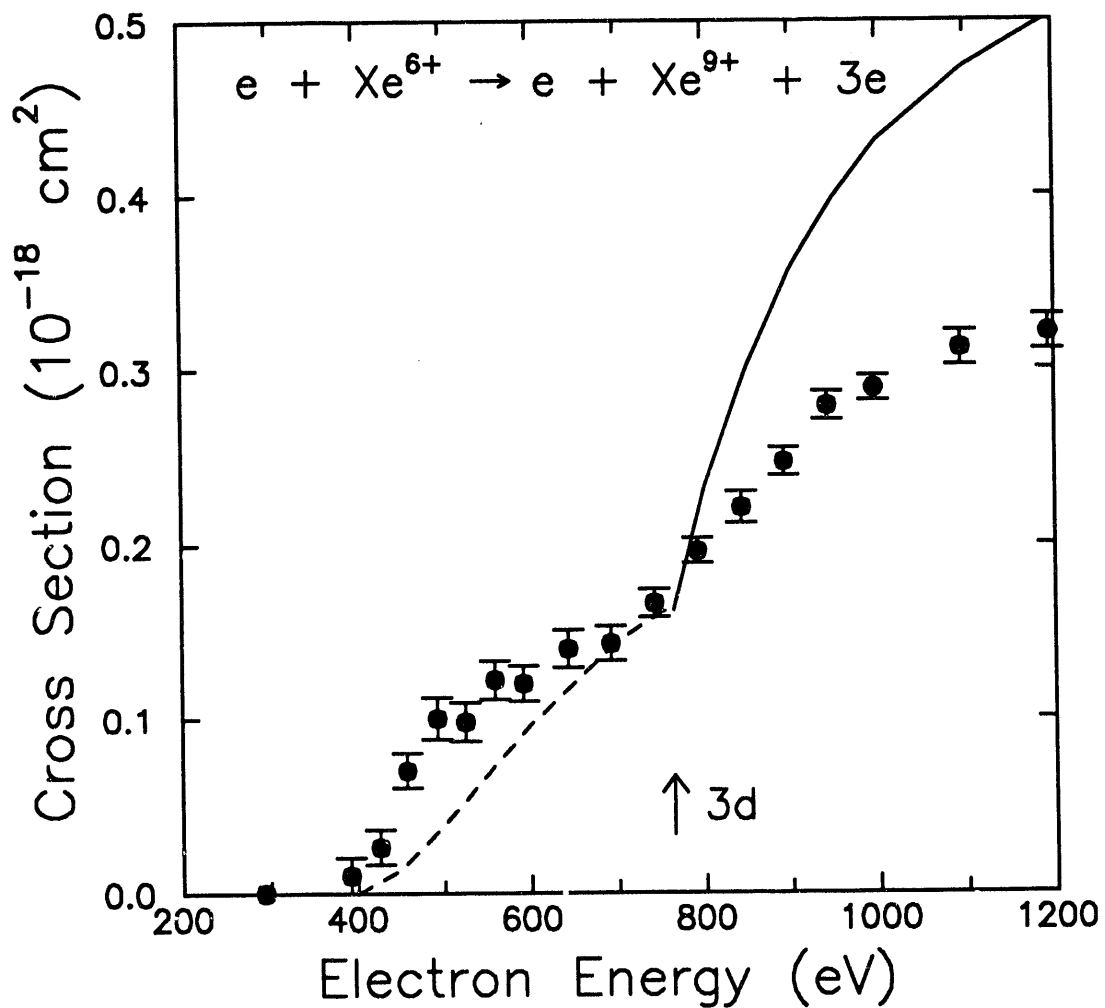
Electron-impact single ionization of Xe^{6+} . Solid squares are the present data [D. C. Gregory *et al.*, unpublished (1986)]; relative uncertainties are smaller than the plotted symbols. The open squares are previously published results (by Gregory and Crandall) with relative uncertainties at the one-standard-deviation level. Distorted-wave calculations by Pindzola *et al.* are shown for direct ionization from the ground configuration (long-dash curve), total ionization for ground-state ions including excitation-autoionization (solid curve), and excitation to a configuration which is bound for ground-state ions but autoionizing for metastable ions (short-dash curve).

ORNL-DWG 94-5791



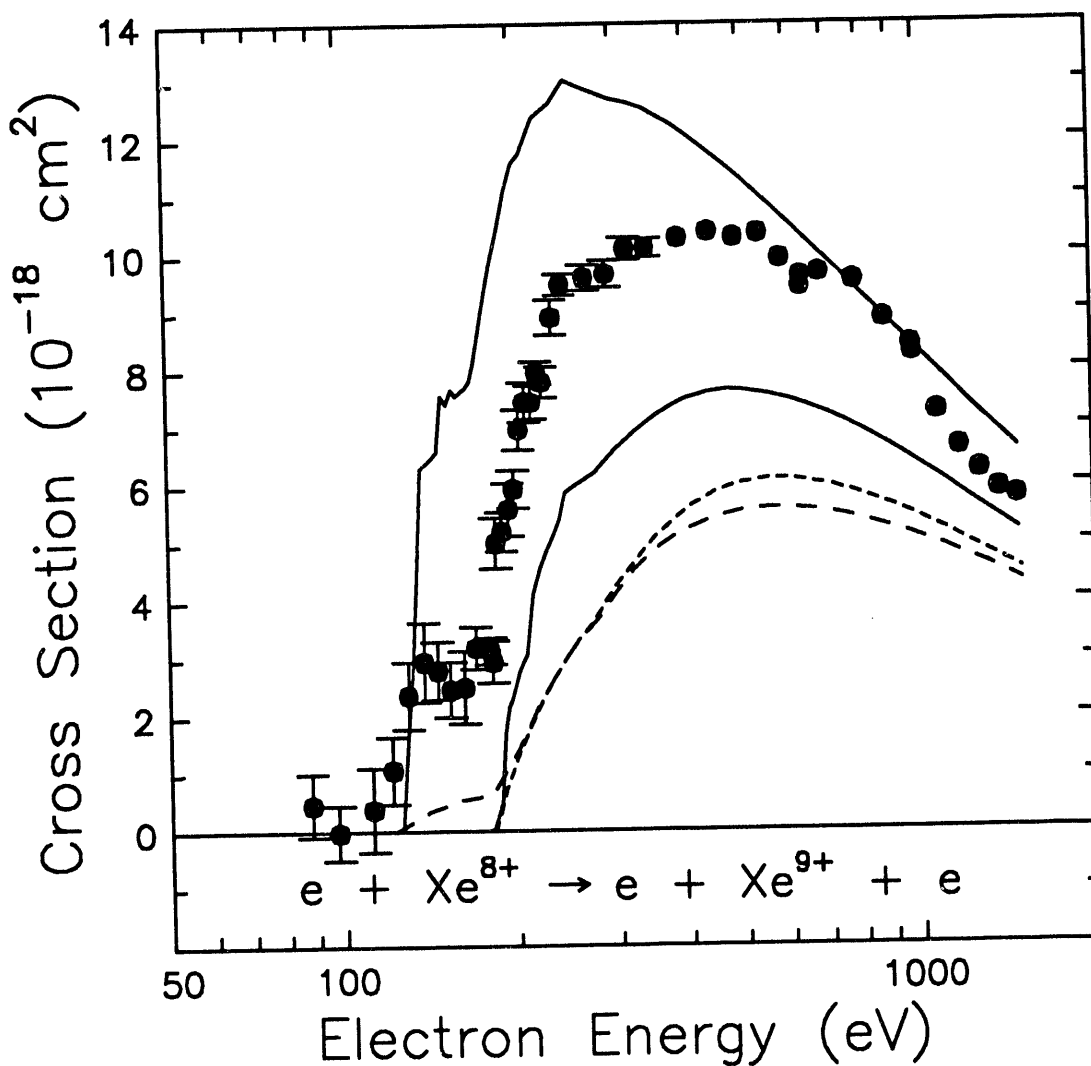
Measured cross sections for double ionization of Xe^{6+} by electron impact. Open squares are the present data [A. M. Howald *et al.*, Phys. Rev. Lett. **56**, 1675 (1986)]; plotted uncertainties are counting statistics at the one-standard-deviation level. The dashed line is a distorted-wave calculation of double ionization due to direct ejection of an inner-shell 4p or 4s electron followed by the emission of an Auger electron.

ORNL-DWG 94-5792



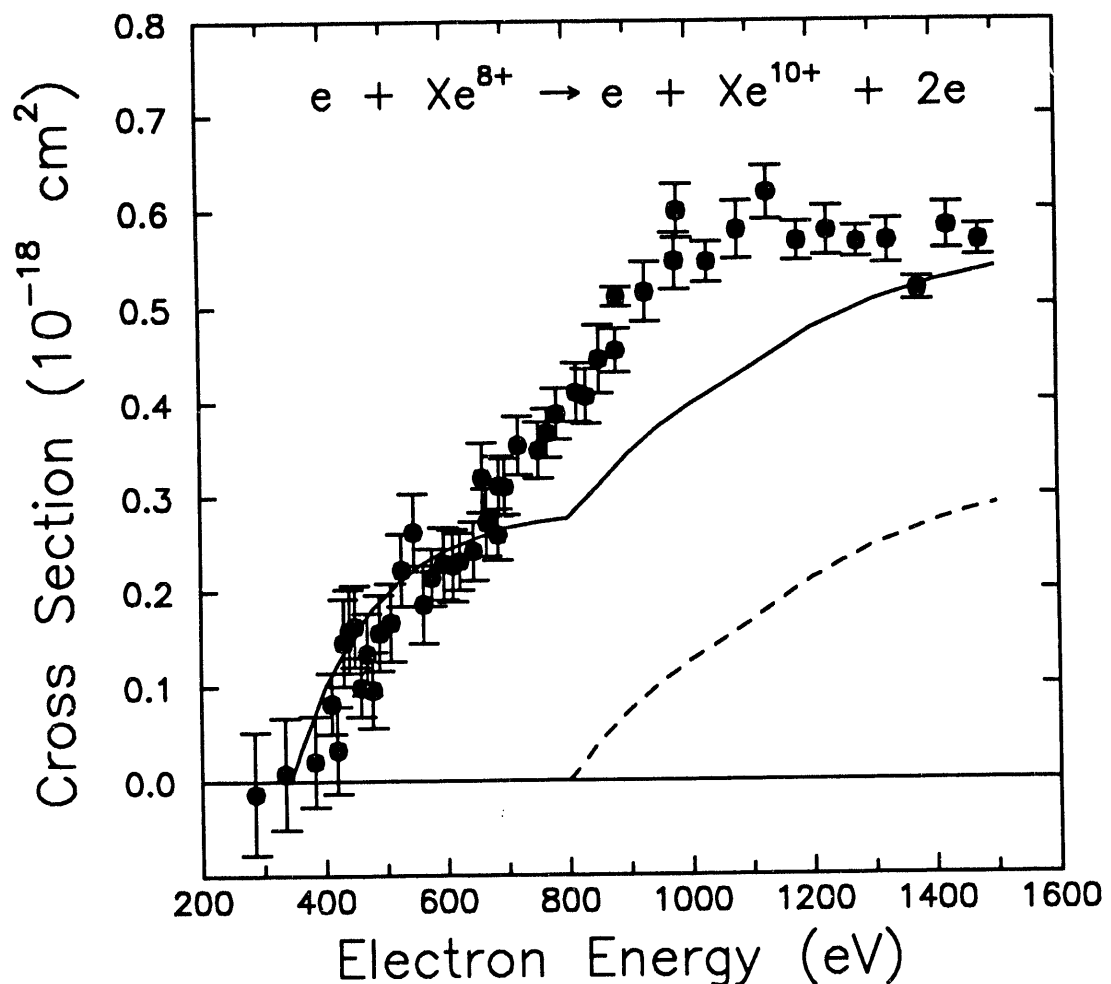
Measured cross sections for triple ionization of Xe^{6+} by electron impact. All triple ionization below 600 eV must be due to multiple-target-electron collisional processes. The data [A. M. Howald *et al.*, Phys. Rev. Lett. 56, 1675 (1986)] are shown with error bars based on counting statistics at the one-standard-deviation level. The dashed line is the BEA classical prediction for the direct ejection of a 4p and a 4d electron; the solid curve is the sum of the BEA result plus distorted-wave calculations for the ejection of a single 3d electron.

ORNL-DWG 94-5793



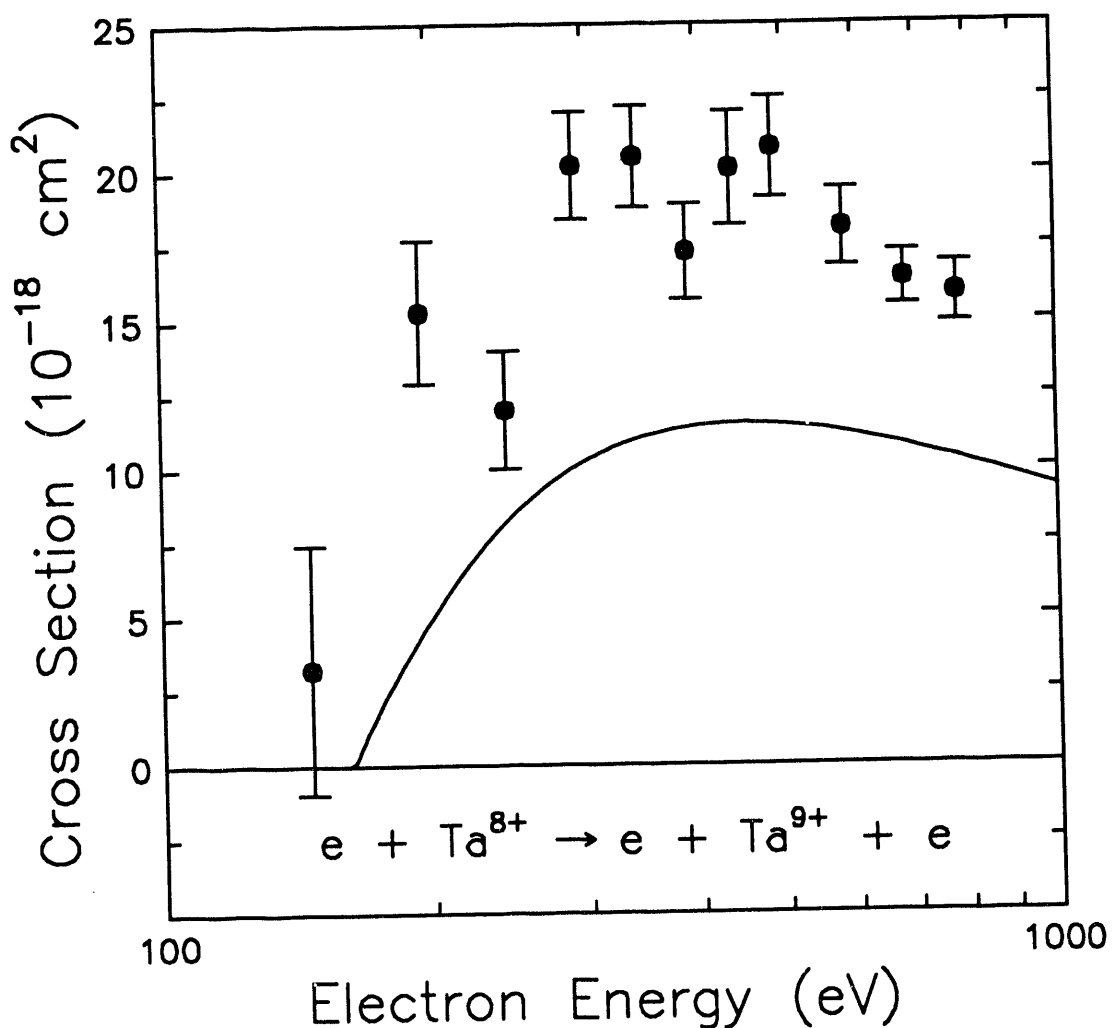
Single ionization of Xe^{8+} by electron impact. The points are the present data [M. E. Bannister *et al.*, Phys. Rev. A 38, 38 (1988)], shown with typical relative uncertainties at the one-standard-deviation level; the dashed curves are DW calculations for direct ionization from the ground (short-dash curve, by Younger) and first-excited (long-dash curve) configurations; the solid curves are CADW calculations for total ionization of $4d^{10}$ ground-state (lower curve) and $4d^95s$ excited-configuration (upper curve) ions.

ORNL-DWG 94-5794



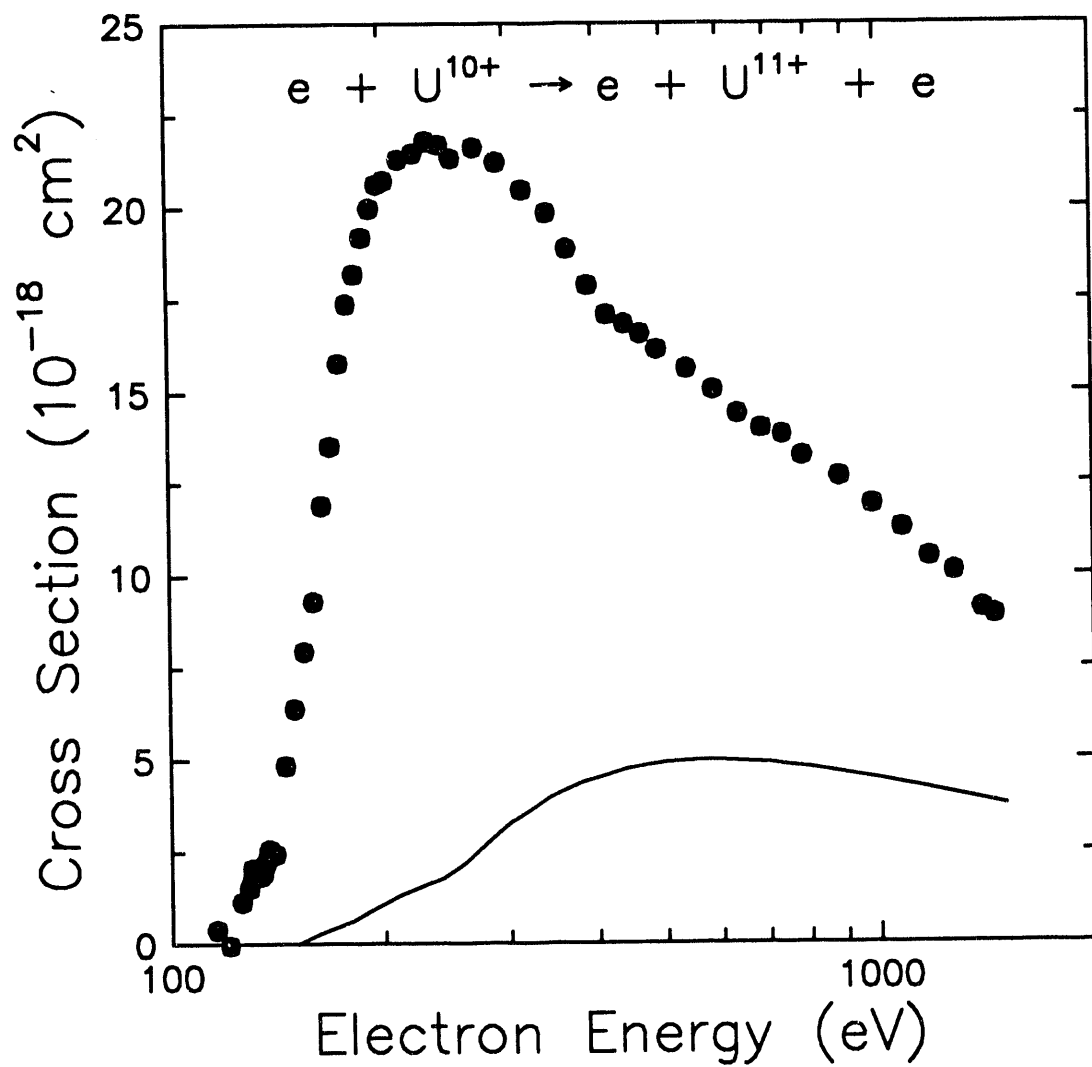
Cross sections for double ionization of Xe^{8+} . The circles are the present data [D. W. Mueller *et al.*, Phys. Rev. A 39, 2381 (1989)], with one-standard-deviation relative uncertainties. The solid line is the Lotz prediction for ionization-autoionization of 4s, 3d, and 3p electrons from metastable Xe^{8+} ($4d^95s$). The dashed curve is the Lotz prediction for ionization of 3d and 3p electrons from the ground state of Xe^{8+} .

ORNL-DWG 92-13483



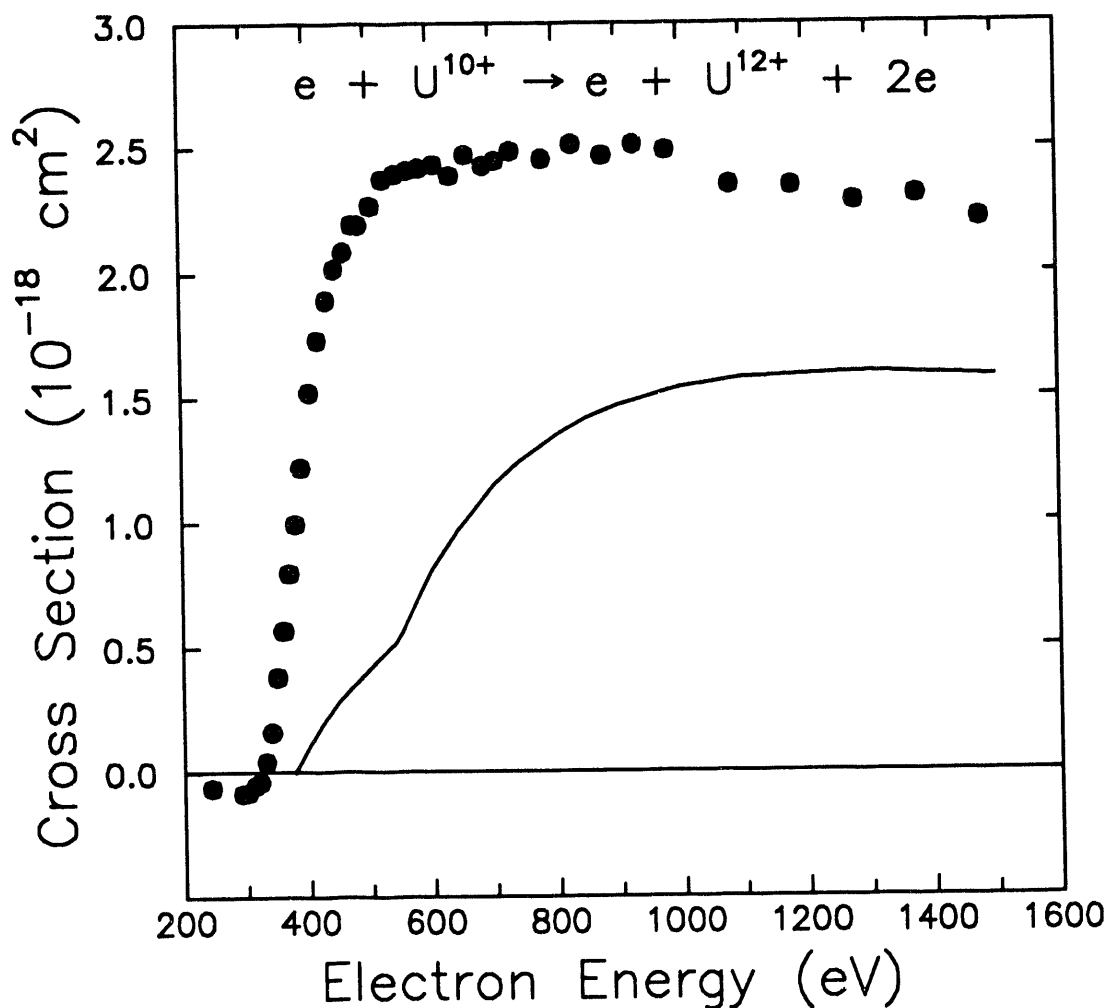
Electron-impact ionization of Ta^{8+} . The data [D. C. Gregory and F. W. Meyer, unpublished (1988)] are shown with one-standard-deviation relative uncertainties. The solid curve is a Lotz calculation for direct ionization of electrons from the ground $4f^{13}5s^25p^4$ configuration.

ORNL-DWG 94-5795



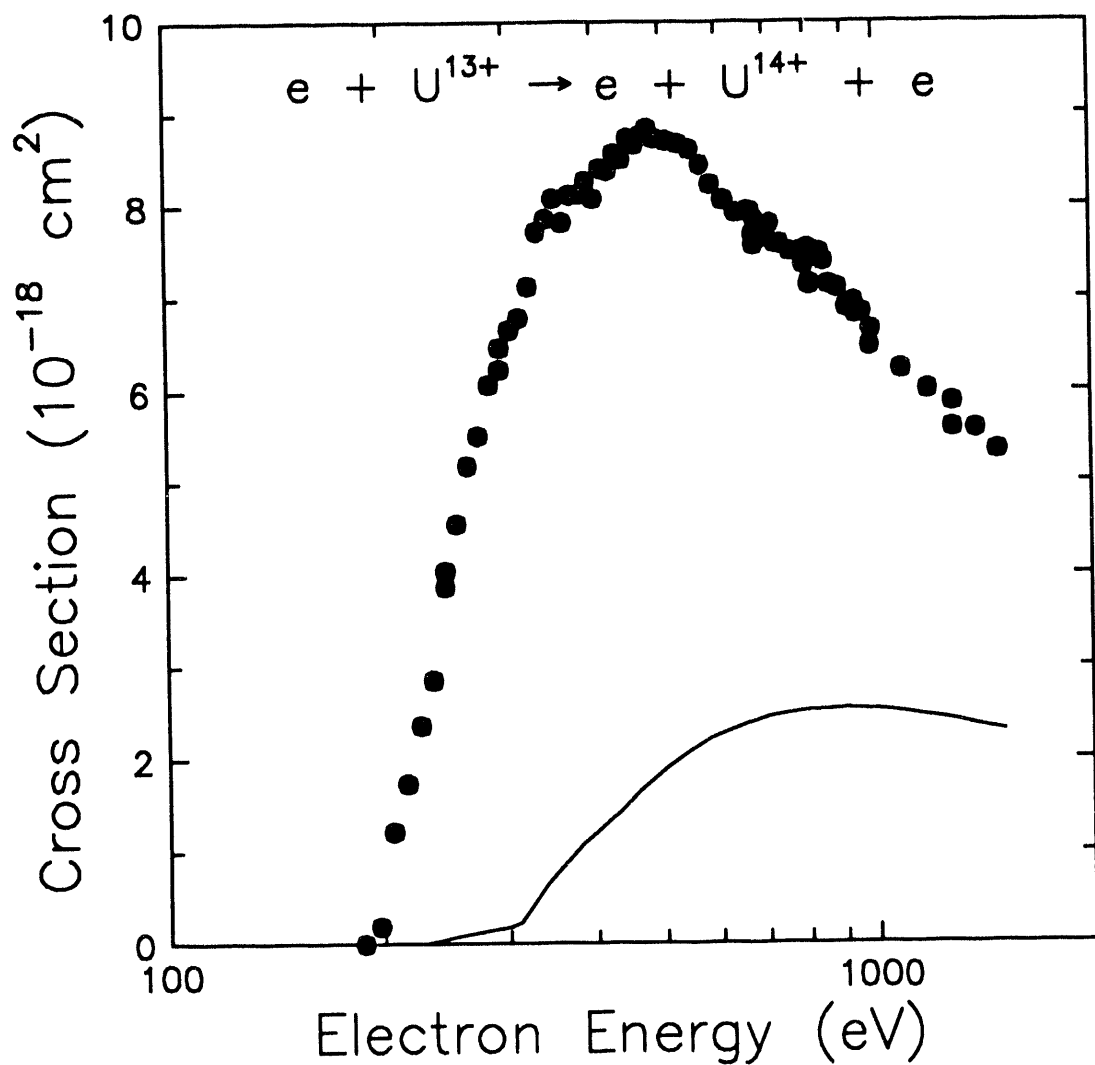
Single ionization cross sections for U^{10+} . The present data [D. C. Gregory *et al.*, Phys. Rev. A 41, 106 (1990)] are shown as solid circles; relative uncertainties at the one-standard-deviation level are smaller than the plotted symbols. The solid curve is a Lotz calculation for direct ionization of ground-configuration $5d^{10}6s^26p^2$ electrons.

ORNL-DWG 94-5796

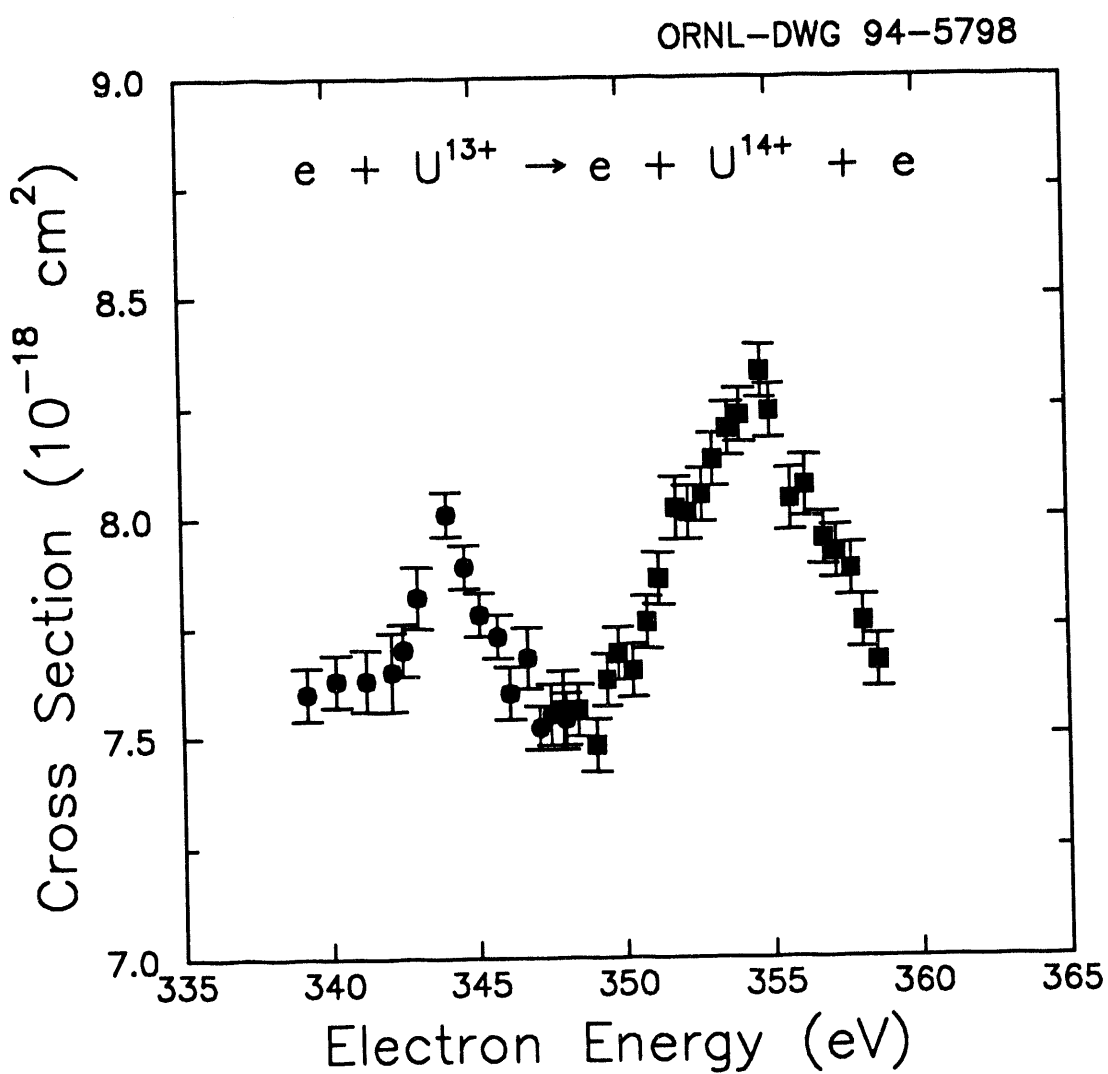


Double ionization cross sections for U^{10+} . The present data [D. C. Gregory *et al.*, Phys. Rev. A 41, 106 (1990)] are shown as solid circles; relative uncertainties at the one-standard-deviation level are smaller than the plotted symbols. The solid curve is a Lotz calculation for direct single ionization of $4f^{14}5s^25p^6$ electrons, which should contribute to double ionization following autoionization.

ORNL-DWG 94-5797

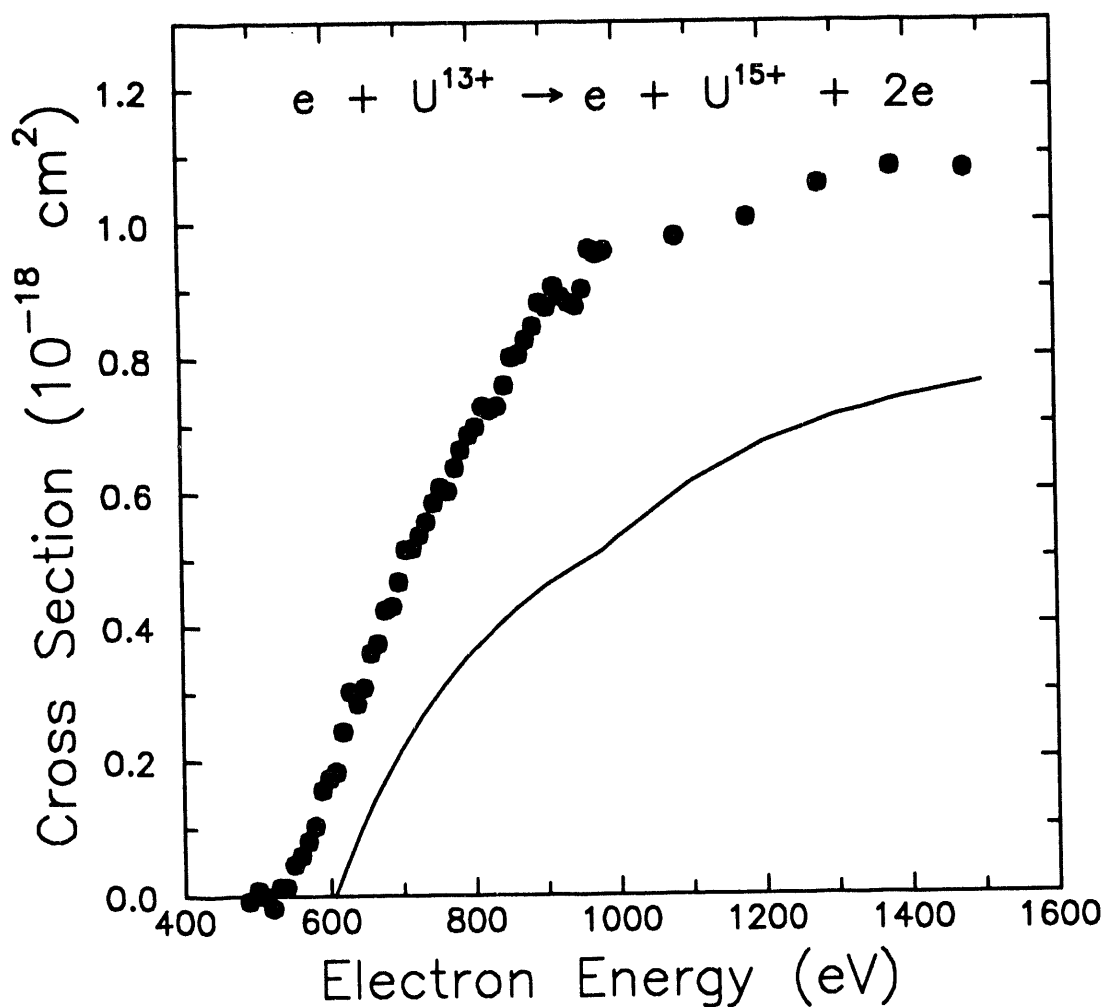


Single ionization cross sections for U^{13+} . The present data [D. C. Gregory *et al.*, Phys. Rev. A **41**, 106 (1990)] are shown as solid circles; relative uncertainties at the one-standard-deviation level are smaller than the plotted symbols. The solid curve is a Lotz calculation for direct ionization of ground-configuration $5p^6 5d^{10} 6s$ electrons.



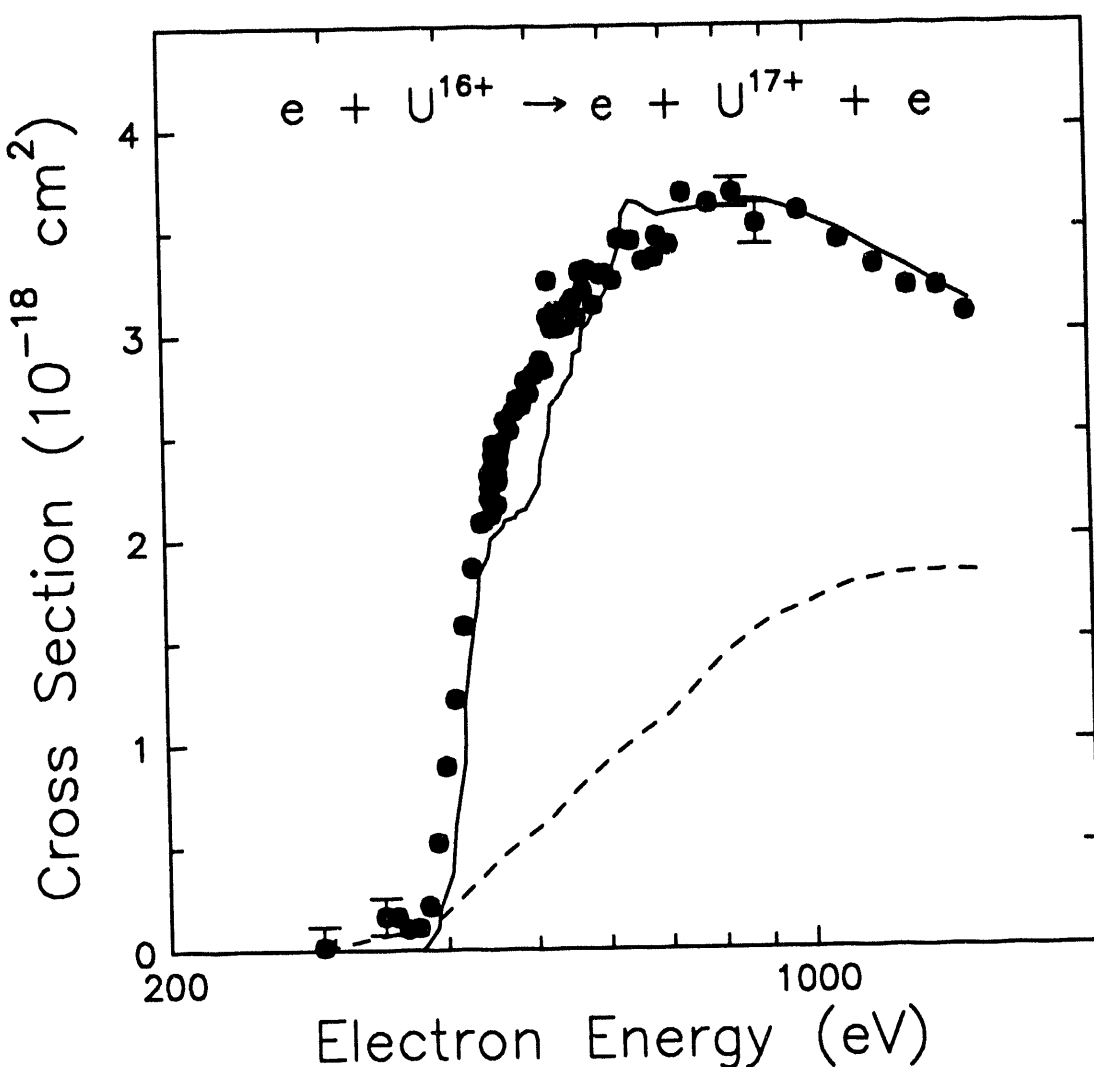
Resonance structures in the single-ionization cross section of U^{13+} . [D. C. Gregory *et al.*, Phys. Rev. A **41**, 106 (1990)] The squares and circles indicate two sets of data with overlapping energy ranges.

ORNL-DWG 94-5799



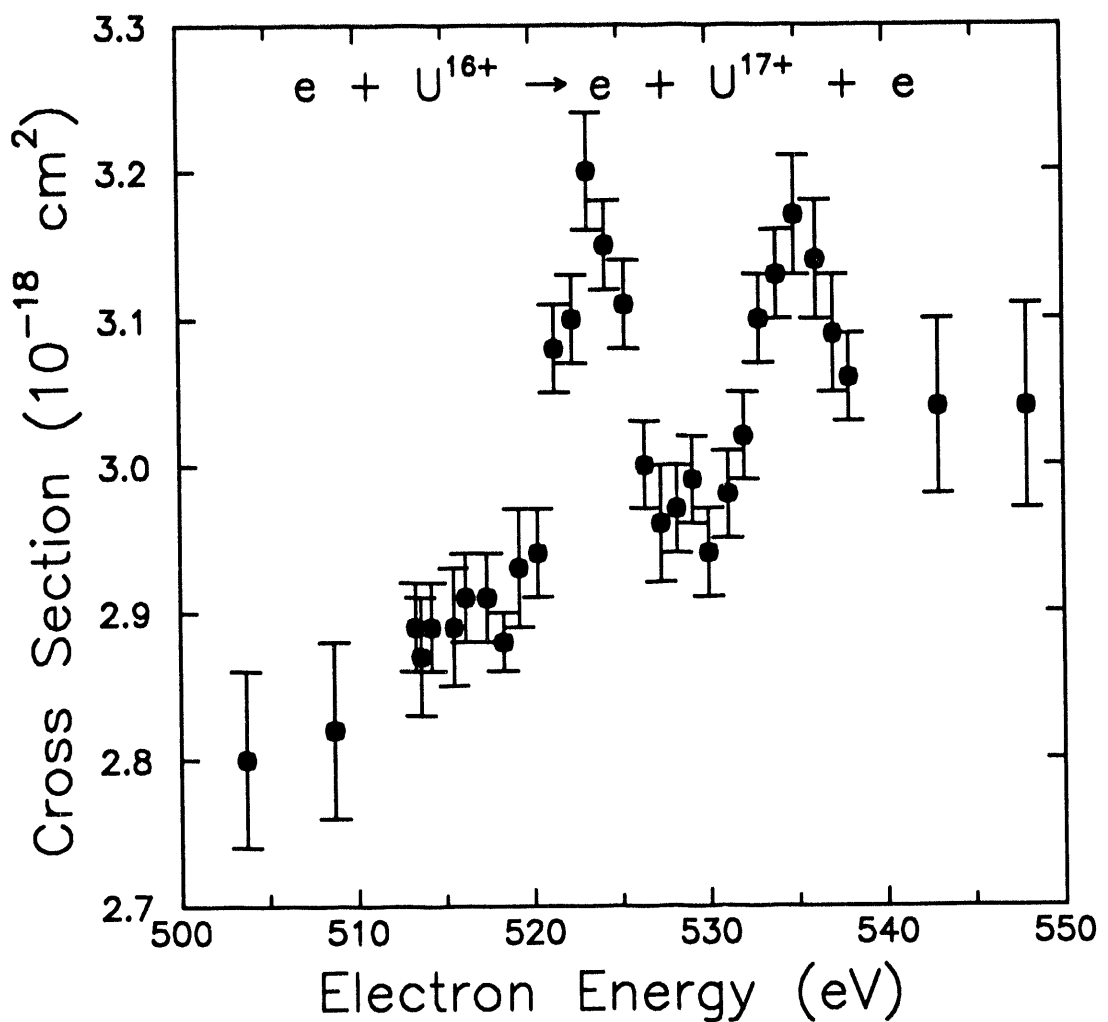
Double ionization cross sections for U^{13+} . The present data [D. C. Gregory *et al.*, Phys. Rev. A 41, 106 (1990)] are shown as solid circles; relative uncertainties at the one-standard-deviation level are smaller than the plotted symbols. The solid curve is a Lotz calculation for direct single ionization of $4\text{d}^{10}4\text{f}^{14}$ electrons, which should contribute to double ionization following autoionization.

ORNL-DWG 94-5800



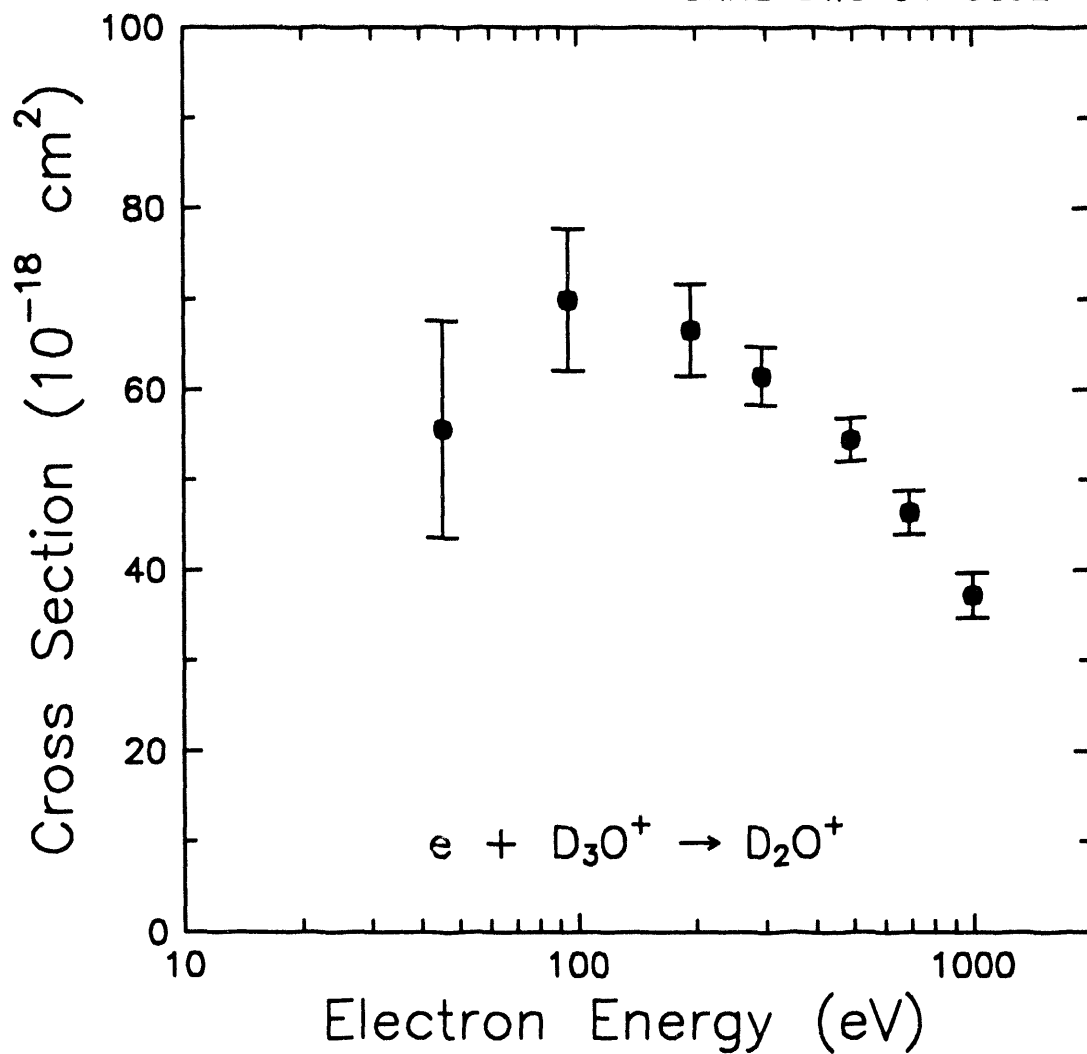
Single ionization cross sections for U^{16+} . The present data [D. C. Gregory *et al.*, Phys. Rev. A **41**, 106 (1990)] are shown as solid circles: relative uncertainties at the one-standard-deviation level are shown where larger than the plotted symbols. The dashed curve is a Lotz calculation for direct ionization of electrons from the metastable $4\text{f}^4 5\text{s}^2 5\text{p}^6 5\text{d}^7 6\text{s}$ configuration. The solid curve is a distorted-wave calculation by Pindzola and Buie for the ground configuration which includes excitation-autoionization effects.

ORNL-DWG 94-5801



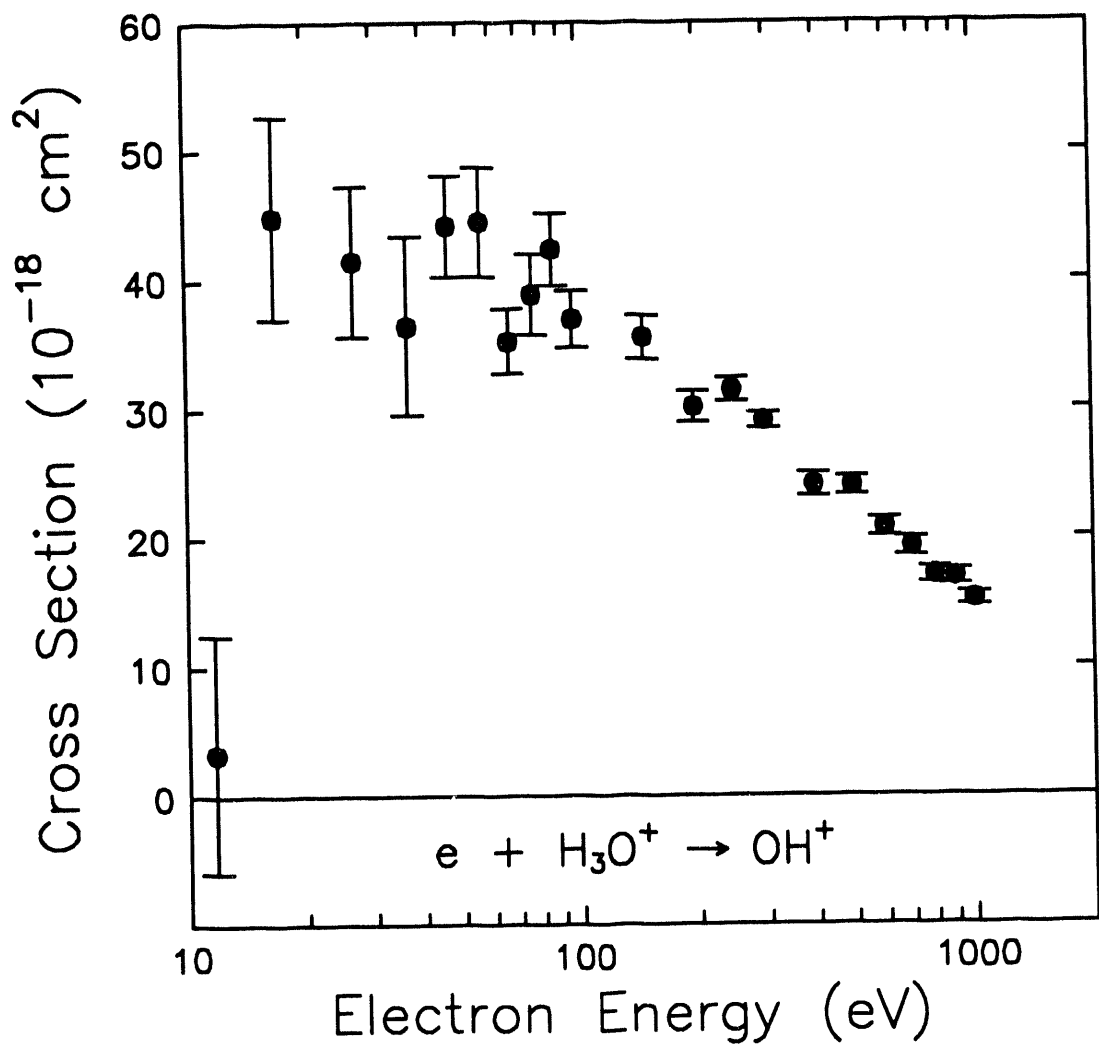
Resonance structures in the single-ionization cross section of U^{16+} . [D. C. Gregory *et al.*, Phys. Rev. A 41, 106 (1990)]

ORNL-DWG 94-5802



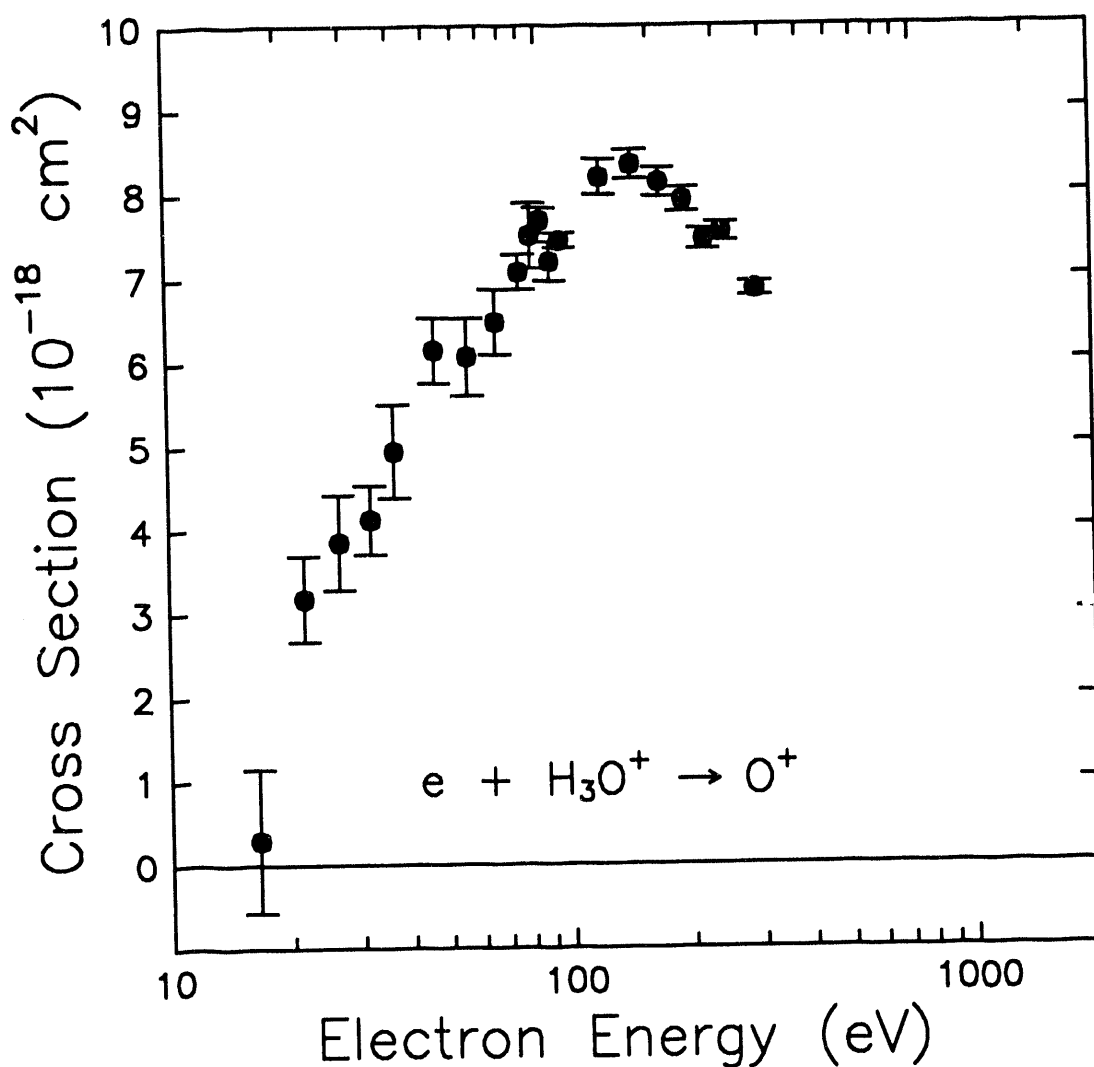
Cross section for D_2O^+ fragment production following electron impact on D_3O^+ , as a function of energy. [P. A. Schulz *et al.*, J. Chem. Phys. 85, 3386 (1986)]

ORNL-DWG 94-5803



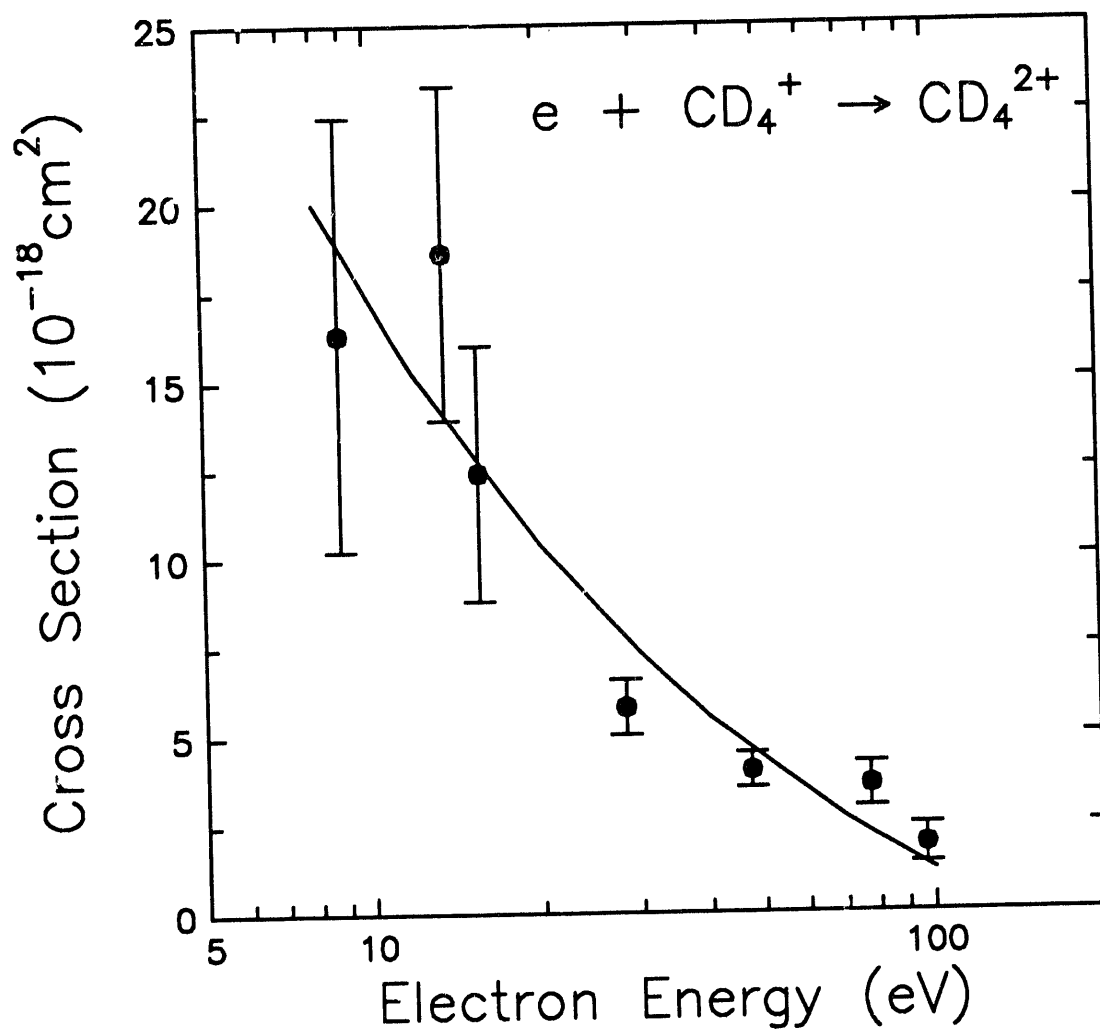
Cross section for OH⁺ fragment production following electron impact on H₃O⁺, as a function of energy. The cross section peaks at the threshold (14 ± 3 eV). [P. A. Schulz *et al.*, J. Chem. Phys. **85**, 3386 (1986)]

ORNL-DWG 94-5804



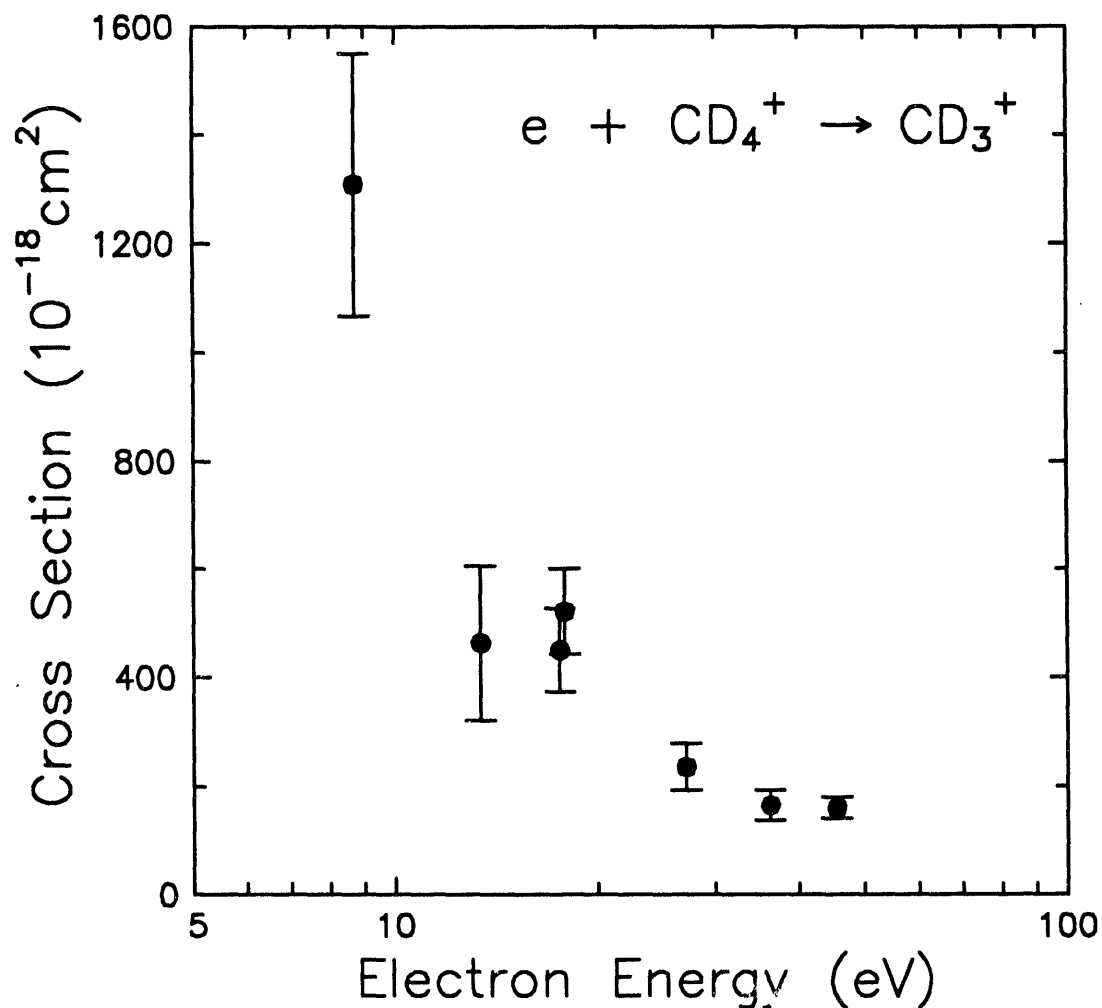
Cross section for O^+ fragment production following electron impact on H_3O^+ , as a function of electron energy. Note that the energy scale is logarithmic, emphasizing the energy region near threshold. [P. A. Schulz *et al.*, J. Chem. Phys. 85, 3386 (1986)]

ORNL-DWG 92-13484



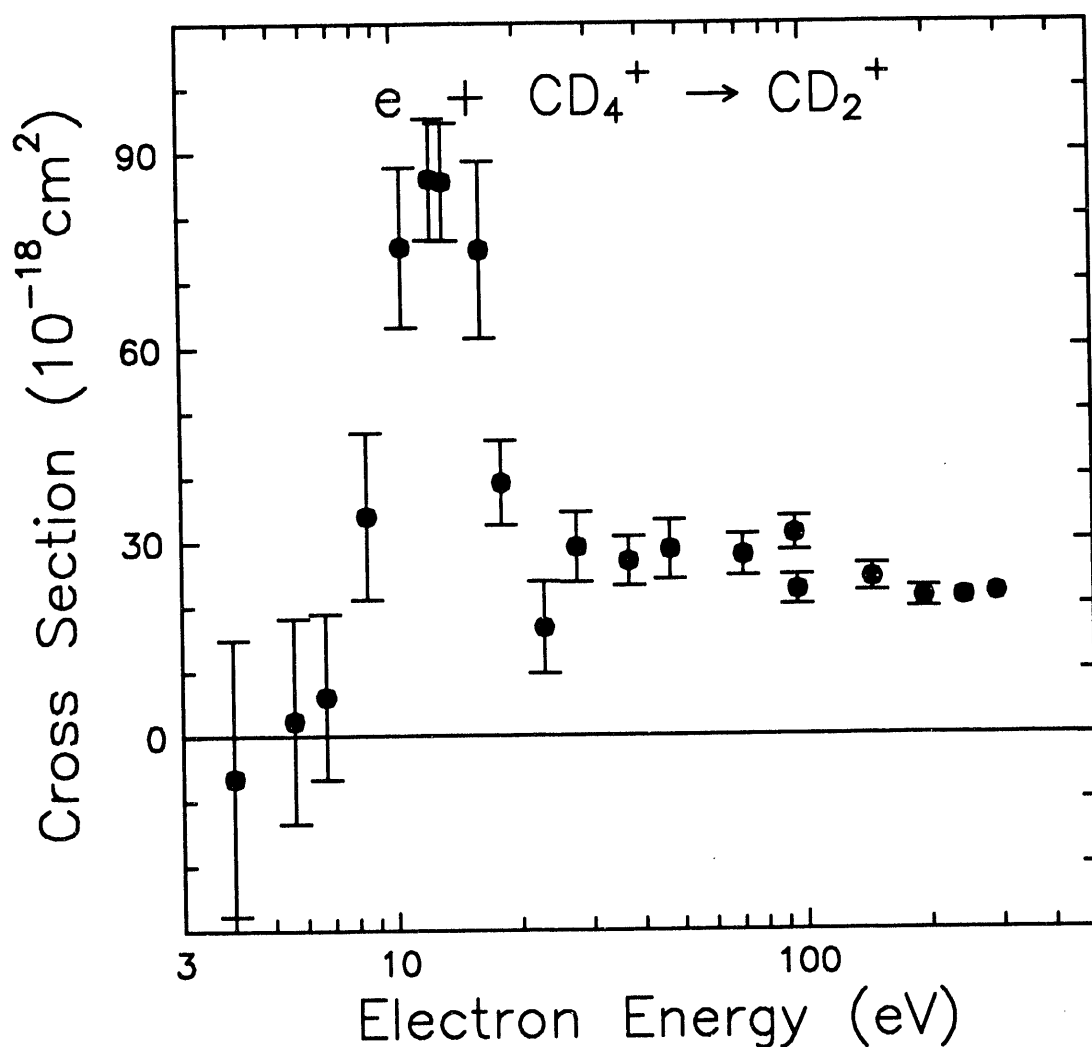
Cross section for ionization of CD_4^+ , producing CD_4^{2+} . No significant features are seen against the "background" cross section, which is represented in the figure by an analytical fit to the data. [D. C. Gregory *et al.*, unpublished (1989)]

ORNL-DWG 92-13485



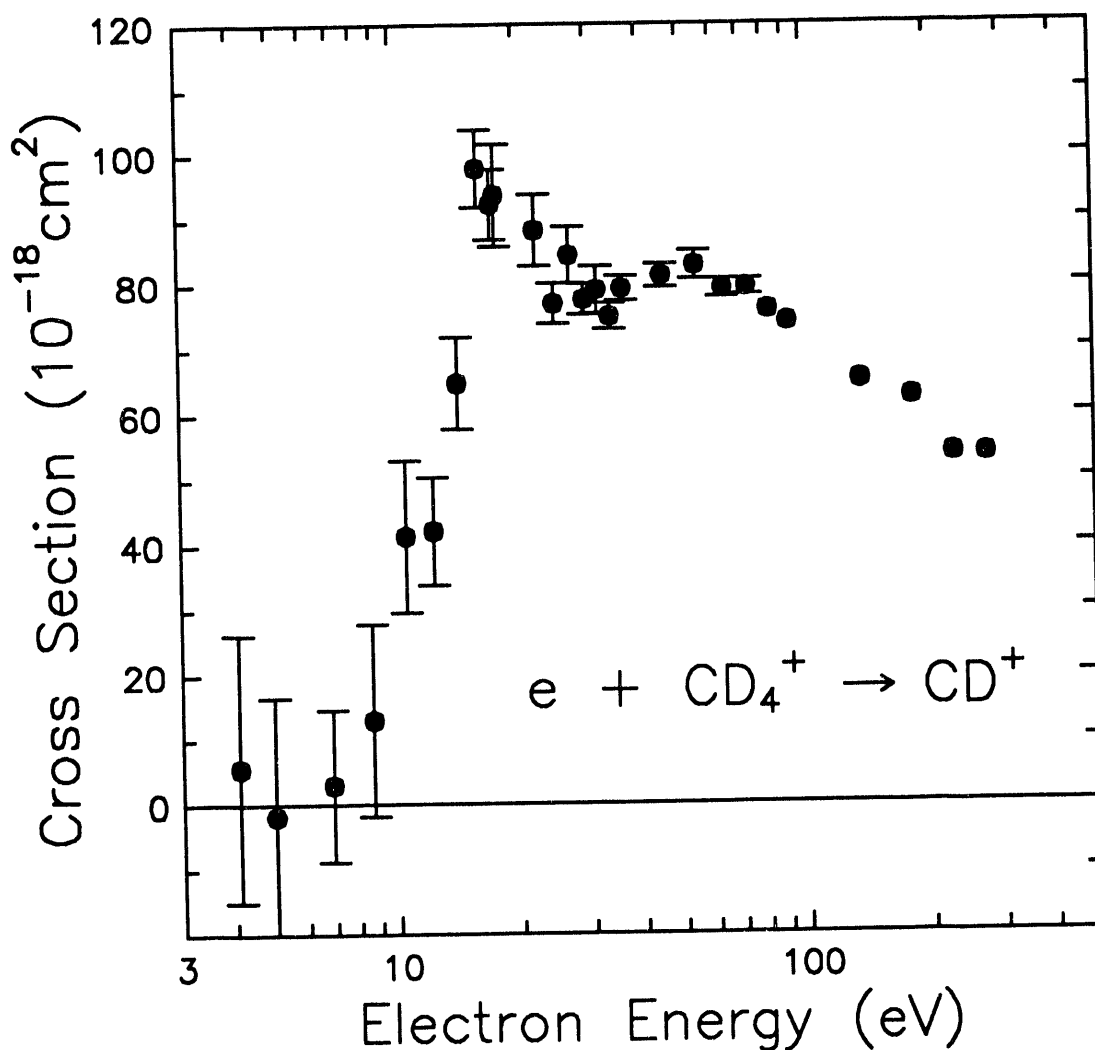
Cross section for the dissociation of CD_4^+ to CD_3^+ . No features are apparent against the overwhelming background signal. [D. C. Gregory *et al.*, unpublished (1989)]

ORNL-DWG 92-13486



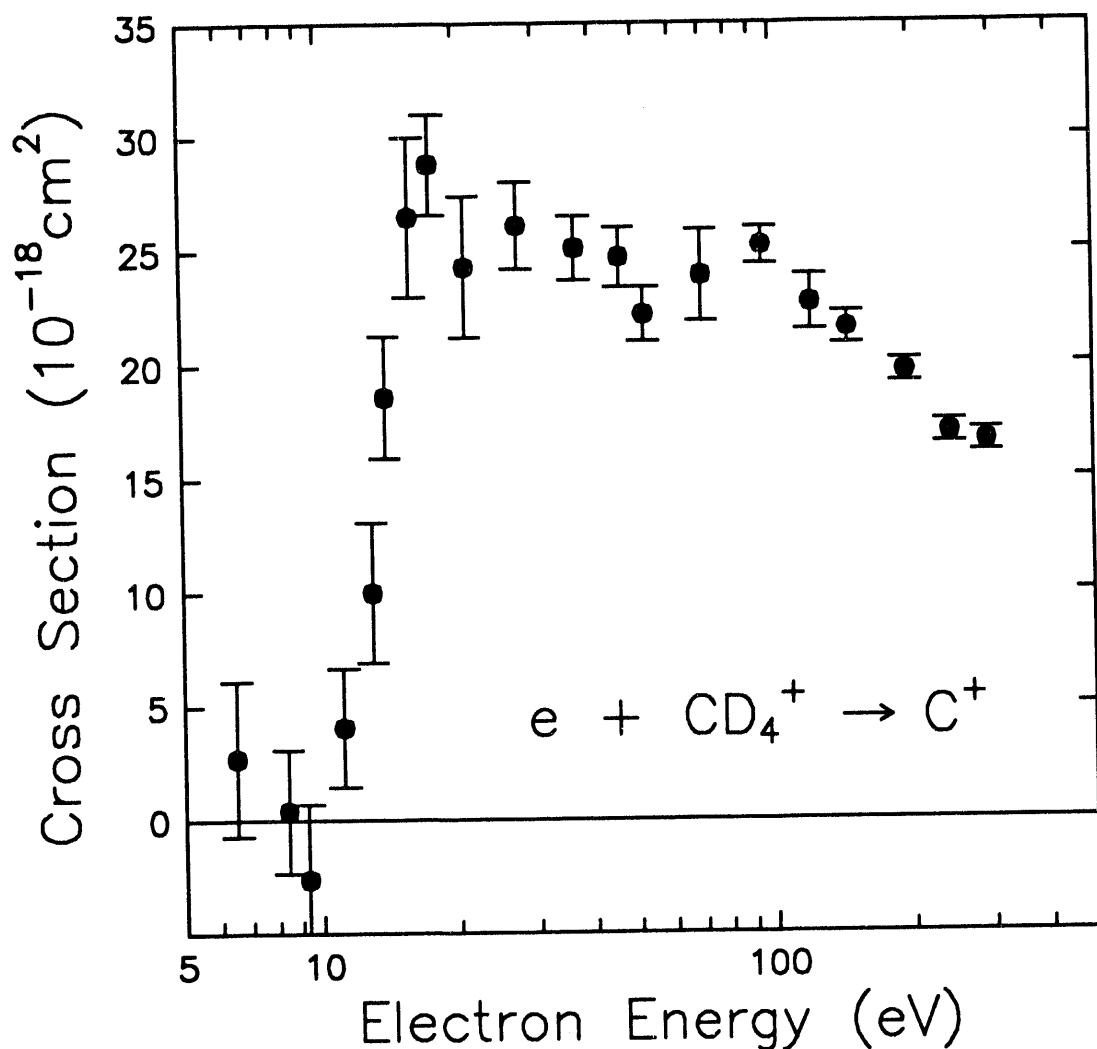
Cross section for the dissociation of CD_4^+ to CD_2^+ . A "background" cross section has been subtracted from the experimental data to emphasize the structure. The subtracted function, $294 \times 10^{-18} E^{1/2}$, where E is the energy in eV, is a reasonable guess, but other forms could as easily have been chosen. [D. C. Gregory *et al.*, unpublished (1989)]

ORNL-DWG 92-13487



Cross section for the dissociation of CD_4^+ to CD^+ . A "background" cross section has been subtracted from the data to emphasize the structure. The subtracted function, $400 \times 10^{-18}/E$, where E is the energy in eV, is a reasonable guess, but other forms could as easily have been chosen. [D. C. Gregory *et al.*, unpublished (1989)]

ORNL-DWG 94-5805



Cross section for the dissociation of CD_4^+ to C^+ . A "background" cross section has been subtracted from the data to emphasize the structure. The subtracted function, $36 \times 10^{-18} E^{-1/2}$, where E is the energy in eV, is a reasonable guess, but other forms could as easily have been chosen. [D. C. Gregory *et al.*, unpublished (1989)]

ORNL/TM-12729

INTERNAL DISTRIBUTION

- | | |
|-------------------------|--|
| 1. J. B. Ball | 36. P. K. Mioduszewski |
| 2-11. M. E. Bannister | 37. S. Ovchinnikov |
| 12. F. E. Bertrand | 38. S. Raman |
| 13. L. G. Christophorou | 39. D. R. Schultz |
| 14. S. Datz | 40. I. A. Sellin |
| 15. P. F. Dittner | 41. J. Sheffield |
| 16. R. A. Dory | 42. J. L. Shinpaugh |
| 17. L. Folkerts | 43. C. R. Vane |
| 18. J. D. Garrett | 44-45. Controlled Fusion Atomic
Data Center |
| 19-28. D. C. Gregory | 46. Central Research Library |
| 29. X. Q. Guo | 47. Document Reference Section |
| 30. C. C. Havener | 48-49. Laboratory Records Department |
| 31. J. T. Hogan | 50. Laboratory Records, RC |
| 32. R. C. Isler | 51. ORNL Patent Section |
| 33. H. F. Krause | 52. Fusion Energy Division Library |
| 34. J. H. Macek | 53. Fusion Engineering Design Center |
| 35. F. W. Meyer | |

EXTERNAL DISTRIBUTION

54. Office of the Assistant Manager for Energy Research and Development, U.S.
Department of Energy Field Office, Oak Ridge, P.O. Box 2000, Oak Ridge, TN 37831
55. V. A. Abramov, Institute Atommoi Energii, IV Kurchatova, 46 Ulitsa Kurchatova,
Moscow D-182, Russia 123182
56. V.V. Afrosimov, AF Ioffe Physical-Technical Institute, St. Petersburg K-21 Russia
194021
57. G. Alber, Fakultat fur Physik, Albert-Ludwigs-Universitat, Hermann-Herder-Strasse 3,
D-79104 Freiburg, Germany
58. M. Ya. Amusia, AF Ioffe Physico-Technical Institute, St. Petersburg, Russia 194021
59. R. Aymar, CEN/Cadarache, Departement de Research sur la Fusion Controlée, F-13108
Saint-Paul-lez-Durance Cedex, France
60. N. R. Badnell, Department of Physics and Applied Physics, University of Strathclyde,
Glasgow G4 0NG, Scotland
61. D. E. Baldwin, Lawrence Livermore National Laboratory, P.O. Box 5511, Livermore,
CA 94550
62. E. C. Beaty, 3005 Stanford Avenue, Boulder, CO 80303-5342
63. P. Beiersdorfer, L-421, Lawrence Livermore National Laboratory, P.O. Box 808,
Livermore, CA 94550
64. D. S. Belic, University of Beograd, P.O. Box 550, Beograd, Yugoslavia
65. E. W. Bell, JILA, Campus Box 440, University of Colorado, Boulder, CO 80309
66. R. D. Bengston, Department of Physics, University of Texas, Austin, TX 78712-1081
67. K. A. Berrington, Department of Theoretical Physics and Applied Mathematics, Queen's
University of Belfast, Belfast BT7 1NN, United Kingdom
68. Bibliothek, Institut für Plasmaphysik, KFA Jülich GmbH, Postfach 1913, D-5170 Jülich,
Federal Republic of Germany

69. Bibliothek, KfK Karlsruhe GmbH, Postfach 3640, K-7500 Karlsruhe 1, Federal Republic of Germany
70. Bibliothek, Max-Planck Institut für Plasmaphysik, Boltzmannstrasse 2, D-8046 Garching, Federal Republic of Germany
71. Bibliothèque, CEN/Cadarache, F-13108 Saint-Paul-lez-Durance, Cedex, France
72. Bibliotheque, Centre de Recherches en Physique des Plasmas, 21 Avenue des Bains, 1007 Lausanne, Switzerland
73. Bibliotheque, Service due Confinement des Plasma, CEA, B.P. 6, 92 Fontenay-aux-Roses (Seine), France
74. M. Bitter, Princeton Plasma Physics Laboratory, P.O. Box 451, Princeton, NJ 08543
75. S.L. Bliman, Centre D'Etudes Nucleaires de Grenoble, 85 X Avenue des Martyrs, F-38041 Grenoble, Cedex, France
76. J. Botero, Nuclear Data Section, IAEA, Wagramerstrasse 5, P.O. Box 100, A-1400 Vienna, Austria
77. F. Brouillard, Institut de Physique, Chemin du Cyclotron 2, B 1348 Louvain-la-Neuve, Belgium
78. P. G. Burke, Department of Theoretical Physics and Applied Mathematics, Queen's University of Belfast, Belfast BT7 1NN, United Kingdom
79. J. Callaway, Department of Physics and Astronomy, Louisiana State University, Baton Rouge, LA 70803-4001
80. J.D. Callen, Department of Nuclear Engineering, University of Wisconsin, 1500 Johnson Drive, Madison, WI 53706-1687
81. R. Camilloni, Istituto Metodologie Avanzate Inorganiche CNR, Area della Ricerca di Roma, CP10, 00016 Monterotondo Scalo, Italy
82. S. J. Chantrenne, Hewlett-Packard Circuit Tech R&D, P.O. Box 10350, Palo Alto, CA 94303
83. M. H. Chen, V Division, L-296, Lawrence Livermore National Laboratory, P.O. Box 808, Livermore, CA 94550
84. Y.S. Chung, JILA, Campus Box 440, University of Colorado, Boulder, CO 80309
85. A. Chutjian, Jet Propulsion Laboratory, Mail Stop 183-601, California Institute of Technology, 4800 Oak Grove Drive, Pasadena, CA 91109
86. C. Cisneros, Instituto de Fisica, Apartado Postal 139-B, Cuernavaca 62191, Mexico
87. R. E. H. Clark, Group X-6, MS B226, Los Alamos National Laboratory, Los Alamos, NM 87545
88. E. J. Clothiaux, Department of Physics, Auburn University, AL 36849-5311
89. C. L. Cocke, Department of Physics, Cardwell Hall, Kansas State University, Manhattan, KS 66502
90. S. A. Cohen, Princeton Plasma Physics Laboratory, P.O. Box 451, Princeton, NJ 08543
91. L.A. Collins, T-4 MS-212, Los Alamos Scientific Laboratory, Los Alamos, NM 87545
92. R.W. Conn, Mechanical, Aerospace, and Nuclear Engineering Dept., 6291 Boelter Hall, University of California, Los Angeles, CA 90024-1597
93. R.D. Cowan, T-Division, MS 212, Los Alamos National Laboratory, P.O. Box 1663, Los Alamos, NM 87544
94. D.H. Crandall, ER54 G242 GTN, Office of Fusion Energy, U.S. Department of Energy, Washington, DC 20585
95. M. D. Crisp, ER-541 GTN, Office of Fusion Energy, U.S. Department. of Energy, Washington, DC 20585

96. J. W. Cuthbertson, MS 13/516, General Atomics, P.O. Box 85608, San Diego, CA 92186
97. A. Dalgarno, Harvard-Smithsonian Center for Astrophysics, 60 Garden Street, MS 14, Cambridge, MA 02138
98. H.E. Dalhed, L-059, Lawrence Livermore National Laboratory, P.O. Box 808, Livermore, CA 94550
99. N. A. Davies, Director, Office of Fusion Energy, Office of Energy Research, ER-50, Germantown, U.S. Department of Energy, Washington, DC 20585
100. S.O. Dean, Fusion Power Associates, 2 Professional Drive, Suite 248, Gaithersburg, MD 20879
101. P. Defrance, Universire Catholique de Louvain, Institut de Physique, B-1348 Louvain la Neuve, Belgium
102. F.J. De Heer, FOM-Institute of Atomic and Molecular Physics, Postbus 41883, 1009 DB Amsterdam, The Netherlands
103. N. Djuric, JILA, Campus Box 440, University of Colorado, Boulder, CO 80309
104. Documentation S.I.G.N., Department de la Physique du Plasma et de la Fusion Controlee, Centre d'Etudes Nucleaires, B.P. No. 85, Centre du Tri, 38041-Cedex, Grenoble, France
105. K.T. Dolder, Department of Atomic Physics, University of Newcastle Upon Tyne, Newcastle-on-Tyne NEI 7RU, United Kingdom
106. R.D. DuBois, Battelle Pacific Northwest Labs, P.O. Box 999, Richland, WA 99352
107. J. L. Duggan, Department of Physics, University of North Texas, Denton, TX 76203
108. G.H. Dunn, JILA, Campus Box 440, University of Colorado, Boulder, CO 80309
109. H. Ehrhardt, Fachbereich Physik, Universitat Kaiserslautern, D-6750 Kaiserslautern, Germany
110. G.A. Eliseev, I.V. Kurchatov Institute of Atomic Energy, P.O. Box 3402, 123182 Moscow, Russia
111. S. Elliot, L-296, Lawrence Livermore National Laboratory, P.O. Box 808, Livermore, CA 94550
112. R.A. Falk, Boeing Aerospace Co., P.O. Box 3999, MS 87-50, Seattle, WA 98124
113. U. Fano, James Franck Institute, Rm. 227, University of Chicago, 5640 S. Ellis Ave., Chicago, IL 60637
114. J.L. Feldman, Code 6691, Naval Research Laboratory, 4555 Overlook Avenue SW, Washington, DC 20375
115. C.F. Fischer, Department of Computer Science, Vanderbilt University, Box 1679 B, Nashville, TN 37235
116. H.K. Forsen, Bechtel Group, Inc., Research Engineering, P.O. Box 3965, San Francisco, CA 94119
117. T.F. Gallagher, Physics Department, University of Virginia, Charlottesville, VA 22901
118. S. Geltman, JILA, Campus Box 440, University of Colorado, Boulder, CO 80309
119. H.B. Gilbody, Department of Pure and Applied Physics, Queen's University of Belfast, Belfast BT7 1NN, United Kingdom
120. J.R. Gilleland, Bechtel Group, Inc., P.O. Box 3965, San Francisco, CA 94119
121. V.A. Glukhikh, Scientific-Research Institute of ElectroPhysical Apparatus, 188631 St. Petersburg, Russia
122. D.E. Golden, University of North Texas, P.O. Box 5308, Denton, TX 76203
123. L.B. Golden, Department of Physics, Worthington Scranton Campus, Pennsylvania State University, 120 Ridge View Drive, Dunmore, PA 18512

124. T. W. Gorczyca, Department of Physics, Auburn University, AL 36849-5311
125. R.W. Gould, Department of Applied Physics, MS 128-95, California Institute of Technology, Pasadena, CA 91125
126. H. R. Griem, Laboratory for Plasma Research, University of Maryland, College Park, MD 20742
127. D.C. Griffin, Department of Physics, Rollins College, Winter Park, FL 32789
128. R.A. Gross, Plasma Research Laboratory, Columbia University, New York, NY 10027
129. Y. Hahn, Department of Physics, University of Connecticut, Storrs, CT 06268
130. M.F.A. Harrison, Culham Laboratory, Room 131/F7, UKAEA Research Group, Abingdon, Oxfordshire, OX 14 3DB, United Kingdom
131. B.E. Hasselquist, Box 292 UMHC, University of Minnesota, 420 Delaware Street SE, Minneapolis, MN 55455
132. R. J. Hawryluk, Princeton Plasma Physics Laboratory, P.O. Box 451, Princeton, NJ 08543
133. A.U. Hazi, L-296, Lawrence Livermore National Laboratory, P.O. Box 808, Livermore, CA 94550
134. R.J.W. Henry, Department of Physics, Miami University, Oxford, OH 45056
135. A.P. Hickman, Molecular Physics Laboratory, SRI International, Menlo Park, CA 94023
136. E. Hinnov, Princeton Plasma Physics Laboratory, P.O. Box 451, Princeton, NJ 08543
137. J.R. Hiskes, L-630, Lawrence Livermore National Lab., Livermore, CA 94550
138. A. M. Howald, MS 15/115, General Atomics, P.O. Box 85608, San Diego, CA 92186
139. J.G. Hughes, Department of Information Systems, University of Ulster, Jordanstown, Co. Antrim, BT 37 OQB, United Kingdom
140. R.A. Hulse, Princeton Plasma Physics Laboratory, P.O. Box 451, Princeton, NJ 08543
141. M. S. Huq, Yale University School of Medicine, Department of Therapeutic Radiation, Hunter Radiation Therapy 215, New Haven, CT 06511-8040
142. M. Inokuti, Environmental Research Division, Argonne National Laboratory, 9700 S. Cass Avenue Bldg. 203, Argonne, IL 60439
143. The Institute of Plasma Physics, Director, P.O. Box 1126, Hefei, Anhui, People's Republic of China
144. Y. Itikawa, Institute of Space and Astronautical Science, 3-1-1 Yoshinodai, Sagamihara 229, Japan
145. V.L. Jacobs, Code 6693, Naval Research Laboratory, 4555 Overlook Avenue SW, Washington, DC 20375
146. G. Jamelot, LSAI, BAL 350, Université Paris-Sud, Ba^t. 350, 91405 Orsay, France
147. R.K. Janev, Nuclear Data Section, IAEA, Wagramerstrasse 5, P.O. Box 100, A-1400 Vienna, Austria
148. C.J. Joachain, Physique Theorique, Faculte des Sciences, Universite Libre de Bruxelles, Code Postal 227, Campus Plaine U.L.B., Boulevard du Triomphe, B-1050, Bruxelles, Belgium
149. Joint Institute for Laboratory Astrophysics, Publications Distribution Center, University of Colorado, Boulder, CO 80309
150. B.M. Johnson, Bldg. 510C, Brookhaven National Laboratory, Upton, NY 11973
151. K.W. Jones, Department of Applied Science, Bldg. 815, Brookhaven National Laboratory, Upton, NY 11973
152. E. Kallne, Physics I, Royal Institute of Technology, S-10044 Stockholm, Sweden
153. Y. Kaneko, Tokyo Metropolitan University, 1-1 Minami-Ohsawa, Hachioji, Tokyo 192-03, Japan

154. T. Kato, Data and Planning Center, National Inst. for Fusion Science, Nagoya 464-01, Japan
155. H.P. Kelly, Department of Physics, University of Virginia, Charlottesville, VA 22901
156. Y.-K. Kim, National Institute of Standards and Technology, Bldg. 221 Room A267, Gaithersburg, MD 20899
157. A.E. Kingston, Department of Theoretical Physics and Applied Mathematics, Queen's University of Belfast, Belfast BT7 1NN, United Kingdom
158. M. Klapisch, Code 6730, Naval Research Laboratory, 4555 Overlook Ave SW, Washington, DC 20375
159. J.L. Kohl, Harvard-Smithsonian Center for Astrophysics, 60 Garden Street, Cambridge, MA 02138
160. T.M. Kojima, Atomic Physics Laboratory, RIKEN, 2-1 Hirosawa, Wako-shi, Saitama 351-01, Japan
161. T.J. Kvale, Department of Physics and Astronomy, University of Toledo, 2801 W. Bancroft Street, Toledo, OH 43606
162. K. J. LaGattuta, X-6 Group B-226, Los Alamos National Laboratory, Los Alamos, NM 87545
163. Y.T. Lee, L-355, Lawrence Livermore National Lab., P.O. Box 808, Livermore, CA 94550
164. Library, Culham Laboratory, UKAEA, Abingdon, Oxfordshire OX14 3DB, United Kingdom
165. Library, FOM Institut voor Plasmaphysica, Rijnhuizen, Edisonbaan 14, 3439 MN Nieuwegein, The Netherlands
166. Library, Institute of Physics, Academia Sinica, Beijing, Peoples Republic of China
167. Library, Japan Atomic Energy Research Institute, Naka Fusion Research Establishment, 801-1 Mukoyama, Naka-machi, Naka-gun, Ibaraki-ken, Japan
168. Library, National Institute for Fusion Science, Chikusa-ku, Nagoya 464-01, Japan
169. Library, International Centre for Theoretical Physics, P.O. Box 586, I-34100 Trieste, Italy
170. Library, JET Joint Undertaking, Abingdon, Oxfordshire OX14 3EA, England
171. Library, Laboratorio Gas Ionizzati, Frascati, Italy
172. Library, Plasma Physics Laboratory, Kyoto University, Gokasho, Uji, Kyoto 611, Japan
173. Library, Princeton Plasma Physics Laboratory, P.O. Box 451, Princeton, NJ 08543
174. P. C. Liewer, MS 138-208, Jet Propulsion Laboratory, 4800 Oak Grove Drive, Pasadena, CA 91109
175. S.I. Lippmann, MS 13/468, General Atomics, P.O. Box 85608, San Diego, CA 92186
176. K.F. Man, Jet Propulsion Laboratory, California Institute of Technology, 4800 Oak Grove Drive, Pasadena, CA 91109
177. J.B. Mann, Los Alamos National Laboratory, P.O. Box 1663, Los Alamos, NM 86544
178. E.S. Marmar, NW17-105, MIT Plasma Fusion Center, 167 Albany Street, Cambridge, MA 02139
179. J.V. Martinez, ER-141, Office of Basic Energy Sciences, U.S. Department of Energy, Washington, DC 20585
180. J.B. McGrory, ER-23 GTN, Office of Fusion Energy, U.S. Department of Energy, Washington, DC 20585
181. E.J. McGuire, Sandia National Laboratories, Orgn. 1231, Albuquerque, NM 87115
182. R. H. McKnight, ER-542 GTN, Office of Fusion Energy, U.S. Department of Energy, Washington, DC 20585

183. D.M. Meade, Princeton Plasma Physics Laboratory, P.O. Box 451, Princeton, NJ 08543
184. W. Mehlhorn, Fakultat fur Physik, Universitat Freiburg, D-7800 Freiburg, Germany
185. A.L. Merts, T-4, MS 212, Los Alamos Scientific Laboratory, Los Alamos, NM 87544
186. D.R. Mikkelsen, Princeton Plasma Physics Laboratory, P.O. Box 451, Princeton, NJ 08543
187. J.B.A. Mitchell, Physics Department, University of Western Ontario, London, ON N6A 3K7, Canada
188. D.L. Moores, Department of Physics and Astronomy, University College London, Gower Street, London WC1E 6BT, United Kingdom
189. T.J. Morgan, Department of Physics, Wesleyan University, Middletown, CT 06457
190. W.L. Morgan, Kinema Research, P.O. Box 1147, Monument, CO 80132
191. R.L. Morse, P.O. Box 1416, Los Alamos, NM 87544
192. A.Z. Msezane, Department of Physics, Clark University, 223 James P. Brawley Drive, Atlanta, GA 30314
193. D. Mueller, Physics Department, University of North Texas, Box 5368, Denton, TX 76203
194. A. Muller, Institut fur Strahlenphysik der Universitat Stuttgart, Allmandring 3, D-70569 Stuttgart, Germany
195. D.W. Norcross, JILA, University of Colorado, Boulder, CO 80309
196. S. Ohtani, National Institute for Fusion Science, Nagoya 464-01, Japan
197. R.E. Olson, Physics Department, University of Missouri-Rolla, Rolla, MO 65401
198. R. Parker, Plasma Fusion Center, Massachusetts Institute of Technology, 167 Albany St., NW16-288, Cambridge, MA 02139
199. O. Pavlichenko, Kharkov Physical-Technical Institute, Academical St. 1, 310108 Kharkov, Ukraine
200. B. Peart, Department of Atomic Physics, University of Newcastle-Upon-Tyne, Newcastle-on-Tyne, NE1 7RU United Kingdom
201. R. D. Petrasso, NW16-132, MIT Plasma Fusion Center, 167 Albany Street, Cambridge, MA 02139
202. R.A. Phaneuf, Department of Physics 220, University of Nevada-Reno, Reno, NV 89557
203. M.S. Pindzola, Physics Department, Auburn University, Auburn, AL 36849-5311
204. Plasma Research Laboratory, Australian National University, P.O. Box 4, Canberra, A.C.T. 2601, Australia
205. D. E. Post, Jr., ITER-San Diego Joint Work Site, 11025 N. Torrey Pines Rd., La Jolla, CA 92037
206. A.K. Pradhan, Department of Astronomy, Ohio State University, Columbus, OH 43210-1106
207. J.F. Reading, Physics Department, Texas A&M University, College Station, TX 77843-4242
208. P.J. Reardon, SSCL, 2250 Beckleymeade Avenue, Dallas, TX 75237
209. C. B. Reddy, Department of Physics, University of North Texas, Denton, TX 76203
210. K. Rinn, Wild Leitz, D-6330 Wetzlar, Germany
211. J.R. Roberts, National Institute of Standards and Technology, Gaithersburg, MD 20899
212. M. Roberts, International Programs, Office of Fusion Energy, Office of Energy Research, ER-52, Germantown, U.S. Department of Energy, Washington, DC 20585
213. F. J. Robicheaux, Department of Physics, Auburn University, AL 36849-5311
214. W.L. Rowan, Fusion Research Center, University of Texas, Austin, TX 78712

215. D.D. Ryutov, Institute of Nuclear Physics, Sovetskaya Street 5, 630090 Novosibirsk, Russia
216. E. Salzborn, Strahlenzentrum der Justus Liebig-Universitat, Leihgesterner Weg 217, D-6300 Giessen, Germany
217. D.H. Sampson, 525 Davey Laboratory, Pennsylvania State University, University Park, PA 16802
218. M. Sataka, Department of Materials Science and Engineering, JAERI, Tokai-mura, Ibaraki-ken 319-11, Japan
219. P. A. Schulz, MIT Lincoln Laboratory, South Road Facility, Lexington, MA 02173-0073
220. G. Scoles, Department of Chemistry, Princeton University, Princeton, NJ 08544
221. M.J. Seaton, Department of Physics and Astronomy, University College London, Gower Street, London WC1E 6BT, United Kingdom
222. V.P. Shevelko, P.N. Lebedev Physical Institute, Russian Academy of Sciences, Leninsky Prospect 53, 117924 Moscow, Russia
223. I. Shpigel, Institute of General Physics, Russian Academy of Sciences, Ulitsa Vavilova 38, Moscow, Russia
224. A.C.H. Smith, Department of Physics and Astronomy, University College London, Gower Street, London WC1E 6BT, United Kingdom
225. J. Smith, Nuclear Data Section, IAEA, Wagramerstrasse 5, P.O. Box 100, A-1400 Vienna, Austria
226. Southwestern Institute of Physics, Deputy Director, P.O. Box 15, Leshan, Sichuan, People's Republic of China
227. R. Srivastava, Department of Physics, University of Roorkee, Roorkee 247667, India
228. W.M. Stacey, School of Nuclear Engineering and Health Physics, Georgia Institute of Technology, Atlanta, GA 30332
229. G. Stefani, Dipartimento di Matematica e Fisica, Universita' di Camerino, 62032 Camerino, Italy
230. D. Steiner, Nuclear Engineering Department, NES Bldg., Tibbetts Ave., Rensselaer Polytechnic Institute, Troy, NY 12181
231. D. R. Swenson, MP-5 H838, Los Alamos National Laboratory, Los Alamos, NM 87545
232. H. Tawara, Data and Planning Center, National Institute for Fusion Science, Nagoya 464-01, Japan
233. S. S. Tayal, Department of Physics, Clark Atlanta University, Atlanta, GA 30314
234. H.S. Taylor, Chemistry Department, University of Southern California, University Park, Los Angeles, CA 90089
235. A. Temkin, Code 680, NASA/Goddard Space Flight Center, Greenbelt, MD 20771
236. J.L. Terry, NW17-176, MIT Plasma Fusion Center, 167 Albany Street, Cambridge, MA 02139
237. Thermonuclear Library, Japan Atomic Energy Research Institute, Tokai, Naka, Ibaraki, Japan
238. K. I. Thomassen, L-637, Lawrence Livermore National Laboratory, P.O. Box 5511, Livermore, CA 94550
239. J.S. Thompson, Department of Physics 220, University of Nevada-Reno, Reno, NV 89557
240. V.T. Tolok, Kharkov Physical-Technical Institute, Academical Street 1, 310108 Kharkov, Russia
241. R. Varma, Physical Research Laboratory, Navrangpura, Ahmedabad-380009, India

- 242. L.J. Wang, Department of Physics and Astronomy, University of Tennessee, 615 McCallie Avenue, Chattanooga, TN 37403-2598
- 243. W. P. West, MS 13/457, General Atomics, P.O. Box 85608, San Diego, CA 92138
- 244. J.F. Williams, Physics Department, University of Western Australia, Perth 6009, Australia
- 245. S.M. Younger, MS E527 NWT/ICF, Los Alamos National Laboratory, Los Alamos, NM 87545
- 246. P.A. Zeijlmans van Emmichoven, Department of Atomic and Interface Physics, Debye Institute, Utrecht University, Princetonplein 5, 3584 CC Utrecht, The Netherlands
- 247. Y. Zhang, Department of Physics, University of North Texas, Denton, TX 76203
- 248-249. Office of Scientific and Technical Information, P.O. Box 62, Oak Ridge, TN 37831

**DATE
FILMED**

10/12/94

END